Improving Maternal and Fetal Cardiac Monitoring Using Artificial Intelligence

A Thesis Submitted to the

College of Graduate and Postdoctoral Studies

In Partial Fulfillment of the Requirements

For the Degree of Doctor of Philosophy

In the Department of Electrical and Computer Engineering

University of Saskatchewan

Saskatoon

By

Mohammad Reza Mohebbian

PERMISSION TO USE

In presenting this thesis in partial fulfillment of the requirements for a Postgraduate degree from the University of Saskatchewan, I agree that the Libraries of this University may make it freely available for inspection. I further agree that permission for copying of this thesis in any manner, in whole or in part, for scholarly purposes may be granted by the professor or professors who supervised my thesis work or, in their absence, by the Head of the Department or the Dean of the College in which my thesis work was done. It is understood that any copying or publication or use of this thesis or parts thereof for financial gain shall not be allowed without my written permission. It is also understood that due recognition shall be given to me and to the University of Saskatchewan in any scholarly use which may be made of any material in my thesis.

DISCLAIMER

Reference in this thesis to any specific commercial products, process, or service by trade name, trademark, manufacturer, or otherwise, does not constitute or imply its endorsement, recommendation, or favoring by the University of Saskatchewan. The views and opinions of the author expressed herein do not state or reflect those of the University of Saskatchewan, and shall not be used for advertising or product endorsement purposes.

Requests for permission to copy or to make other uses of materials in this thesis in whole or part should be addressed to:

Dean

College of Graduate and Postdoctroral Studies

University of Saskatchewan

116 Thorvaldson Building, 110 Science Place

Saskatoon, SK S7N 5C9 Canada

Or

Head of Department of Electrical and Computer Engineering

57 Campus Drive

University of Saskatchewan,

Saskatoon, SK, S7N 5A9 Canada

Abstract

Early diagnosis of possible risks in the physiological status of fetus and mother during pregnancy and delivery is critical and can reduce mortality and morbidity. For example, early detection of life-threatening congenital heart disease may increase survival rate and reduce morbidity while allowing parents to make informed decisions. To study cardiac function, a variety of signals are required to be collected. In practice, several heart monitoring methods, such as electrocardiogram (ECG) and photoplethysmography (PPG), are commonly performed. Although there are several methods for monitoring fetal and maternal health, research is currently underway to enhance the mobility, accuracy, automation, and noise resistance of these methods to be used extensively, even at home. Artificial Intelligence (AI) can help to design a precise and convenient monitoring system. To achieve the goals, the following objectives are defined in this research:

The first step for a signal acquisition system is to obtain high-quality signals. As the first objective, a signal processing scheme is explored to improve the signal-to-noise ratio (SNR) of signals and extract the desired signal from a noisy one with negative SNR (i.e., power of noise is greater than signal). It is worth mentioning that ECG and PPG signals are sensitive to noise from a variety of sources, increasing the risk of misunderstanding and interfering with the diagnostic process. The noises typically arise from power line interference, white noise, electrode contact noise, muscle contraction, baseline wandering, instrument noise, motion artifacts, electrosurgical noise. Even a slight variation in the obtained ECG waveform can impair the understanding of the patient's heart condition and affect the treatment procedure. Recent solutions, such as adaptive and blind source separation (BSS) algorithms, still have drawbacks, such as the need for noise or desired signal model, tuning and calibration, and inefficiency when dealing with excessively noisy signals. Therefore, the final goal of this step is to develop a robust algorithm that can estimate noise, even when SNR is negative, using the BSS method and remove it based on an adaptive filter.

The second objective is defined for monitoring maternal and fetal ECG. Previous methods that were non-invasive used maternal abdominal ECG (MECG) for extracting fetal ECG (FECG). These methods need to be calibrated to generalize well. In other words, for each new subject, a calibration with a trustable device is required, which makes it difficult and time-consuming. The calibration is also susceptible to errors. We explore deep learning (DL) models for domain mapping, such as Cycle-Consistent Adversarial Networks, to map MECG to fetal ECG (FECG) and vice versa. The advantages of the proposed DL method over state-of-the-art approaches, such as adaptive filters or blind source separation, are that the proposed method is generalized well on unseen subjects. Moreover, it does not need calibration and is not sensitive to the heart rate variability of mother and fetal; it can also handle low signal-to-noise ratio (SNR) conditions.

Thirdly, AI-based system that can measure continuous systolic blood pressure (SBP) and diastolic blood pressure (DBP) with minimum electrode requirements is explored. The most common method of measuring blood pressure is using cuff-based equipment, which cannot monitor blood pressure continuously, requires calibration, and is difficult to use. Other

solutions use a synchronized ECG and PPG combination, which is still inconvenient and challenging to synchronize. The proposed method overcomes those issues and only uses PPG signal, comparing to other solutions. Using only PPG for blood pressure is more convenient since it is only one electrode on the finger where its acquisition is more resilient against error due to movement.

The fourth objective is to detect anomalies on FECG data. The requirement of thousands of manually annotated samples is a concern for state-of-the-art detection systems, especially for fetal ECG (FECG), where there are few publicly available FECG datasets annotated for each FECG beat. Therefore, we will utilize active learning and transfer-learning concept to train a FECG anomaly detection system with the least training samples and high accuracy. In this part, a model is trained for detecting ECG anomalies in adults. Later this model is trained to detect anomalies on FECG. We only select more influential samples from the training set for training, which leads to training with the least effort.

Because of physician shortages and rural geography, pregnant women's ability to get prenatal care might be improved through remote monitoring, especially when access to prenatal care is limited. Increased compliance with prenatal treatment and linked care amongst various providers are two possible benefits of remote monitoring. If recorded signals are transmitted correctly, maternal and fetal remote monitoring can be effective. Therefore, the last objective is to design a compression algorithm that can compress signals (like ECG) with a higher ratio than state-of-the-art and perform decompression fast without distortion. The proposed compression is fast thanks to the time domain B-Spline approach, and compressed data can be used for visualization and monitoring without decompression owing to the B-spline properties. Moreover, the stochastic optimization is designed to retain the signal quality and does not distort signal for diagnosis purposes while having a high compression ratio.

In summary, components for creating an end-to-end system for day-to-day maternal and fetal cardiac monitoring can be envisioned as a mix of all tasks listed above. PPG and ECG recorded from the mother can be denoised using deconvolution strategy. Then, compression can be employed for transmitting signal. The trained CycleGAN model can be used for extracting FECG from MECG. Then, trained model using active transfer learning can detect anomaly on both MECG and FECG. Simultaneously, maternal BP is retrieved from the PPG signal. This information can be used for monitoring the cardiac status of mother and fetus, and also can be used for filling reports such as partogram.

Acknowledgment

This thesis would not have been possible, or at least not what it looks like now, without the help and guidance of many people. These few lines are not enough to express my gratitude to all of them.

I would like to express my deepest gratitude toward my supervisor, Dr. Khan A. Wahid, for his criticism, patience, invaluable support, and guidance through my research program at the University of Saskatchewan. It has indeed been an honor and rewarding experience to work under his supervision. I have learned important lessons on the skills and values of conducting research.

I would also like to extend my gratitude to Dr. Anh Dinh, Dr.Babyn, and Dr. Marateb for helping me develop my knowledge and skills and collaborating in writing papers with me, and inspiring me with their ideas. To my loving wife, my dearest parents, and my caring sibling, I dedicate this thesis. I am also thankful to my colleagues and lab mates.

My deepest love and gratitude belong to my beloved wife, Roxana Samani, for her tremendous understanding, support, and encouragement during this study. Finally, I wish to express my appreciation to all of those who gave me help when I studied at the University of Saskatchewan

Table of Contents

List of Figures

List of Tables

ABBREVIATIONS

ABP	Arterial Blood Pressure
ACO	Ant Colony Optimization
AECG	Abdominal Electrocardiogram
AI	Artificial Intelligence
APG	Acceleration of Photoplethysmogram
BP	Blood Pressure
CF	Conventional Feature
CKC	Convolution Kernel Compensation
CNN	Convolutional Neural Network
CR	Compression Ratio
CTG	Cardiotocography
DBP	Diastolic Blood Pressure
DL	Deep Learning
ECG	Electrocardiogram
FECG	Fetal Electrocardiogram
FHR	Fetal Heart Rate
FP-CKC	Fixed-Point Convolution Kernel Compensation
GAN	Generative Adversarial Networks
GMDH	Group Method of Data Handling
ICA	Independent Component Analysis
LSTM	Long Short Term Memory
MAE	Mean Average Error
MCG	Magnetocardiography
MECG	Maternal Electrocardiogram
ML	Machine Learning
NI-FECG	Non-Invasive Fetal Electrocardiogram
PPG	Photoplethysmogram
PRD	Percentage Root Difference
PSO	Particle Swarm Optimization
RBF	Radial Basis Function
ReLU	Rectified Linear Unit
RF	Random Forest
RMSE	Root Mean Square Error
SBP	Systolic Blood Pressure

SER	Signal to Error Ratio
SNR	Signal to Noise Ratio
SVM	Support Vector Machine
t-SNE	t-Distributed Stochastic Neighbor Embedding
VPG	Velocity of Photoplethysmogram
WEDD	Wavelet Energy Diagnosis Distortion
WSN	Wireless Sensor Network

1 INTRODUCTION

1.1 Background

Each year, 2.65 million stillbirths are estimated to occur worldwide, with 98% occurring in low- and middle-income countries and more than 45% after delivery [1]. Besides stillbirths, the rate of congenital disabilities is increasing; while most defects happen in the first month of pregnancy, wherein the heart is forming [2]. The most crucial period of fetus development is between 3 and 7 weeks of pregnancy because the heart is the first formed organ [3]. About 1% of fetuses are found to have heart arrhythmias. 10% percent of these arrhythmias are thought to be potential causes of morbidity [4]. Obstetricians will be able to make the best decisions before and after delivery if the fetal heart is carefully monitored [5]. One of the essential ways to reduce stillbirth and defect is monitoring the fetal status, especially cardiac status, to diagnose and treat early problems in the early stages.

Although there are various ways to monitor the health status of fetuses and mothers, there is research still investigating to improve portability, precision, automation, and robustness against noise of these methods to be used widely even in the home. The best way to monitor a fetus's cardiac activity is to use magnetocardiography (MCG). However, the expensive cost of MCG makes it expensive for low- and middle-income economies [6]. Cardiotocography (CTG) and Doppler ultrasound are two current methods that have certain drawbacks. CTG, for example, can be used to determine the fetal heart rate (FHR) during the third trimester of pregnancy (after 28 weeks of pregnancy) and solely gives information on ventricular blood flow [7]. The widespread use of CTG monitoring in hospitals has also increased cesarean section deliveries' prevalence [8]. Compared to CTG diagnosis, the signal quality of electrocardiography (ECG) offers better findings even at 20 weeks of pregnancy [7]. The fetal ECG (FECG) can be measured invasively by placing an electrode on the fetus's scalp, but this can only be done after cervical dilation [9], which puts the fetus and the mother in danger. The FECG signal can also be measured by electrodes on the mother's abdomen (AECG) [10]. However, the FECG extraction is still under effect by many factors such as noises, artifacts, algorithm tuning, and lack of enough clinical data for validation. Nevertheless, the FECG is one of the best signals that can used for monitoring status of fetus and improving the FECG extraction technique is crucial for improving fetal heart status monitoring.

There some structural differences between Fetal and adult hearts [11]. The left ventricle pumps blood throughout the body after birth, whereas the right ventricle pumps blood to the lungs for oxygenation. On the other hand, the placenta provides fetal oxygen; hence, blood is no longer pushed to the lungs. Alternatively, both ventricles work together to circulate blood to the body (including the lungs). While the mechanical functionality of the fetal heart differs from the adult heart, its electrical activity is comparable beat to beat [12]. Adults and fetuses show comparable ECG patterns morphologically, but the relative amplitudes of the fetal

complexes fluctuate throughout pregnancy and even after delivery [13]. For instance, the T-waves, which are very weak for fetuses and infants, undergo the most significant alteration.

Another signal that can be used for day-to-day cardiac monitoring is Photoplethysmography (PPG). PPG is a common optical technique for monitoring skin blood volume, pulse rate, and oxygenation changes. The PPG signal contains components aligned with both cardiac and respiratory rhythms and has been used to monitor heart and respiration rates [14]. Furthermore, PPG is easier to be recorded compared to ECG. ECG requires at least three electrodes to record the signal, while the PPG can be measured by only one connection. Besides, ECG is highly sensitive to subject motion, while many PPG-based devices in the market are used for health monitoring [15]. PPG and ECG are used in some studies to predict blood pressure [16]. Automatic blood pressure (BP) monitors are another well-known technology that is occasionally employed for day-to-day cardiac monitoring [17], [18] and is also essential for partograms [19]. However, all current precise BP measurement methods are based on a cuff that requires a second person with expertise. Moreover, the cuff is sensitive to movement, and cuff-based devices require calibration. In this regard, improving PPG signal interpretation for measuring BP without the need for ECG is merit.

Traditional ECG uses twelve electrodes for measuring heart activity for a short time. Holter is another standard method for recording ECG that records the heart activity for 24 hours or more [20]. Besides, emerging wireless sensor networks (WSNs) and the internet of things helped bring new technologies like wearable and WSN-based ECGs, which need transmitting signals [21]. Depending on application types, the ECG signal can be recorded with 100 to 500 Hz sampling frequency [22], and as an example, three channels of 24 hours ECG can typically take over two hundred megabytes. Therefore, transmitting signal is a challenge that would be more difficult with increasing resolution, sampling frequency, number of channels, and number of signals. Signal compression is one of the solutions for sending and storing signals [23]. However, the compressing and decompressing parts need to be fast and with the most negligible loss, especially for monitoring vital signs, which are very important to be visualized precisely and in real-time.

Artificial intelligence (AI) has achieved enormous popularity in the medical field in the last few years [24], [25]. Various AI systems are undergoing massive study to maximize the efficiency of routine clinical diagnosis and make the routine simpler. It can be exceedingly complex, even for experienced physicians, to accurately detect possible cardiac disorders from different signals. Not only is it inconvenient for subjects and technicians to record multiple signals, but increasing the number of signals increases the potential for noise, making diagnosis more difficult.

The general task of software development is to code a computer program based on an algorithm that produces a given output for a particular input. This perspective is modified by machine learning since portions of the computer program remain undetermined. The primary objective of training an AI model is to find a generalizable model that is appropriate even for new data samples that have not been used in the training phase. New data samples can also be correctly processed for such a model and, thus, the computer can learn to deal with new scenarios. For all activities with such a learning aspect, the generic term 'artificial intelligence'

is currently known. However, in a human way of thinking, all approaches used are still not "intelligent," but rather deal with various kinds of pattern recognition.

In the aspect of the learning procedure, AI can be categorized into five different methods, including supervised learning, unsupervised learning [26], semi-supervised learning [27], self-supervised learning [28], and reinforcement learning [29]. Machine learning for several years worked primarily on hand-crafted features, where a statistical explanation of patterns was utilized, e.g., texture and color. In recent years, the concept of hand-crafted features has shifted to "deep learning" (DL) [30] approaches, where an artificial neural network trains not only the classifier but also extracts features. Figure 1.1 shows an overview of different AI categories and their relations.

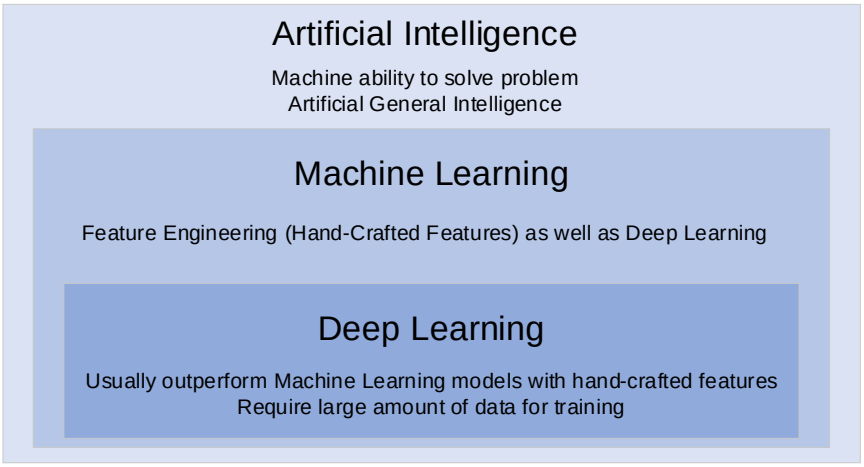

Figure 1-1. Overview of different AI categories and their relations.

Deep learning has been one of the most effective machine learning techniques in the last decade [31]. A deep learning model requires the availability of a large dataset for training to learn the dataset's interesting features; accordingly, training the model with a limited dataset typically results in an overfitted model. Transfer learning (TL) is a popular technique for dealing with data limitation [32] that obtain information in one problem domain and transferring it to a different but similar problem. For example, the knowledge learned while identifying adult ECG anomalies may be applied to classifying FECG anomalies. The transfer learning models usually require to be fine-tuned on a small portion of new domain data. This can decrease the effort of labeling large number of datasets, however, manually annotating data is still costly and time-consuming, especially when subject expertise is required.

Overall, the AI can improve maternal and fetal heart monitoring to reduce fetal defect, stillbirth, and maternal fatality. This improvement contains but is not limited to: denoising recorded signals for better diagnosis, improving FECG extraction quality using AECG, predicting BP from only PPG, detecting anomaly from least annotated FECG signals, and compressing signals for storing or off-line processing.

1.2 Literature review

The first step after recording signals is to filter and clean them from the noises and artifacts. Different types of digital filters such as finite impulse response and infinite impulse response filters [33], [34] have been utilized to eliminate signal noises. These filters work when the parameters of signals and channels are well-known. However, they cannot efficiently remove all types of noises when signals are nonstationary [35]. In this regard, adaptive filters are introduced to adapt filter coefficients according to signal changes in time.

Nevertheless, adaptive filters have some disadvantages, e.g., the convergence rate depends on the input signal's power spectral density [36]. Hence, if the power spectrum of signals has a flat and uniform component in all available frequencies which means that the input signal filter is white, the convergence rate of minimum mean-square is excellent. However, colored noise will drop the efficiency substantially. Therefore, the least mean squares (LMS) and recursive least square (RLS), which converge to Weiner optimal solution, are designed to handle narrowband frequency, and according to the literature [37], even a primary adaptive filter such as LMS can reduce the noise from nonstationary signals. Another drawback of an adaptive filter is the prior knowledge about the desired signal or noise, which is paramount [37]. Occasionally, using a template of a well-known shape of the signal, such as one ECG or PPG epoch, can reduce the chance of detecting abnormality and artifacts [38]. Therefore, blind source separation methods such as independent component analysis (ICA) and principal component analysis have emerged for noise removal; However, in meager SNR circumstances, these methods are not sufficient and need further post-processing [39]–[42].

Many methods tried to extract QRS waves; however, in decomposing the FECG, other parts should also be considered. To the best of our knowledge, there is no research for extracting all FECG components from MECG. Moreover, using a general model that can be used for different subjects with different electrode displacements, maternal and fetal age requires more investigation. Since the time series of ECG QRS can give lots of information about cardiac statuses, such as heart rate, various research aimed to extract QRS of FECG from MECG. Behar *et al.* [43] evaluated recurrent neural network (RNN), principal component analysis (PCA), least mean square (LMS), and recursive least square (RLS), and template subtraction for fetal QRS detection from MECG [44]. They trained on 30 seconds of the NI-FECG dataset, used a 50 ms matching window, and achieved a 97.2% F1-score as the best results acquired by RNN. They also reported results of the trained model on a single dataset as external validation of 90.2% with the same network. The Encoder-Decoder method [45] and SVD-SW [46] approaches are also utilized on the same task on the Abdominal and Direct FECG (A&D FECG) dataset and achieved 94.1% and 99.4% F1-score. Behar et al. [47] used a combination of template subtraction and ICA and achieved a 95.9% F1-score on the NI-FECG dataset. Varanini et al. [48] proposed a signal extraction technique based on ICA and a post-processing method specialized for detecting the QRS on the NI-FECG challenge dataset and obtained a 99 % F1 score. Warmerdam et al. [49] used a multichannel hierarchical probabilistic system, incorporating ECG waveform and heart rate predictive models to detect fetal R peaks in the NI-FECG challenge dataset. They reported that only 99.6% accuracy did not provide sensitivity or F1-Score for better comparison. However, their accuracy outperformed Varanini et al. [48] method with an accuracy of 98.6%.

By extracting high-quality FECG from AECG, the potential of accurate anomaly detection from FECG can be raised. Despite the high similarity of adult ECG and FECG, adult ECG processing has made significant advances in modern medicine [50], but FECG processing remains a significant issue [51]. Todays, fetal monitoring is only focused on the fetal heart rate [52]. The abnormal fetal heartbeat usually is categorized as tachyarrhythmia (faster than 160 beats per minute) or bradyarrhythmia (slower than 120 beats per minute). However, detecting the fetal abnormal heartbeat rhythm does not consider the waveform features of the FECG, which are the basis of cardiac assessment in both children and adults. The technology to accurately measure FECG is mainly unavailable, which is the fundamental reason for its exclusion from clinical settings. As a result, there has not been much study linking ECG features to FECG outcomes on a broad scale. Moreover, the lack of gold standard datasets for FECG anomaly detection is another reason FECG arrhythmia detection needs more research. It is partly due to the absence of comprehensive clinical information about fetal cardiac function and partly due to the low signal-to-noise ratio of FECG compared to the maternal ECG [51].

Blood pressure is an essential signal for monitoring cardiac status; however, most of the current devices work based on the cuff, which usually needs a second person to perform the measurement and is not capable of continuous monitoring. Various methods tried to estimate continuous BP by alternative easy-recording signals. PPG, age, weight, height, and gender were used by Liu *et al.* [53] to predict continuous BP. Poon and Zhang [54] calculated DBP and SBP using Moens Korteweg's method after extracting pulse transit time (PTT) from PPG and ECG in 45 seconds. For DBP and SBP, the mean difference of 2.8 ± 6.8 mmHg and 0.9 ± 5.6 mmHg was achieved, respectively. Zheng *et al*. developed a wearable wristband for monitoring SBP using PTT analysis in 30-minute intervals of ECG and PPG, with a root mean square error of 2.8 8.2 mmHg (RMSE) [55]. Nevertheless, having a technique to extract continuous BP with the minimal instrument and higher accuracy requires more research.

Signal compression is another scope that requires quality improvement to make transmission, storing, and monitoring more efficient. Polania *et al*. [56] performed simultaneous orthogonal matching pursuit and could achieve a 2.5% percentage root-mean-square difference (PRD), with a 7.2 compression ratio (CR). Mamaghanian *et al*. [57] compared discrete wavelet transform (DWT) and sparse binary sensing and reported a real-time performance for the sparse binary method but with low precision with 9% PRD. Chae *et al*. [58] also used a modified TH-DWT and only tested one signal. Moreover, there is no systematic real-time validation. Elgandi and Ward [59] used adaptive linear predictors and obtained a compression ratio of 6.4 along with QRS detection. Jha CK [60] combined wavelet transform, and empirical mode decomposition could achieve a 21.5 compression ratio and 6.8 % PRD. Still, there is some chance to design an efficient method to have better PRD respecting CR.

1.3 Research objectives

An end-to-end system is required to monitor the maternal and fetal cardiac systems. Here, at first, the PPG and AECG signal is recorded from the mother. Then, a denoising algorithm is applied to each signal to remove artifacts and noises. Next, the AECG is converted to FECG; algorithms to detect anomaly is applied on it. Simultaneously, anomalies on maternal ECG are

detected with another model. BP is extracted from the PPG signal. It is shown that during pregnancy, both low and high diastolic blood pressures are linked to small babies and high perinatal mortality [61]. All these data can be compressed and used to fill the partogram or can be used individually for investigating a specific issue.

For improving cardiac monitoring using AI, the following objectives are taken into consideration which is shown in Figure 1.2:

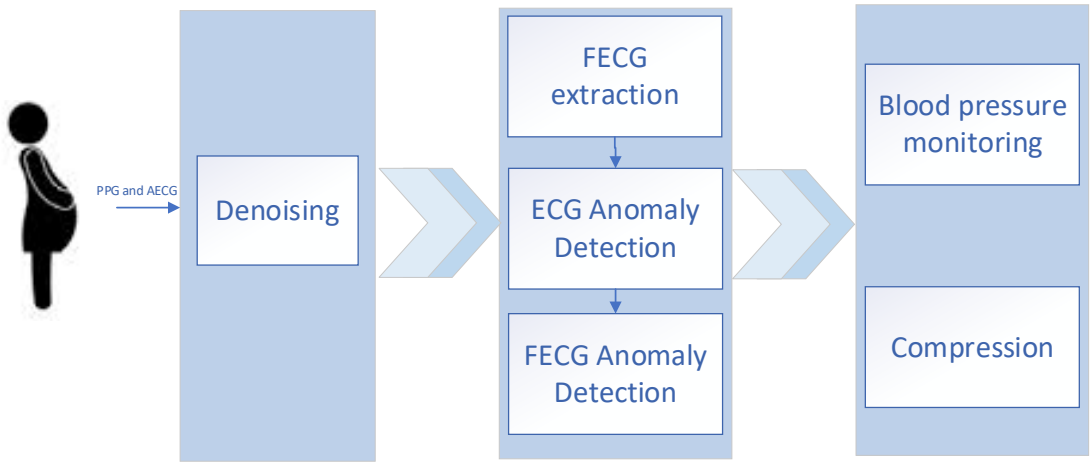

Figure 1-2. The block diagram of the proposed methods that are addressed in the thesis and their relation.

1. To explore signal processing schemes to improve the quality of recorded biomedical signals and make a robust denoising method against high amplitude noise. The proposed method should extract the desired signal even the signal-to-noise ratio (SNR) of the input signal is negative, which means noise with a higher amplitude distorted signal. It is worth mentioning that the noise is added to the signal, but it can be convolved to the original signal.

2. To explore an efficient method using AI to extract FECG from maternal ECG. Many approaches have been used to extract QRS waves; however, FECG has other components that must be considered while deconstructing it. Furthermore, developing a general model that can be used for various subjects with various electrode displacements requires more research. We further followed this aim with two approaches:

    - Since generative models have shown promising results in mapping data, deep generative methods [62] are investigated to map MECG to FECG and vice versa. Moreover, the attention mechanism [63], which has shown high performance for sequence-to-sequence processing in natural language processing, is utilized for biomedical signals. We also explored recent DL training advances and used CycleGAN to simplify the training using unpaired data.

- Deconvolution strategy, which is a combination of adaptive filter and blind source separation, can be used for FECG extraction and can be used for noise extraction.

3. To investigate the use of AI for anomaly detection from FECG. Although much research is developed around adult ECG anomaly detection due to enough publicly available datasets, there is limited research for FECG anomaly detection. In this objective, recent advances in deep learning, including transfer learning and active learning, are investigated to transfer a model from adult ECG anomaly detection to FECG anomaly detection. The transferred model is trained using active learning by help an expert, helping to train a model with the least annotated FECG samples for fine-tuning.

4. To explore the use of AI for estimating blood pressure (BP) using only PPG signals. It will help the mother be monitored with minimal instrument and allow continuous BP and PPG using only one channel. Recent studies [62] showed a correlation between maternal blood pressure, the weight of the birth, and parental mortality. Hence, it is important to have blood pressure monitoring in an end-to-end cardiac monitoring system.

5. A compression scheme is investigated to use a monitoring system in remote distances to reduce the bandwidth required for sending signals. The proposed compression enables the day-to-day in-home monitoring of pregnant women. An optimized signal compression scheme is investigated to maintain the quality along with a high compression ratio. Although there is much research about signal compression, compression and reconstruction performance may be enhanced even further. The contribution is improving the state-of-the-art algorithm's performance and designing a new algorithm not to distort features that are important in diagnosis. Due to using the time-domain and B-Spline technique, the data compression is fast and compressed data can be used for visualization and monitoring purposes without decompression owing to B-spline characteristics.

Therefore, a combination of all these tasks can be applied to an end-to-end maternal and fetal cardiac monitoring system.

1.4 Organization of the thesis

The thsis is organized in a manuscript-based style. The first chapter of the thesis presents an overview about importance of maternal and fetal cardiac monitoring, motivation of the thesis, objectives and research. The main content and contribution of the thesis are included in the form of published or under review manuscripts. The remainder of the thesis organized as follows:

Chapter 2 presents a novel technique for denoising biomedical signals that are degraded with high amplitude noises, in which target signal is not visible and extractable using conventional methods. This assists in the development of a reliable and high-precision biomedical signal recording stage, which is the first and most essential step in signal monitoring analysis and diagnosis. It may also allow us to claim that we can record signals on portable devices.

The manuscript in chapter 3 describes the development of an algorithm for extracting FECG from abdominal maternal ECG. The proposed method has some unique features. First,

it is trained using unpaired fetus and mother ECG samples which means it eliminated the difficulty of synronization signals during recording. Second, the calibration and use of various datasets during the test revealed that it has strong generalization to operate with a variety of maternal and fetal ages. Finally, this work helps to obtain high quality FECG for diagnosis aims that paves the way for the next step that is anomaly detection on FECG, which is discussed in chapter 4.

The manuscript in chapter 4 presents a new method for training a deep learning model. The new method of training helps to obtain high performance with least annotation effort and computational resources. A mix of active learning and transfer learning is utilised to achieve this goal, while the sampling approach for picking the optimum training sample is modified.

Chapter 5 changes the focus from fetal cardiac monitoring to maternal cardiac monitoring and devised a method that can measure blood pressure continuously, cuff-less, with high precision and least electrode connection. This chapter describes a machine learning technique that uses solely PPG inputs for blood pressure measurement. A prototype device is used for collecting samples and it is tested and compared to a cuff-based, gold standard blood pressure device.

The manuscript in chapter 6 presents a compression algorithm for ECG. The manuscript's contribution is to improve the present state-of-the-art algorithm's performance and to develop a new technique that does not distort important diagnostic traits from the signal, while having fast decompression to be used in future portable devices. Finally the summary of accomplishment and future recommendation are presented in chapter 7.

1.5 Reference

[1] Z. A. Bhutta *et al.*, "Stillbirths: what difference can we make and at what cost?," *The Lancet*, vol. 377, no. 9776, pp. 1523–1538, 2011.

[2] B. Q. Dong *et al.*, "Study on the characteristics of major birth defects in 1.69 million cases of fetus in Guangxi Zhuang autonomous region," *Zhonghua liu xing bing xue za zhi= Zhonghua liuxingbingxue zazhi*, vol. 40, no. 12, pp. 1554–1559, 2019.

[3] J. G. Och, "Computer-assisted assessment of fetal growth and development," in *The Seventh Annual Symposium on Computer Applications in Medical Care, 1983. Proceedings.*, 1983, pp. 185–187.

[4] J. A. Behar, L. Bonnemains, V. Shulgin, J. Oster, O. Ostras, and I. Lakhno, "Noninvasive fetal electrocardiography for the detection of fetal arrhythmias," *Prenatal diagnosis*, vol. 39, no. 3, pp. 178–187, 2019.

[5] E. Keenan, C. Karmakar, F. C. Brownfoot, and M. Palaniswami, "Personalized Anatomic Modeling for Noninvasive Fetal ECG: Methodology and Applications," *IEEE Transactions on Instrumentation and Measurement*, vol. 70, pp. 1–12, 2021.

[6] S. Strand, W. Lutter, J. F. Strasburger, V. Shah, O. Baffa, and R. T. Wakai, "Low-cost fetal magnetocardiography: a comparison of superconducting quantum interference device and optically pumped magnetometers," *Journal of the American Heart Association*, vol. 8, no. 16, p. e013436, 2019.

[7] R. G. Sæderup, H. Zimmermann, D. H. Eiríksdóttir, J. Hansen, J. J. Struijk, and S. Schmidt, "Comparison of cardiotocography and fetal heart rate estimators based on non-invasive fetal ECG," in *2019 Computing in Cardiology (CinC)*, 2019, p. Page 1-Page 4.

[8] P. Chetandas, S. Zahiruddin, N. Jabeen, R. Baloch, and F. Shaikh, "Increasing rate of Caesarean Section Due to Non-Reassuring Cardiotocography," *Open Journal of obstetrics and gynecology*, vol. 7, no. 3, pp. 351–357, 2017.
[9] T. Y. Euliano, S. Darmanjian, M. T. Nguyen, J. D. Busowski, N. Euliano, and A. R. Gregg, "Monitoring fetal heart rate during labor: a comparison of three methods," *Journal of pregnancy*, vol. 2017, 2017.
[10] A. Agostinelli *et al.*, "Noninvasive fetal electrocardiography: an overview of the signal electrophysiological meaning, recording procedures, and processing techniques," *Annals of Noninvasive Electrocardiology*, vol. 20, no. 4, pp. 303–313, 2015.
[11] E. Hernandez-Andrade, M. Patwardhan, M. Cruz-Lemini, and S. Luewan, "Early evaluation of the fetal heart," *Fetal diagnosis and therapy*, vol. 42, no. 3, pp. 161–173, 2017.
[12] A. V. Rajesh and R. Ganesan, "Comprehensive study on fetal ECG extraction," in *2014 International Conference on Control, Instrumentation, Communication and Computational Technologies (ICCICCT)*, 2014, pp. 1187–1192.
[13] N. J. Randall, P. J. Steer, and I. A. Sutherland, "Detection of the fetal ECG during labour by an intrauterine probe," *Journal of biomedical engineering*, vol. 10, no. 2, pp. 159–164, 1988.
[14] A. Johansson, P. Å. Öberg, and G. Sedin, "Monitoring of heart and respiratory rates in newborn infants using a new photoplethysmographic technique," *Journal of clinical monitoring and computing*, vol. 15, no. 7, pp. 461–467, 1999.
[15] T. Wu, F. Wu, C. Qiu, J.-M. Redouté, and M. R. Yuce, "A rigid-flex wearable health monitoring sensor patch for IoT-connected healthcare applications," *IEEE Internet of Things Journal*, vol. 7, no. 8, pp. 6932–6945, 2020.
[16] Y. Yoon, J. H. Cho, and G. Yoon, "Non-constrained blood pressure monitoring using ECG and PPG for personal healthcare," *Journal of medical systems*, vol. 33, no. 4, pp. 261–266, 2009.
[17] C. J. H. Johnson and J. H. Kerr, "Automatic blood pressure monitors A clinical evaluation of five models in adults," *Anaesthesia*, vol. 40, no. 5, pp. 471–478, 1985.
[18] G. D. James and L. M. Gerber, "Measuring arterial blood pressure in humans: Auscultatory and automatic measurement techniques for human biological field studies," *American Journal of Human Biology*, vol. 30, no. 1, p. e23063, 2018.
[19] K. C. Ashish, J. Wrammert, R. B. Clark, U. Ewald, and M. Målqvist, "Inadequate fetal heart rate monitoring and poor use of partogram associated with intrapartum stillbirth: a case-referent study in Nepal," *BMC pregnancy and childbirth*, vol. 16, no. 1, pp. 1–11, 2016.
[20] C. K. Jha and M. H. Kolekar, "Classification and compression of ECG signal for holter device," in *Biomedical signal and image processing in patient care*, IGI Global, 2018, pp. 46–63.
[21] M. Rosu and S. Pasca, "WBAN based long term ECG monitoring," in *Wearable technologies: concepts, methodologies, tools, and applications*, IGI Global, 2018, pp. 952–971.
[22] S. S. Qurraie and R. G. Afkhami, "ECG arrhythmia classification using time frequency distribution techniques," *Biomedical engineering letters*, vol. 7, no. 4, pp. 325–332, 2017.
[23] A. F. Hussein, S. J. Hashim, A. F. A. Aziz, F. Z. Rokhani, and W. A. W. Adnan, "A real time ECG data compression scheme for enhanced bluetooth low energy ECG system power consumption," *Journal of Ambient Intelligence and Humanized Computing*, pp. 1–14, 2017.
[24] F. Pesapane, M. Codari, and F. Sardanelli, "Artificial intelligence in medical imaging: threat or opportunity? Radiologists again at the forefront of innovation in medicine," *European Radiology Experimental*, vol. 2, no. 1, p. 35, Oct. 2018, doi: 10.1186/s41747-018-0061-6.
[25] R. Vashistha, A. K. Dangi, A. Kumar, D. Chhabra, and P. Shukla, "Futuristic biosensors for cardiac health care: an artificial intelligence approach," *3 Biotech*, vol. 8, no. 8, pp. 1–11, 2018.
[26] H. B. Barlow, "Unsupervised learning," *Neural computation*, vol. 1, no. 3, pp. 295–311, 1989.
[27] T. Hastie, R. Tibshirani, and J. Friedman, "Overview of supervised learning," in *The elements of statistical learning*, Springer, 2009, pp. 9–41.
[28] X. Liu *et al.*, "Self-supervised learning: Generative or contrastive," *arXiv preprint arXiv:2006.08218*, vol. 1, no. 2, 2020.
[29] R. S. Sutton and A. G. Barto, *Reinforcement learning: An introduction*. MIT press, 2018.

[30] I. Goodfellow, Y. Bengio, A. Courville, and Y. Bengio, *Deep learning*, vol. 1, no. 2. MIT press Cambridge, 2016.
[31] Z. Ebrahimi, M. Loni, M. Daneshtalab, and A. Gharehbaghi, "A review on deep learning methods for ECG arrhythmia classification," *Expert Systems with Applications: X*, vol. 7, p. 100033, 2020.
[32] J.-H. Jang, T. Y. Kim, and D. Yoon, "Effectiveness of Transfer Learning for Deep Learning-Based Electrocardiogram Analysis," *Healthcare informatics research*, vol. 27, no. 1, pp. 19–28, 2021.
[33] J. A. Van Alsté and T. S. Schilder, "Removal of Base-Line Wander and Power-Line Interference from the ECG by an Efficient FIR Filter with a Reduced Number of Taps," *IEEE Transactions on Biomedical Engineering*, 1985, doi: 10.1109/TBME.1985.325514.
[34] D. Ricciardi *et al.*, "Impact of the high-frequency cutoff of bandpass filtering on ECG quality and clinical interpretation: A comparison between 40 Hz and 150 Hz cutoff in a surgical preoperative adult outpatient population," *Journal of Electrocardiology*, vol. 49, no. 5, pp. 691–695, 2016, doi: 10.1016/j.jelectrocard.2016.07.002.
[35] S. L. Joshi, R. A. Vatti, and R. V. Tornekar, "A survey on ECG signal denoisingtechniques," 2013. doi: 10.1109/CSNT.2013.22.
[36] K. Bartyzel, "Adaptive Kuwahara filter," *Signal, Image and Video Processing*, 2016, doi: 10.1007/s11760-015-0791-3.
[37] J. Dhiman, S. Ahmad, K. Gulia, and A. Professor, "Comparison between Adaptive filter Algorithms (LMS, NLMS and RLS)," 2013.
[38] E. Ebrahimzadeh, M. Pooyan, S. Jahani, A. Bijar, and S. K. Setaredan, "ECG SIGNALS NOISE REMOVAL: SELECTION AND OPTIMIZATION OF THE BEST ADAPTIVE FILTERING ALGORITHM BASED ON VARIOUS ALGORITHMS COMPARISON," *Biomedical Engineering: Applications, Basis and Communications*, 2015, doi: 10.4015/S1016237215500386.
[39] A. Karimi Rahmati, S. K. Setarehdan, and B. N. Araabi, "A PCA/ICA based Fetal ECG Extraction from Mother Abdominal Recordings by Means of a Novel Data-driven Approach to Fetal ECG Quality Assessment.," *Journal of biomedical physics & engineering*, 2017.
[40] M. Varanini, G. Tartarisco, L. Billeci, A. Macerata, G. Pioggia, and R. Balocchi, "A multi-step approach for non-invasive fetal ECG analysis," *Proc. 40th Computing in Cardiology Conf. (CinC)*, 2013.
[41] A. Gupta, M. C. Srivastava, V. Khandelwal, and A. Gupta, "A novel approach to fetal ECG extraction and enhancement using Blind Source Separation (BSS-ICA) and adaptive fetal ECG enhancer (AFE)," 2007. doi: 10.1109/ICICS.2007.4449716.
[42] R. Martinek *et al.*, "Comparative effectiveness of ICA and PCA in extraction of fetal ECG from abdominal signals: Toward non-invasive fetal monitoring," *Frontiers in Physiology*, 2018, doi: 10.3389/fphys.2018.00648.
[43] J. Behar, A. Johnson, G. D. Clifford, and J. Oster, "A comparison of single channel fetal ECG extraction methods," *Annals of biomedical engineering*, vol. 42, no. 6, pp. 1340–1353, 2014.
[44] J. Pan and W. J. Tompkins, "A real-time QRS detection algorithm," *IEEE transactions on biomedical engineering*, no. 3, pp. 230–236, 1985.
[45] W. Zhong, L. Liao, X. Guo, and G. Wang, "Fetal electrocardiography extraction with residual convolutional encoder–decoder networks," *Australasian Physical & Engineering Sciences in Medicine*, vol. 42, no. 4, pp. 1081–1089, 2019.
[46] N. Zhang *et al.*, "A novel technique for fetal ECG extraction using single-channel abdominal recording," *Sensors*, vol. 17, no. 3, p. 457, 2017.
[47] J. Behar, J. Oster, and G. D. Clifford, "Combining and benchmarking methods of foetal ECG extraction without maternal or scalp electrode data," *Physiological measurement*, vol. 35, no. 8, p. 1569, 2014.
[48] M. Varanini, G. Tartarisco, L. Billeci, A. Macerata, G. Pioggia, and R. Balocchi, "An efficient unsupervised fetal QRS complex detection from abdominal maternal ECG," *Physiological measurement*, vol. 35, no. 8, p. 1607, 2014.
[49] G. J. Warmerdam, R. Vullings, L. Schmitt, J. O. Van Laar, and J. W. Bergmans, "Hierarchical probabilistic framework for fetal R-peak detection, using ECG waveform and heart rate information," *IEEE Transactions on Signal Processing*, vol. 66, no. 16, pp. 4388–4397, 2018.

[50] H. Li and P. Boulanger, “A survey of heart anomaly detection using ambulatory Electrocardiogram (ECG),” *Sensors*, vol. 20, no. 5, p. 1461, 2020.
[51] M. Anisha, S. S. Kumar, E. E. Nithila, and M. Benisha, “Detection of Fetal Cardiac Anomaly from Composite Abdominal Electrocardiogram,” *Biomedical Signal Processing and Control*, vol. 65, p. 102308, 2021.
[52] M. Suganthy, S. I. Joy, and P. Anandan, “Detection of fetal arrhythmia by adaptive single channel electrocardiogram extraction,” *Physical and Engineering Sciences in Medicine*, pp. 1–10, 2021.
[53] M. Liu, L.-M. Po, and H. Fu, “Cuffless blood pressure estimation based on photoplethysmography signal and its second derivative,” *International Journal of Computer Theory and Engineering*, vol. 9, no. 3, p. 202, 2017.
[54] C. C. Y. Poon and Y. T. Zhang, “Cuff-less and noninvasive measurements of arterial blood pressure by pulse transit time,” in *2005 IEEE engineering in medicine and biology 27th annual conference*, 2006, pp. 5877–5880.
[55] Ya-Li Zheng, B. P. Yan, Yuan-Ting Zhang, and C. C. Y. Poon, “An Armband Wearable Device for Overnight and Cuff-Less Blood Pressure Measurement,” *IEEE Trans. Biomed. Eng.*, vol. 61, no. 7, pp. 2179–2186, Jul. 2014, doi: 10.1109/TBME.2014.2318779.
[56] L. F. Polania, R. E. Carrillo, M. Blanco-Velasco, and K. E. Barner, “Compressed sensing based method for ECG compression,” in *2011 IEEE international conference on acoustics, speech and signal processing (ICASSP)*, 2011, pp. 761–764.
[57] H. Mamaghanian, N. Khaled, D. Atienza, and P. Vandergheynst, “Compressed sensing for real-time energy-efficient ECG compression on wireless body sensor nodes,” *IEEE Transactions on Biomedical Engineering*, vol. 58, no. 9, pp. 2456–2466, 2011.
[58] D. H. Chae, Y. F. Alem, S. Durrani, and R. A. Kennedy, “Performance study of compressive sampling for ECG signal compression in noisy and varying sparsity acquisition,” in *2013 IEEE International Conference on Acoustics, Speech and Signal Processing*, 2013, pp. 1306–1309.
[59] M. Elgendi, A. Mohamed, and R. Ward, “Efficient ECG compression and QRS detection for e-health applications,” *Scientific reports*, vol. 7, no. 1, pp. 1–16, 2017.
[60] C. K. Jha and M. H. Kolekar, “Empirical mode decomposition and wavelet transform based ECG data compression scheme,” *IRBM*, vol. 42, no. 1, pp. 65–72, 2021.
[61] P. J. Steer, M. P. Little, T. Kold-Jensen, J. Chapple, and P. Elliott, “Maternal blood pressure in pregnancy, birth weight, and perinatal mortality in first births: prospective study,” *Bmj*, vol. 329, no. 7478, p. 1312, 2004.
[62] S. Oh, Y. Jung, S. Kim, I. Lee, and N. Kang, “Deep generative design: Integration of topology optimization and generative models,” *Journal of Mechanical Design*, vol. 141, no. 11, 2019.
[63] A. Vaswani *et al.*, “Attention is all you need,” *arXiv preprint arXiv:1706.03762*, 2017.

2 SINGLE CHANNEL HIGH NOISE LEVEL ECG DECONVOLUTION USING OPTIMIZED BLIND ADAPTIVE FILTERING AND FIXED-POINT CONVOLUTION KERNEL COMPENSATION

The first step for monitoring maternal and fetal signal is recording signals. Various noises, including fetus activity, such as fetal brain activity, and maternal activity, like heart activity, uterine contraction, electromyogram (EMG), and movement, degrade recorded signals. It is worth noting that the amplitude of the maternal ECG is substantially higher than FECG, and both overlap in temporal and frequency domains. As a result, obtaining and interpreting the FECG waveform properly is difficult and requires appropriate signal filtering before processing. Furthermore, both baseline wandering and power line interference are major sources of noise. As another instance, photoplethysmography (PPG), which is now the industry standard for continuous heart rate (HR) monitoring for everyday usage because its simplicity, portability, and low-cost, still suffers from noises due to signals cross over, diverse skin tone, and EMG. Therefore, this chapter contributes to removing noise from signals as first step to make signals appropriate for further analysis.

Finite Impulse Response and Infinite Impulse Response filters work when the signal and channel characteristics are known. When signals are nonstationary, however, they are unable to effectively eliminate all types of noise. The convergence rate of adaptive filters also is highly depended on the power spectral density of the input signal and colored noise can drop their efficiency. Furthermore, in low-SNR situations, blind source separation methods are insufficient, and further post-processing is required. A deconvolution strategy based on combination of adaptive filter and convolution kernel compensation is utilized to deconvolve noise and signal. Not only this process is used for denoising noisy signals that have higher noise power than signal power, but also it can be used for extracting FECG from MECG since MECG can assumed as a high-power noise in abdominal ECG respecting to FECG. The proposed method in this chapter introduces a robust denoising method that can be used for highly degraded recorded ECG, like ones recorded using wearable device or smart-clothing platforms.

The analysis and findings of this chapter is reported in the below mentioned published journal manuscript. The student contributed in the main idea, implementing code, writing the original draft, evaluation and revision of the manuscript.

Mohebbian, M.R., Alam, M.W., Wahid, K.A. and Dinh, A., 2020. Single channel high noise level ECG deconvolution using optimized blind adaptive filtering and fixed-point convolution kernel compensation. *Biomedical Signal Processing and Control*, *57*, p.101673.

Single Channel High Noise Level ECG deconvolution using Optimized Blind Adaptive Filtering and Fixed-Point Convolution Kernel Compensation

Mohammad Reza Mohebbian[1], Mohammad Wajih Alam, Khan A. Wahid, Anh Dinh

Department of Electrical and Computer Engineering, University of Saskatchewan S7N 5A9, Saskatoon, Saskatchewan, Canada

Abstract

An electrocardiogram (ECG) is used to record the electrical activity of the heart. However, ECG signals are susceptible to the noise from various sources which increases the probability of misinterpretation and can affect the diagnostic process. Traditional noise cancellation techniques, which uses finite and deterministic coefficient, are not efficient, since the ECG signals are non-stationary. Thus, adaptive filters are commonly utilized on such signal as they can adjust their coefficient according to the changing nature of non-stationary signal. Adaptive algorithms still have a disadvantage that they require the model of noise or desired signal. In this work, a novel algorithm is introduced based on fixed-point convolution kernel compensation for finding a model for using an adaptive filter; then a recursive least square method is used for completing steps of deconvolution of the ECG signal. The deconvolution method can be used for denoising ECG signals in very low signal to noise ratio circumstances and also can be used in blind source separation applications such as separation of fetal ECG from maternal ECG. ECG signals were utilized in this study are taken from the MIT-BIH Arrhythmia database for showing the performance of the algorithm on denoising applications. The results demonstrate that the proposed algorithm renders a much-improved performance in removing the noise from ECG signals, especially in a scenario where signal to noise ratio is negative. Moreover, the noninvasive fetal ECG dataset (NI-FECG) provided by Physionet is also used for fetal ECG extraction by a single thoracic channel. By comparing fetal ECG extraction methods in the literature and the proposed method, it reveals that the proposed method can extract the QRS complex of fetal ECG by a single thoracic channel as accurate as other methods which use abdominal channels.

Keywords: Blind adaptive filter, Blind source separation, Fetal ECG, Deconvolution

2.1 Introduction

The electrocardiogram (ECG) is an essential tool used for diagnosis of heart disorders. It is a non-invasive recording of heart activity that is typically measured by connecting electrodes on the surface of the specific parts of the human body (chest, arms, hands or legs) [1]. However, with the introduction of new technology (Body Area Network or Body Sensor Network), wearable or implantable devices are getting popular which can monitor the vital signs continuously [2]. Although the introduction of these wearable devices have revolutionized personal healthcare, the obtained ECG signal from these devices is significantly distorted with noises (baseline drift and

motion artifacts) [2]. Since ECG can aid in the comprehensive analysis of the heart activity of a patient and can also help in detecting aberrations such as cardiac infractions, unequal beat intervals, the obtained signal should be very accurate. The signals obtained at the surface of the body is weak, have low amplitude and is often susceptible to noise from different sources. These noises are typical results of basic measurement and instrumentation faults. The noises typically arise from power line interference, white noise, electrode contact noise, muscle contraction, baseline wandering, and instrument noise, motion artifacts, electrosurgical noise[3]. Even a slight variation in the obtained ECG waveform can impair the understanding of the heart condition of the patient and can affect the treatment procedure [4], [5]. Thus, it is necessary to remove noise as it will help in obtaining the data which is an accurate representation of the heart's functionality.

Different types of digital filters such as Finite Impulse Response and Infinite Impulse Response filter [5], [6] have been utilized in order to eliminate ECG noises. These filters work when parameters of signals and channels are well-known. However, they cannot remove all type of noises efficiently, when signals are nonstationary [8]. In this regard, adaptive filters are introduced to adapt coefficients of filter according to signal changes in time. Nevertheless, adaptive filters have some disadvantages, e.g., the convergence rate is highly depended on the power spectral density of the input signal [9]. Hence, if the power spectrum of signals has a flat and uniform component in all available frequencies which means that the input signal filter is white, the convergence rate of minimum mean-square is excellent. However, colored noise, will drop the efficiency substantially. Therefore, the least mean squares (LMS) and Recursive least square (RLS) which converge to Weiner optimal solution are designed to handle narrowband frequency, and according to the literature [10], even a primary adaptive filter such as LMS can reduce the noise from nonstationary signals. Another drawback of an adaptive filter is the prior knowledge about the desired signal or noise which is paramount [10]. Occasionally, using a template of a well-known shape of ECG epoch as the desired signal, can reduce the chance of detecting abnormality and artifacts [11]. Therefore, blind source separation methods such as independent component analysis (ICA) and principal component analysis are emerged for ECG noise removal; However, in meager SNR circumstances, these methods are not sufficient and need further post-processing [12]–[15].

In this work, a robust algorithm is introduced for deconvolution of ECG signal. The proposed algorithm is tested in two ways. First, the proposed algorithm is utilized for single-channel ECG denoising in very low signal to noise ratio condition. Second, the proposed method is used for extracting QRS complex from maternal ECG by a single thoracic channel. This method is based on the fixed-point convolution kernel compensation (FP-CKC) and recursive least square (RLS) method which is combined with particle swarm optimization (PSO). The rest of the paper is organized as follows: in the next section, information about the signals and formulation of methods used in this study is presented. Section 3 provides the results of the proposed method. The discussion is provided in section 4, along with conclusions.

2.2 Materials and methods

An overall block diagram of the proposed algorithm is shown in Figure. 2.1. As can be seen from the Figure, the signal should first pass from a sliding window. The zero centering and

whitening should be applied on every window separately. Then, every sample of the window is used for the initial point of FP-CKC. The average of separated components is calculated and considered as the noise model or decomposed signal. The adaptive filter using the RLS algorithm and calculated noise model is applied on the signal window in the next step. Further information about each step is provided in detail in the following sub-sections.

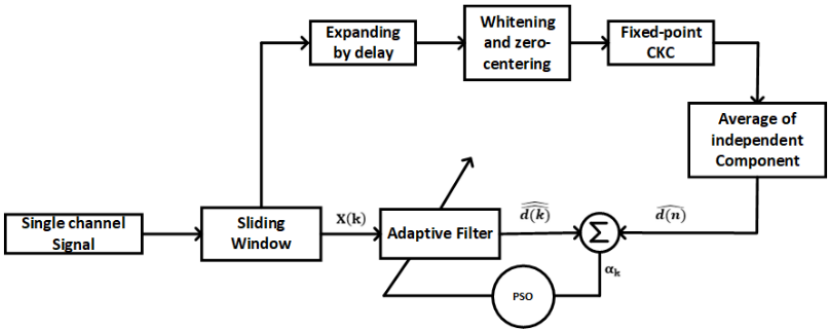

Figure 2-1. The block diagram of the proposed algorithm for signal deconvolution.

2.2.1 Dataset

In this work, MIT-BIH Arrhythmia Database [16] is used in order to assess the performance of the proposed algorithm. This database consists of different types of noisy as well as noise-free ECG signals. The ECG recordings were acquired from BIH Arrhythmia Laboratory which studied 47 subjects and recorded 48 two channel ambulatory ECG recordings of half-hour lengths. This database contains 15 different types of ECG signals, heartbeats, signal loss, and various kinds of noises (e.g., Baseline wanders and muscle artifacts). 20 recordings (24 hour length) of noise-free signals were selected randomly from a set of 4000 which were obtained from a mixed population of outpatients (about 40%) and inpatients (about 60%). The recordings were then digitized at 360 samples/second/channel which had 11 bit resolution over 10mV range. The SNR of the original signal (before adding noise) is not presented in the database specification. For each signal, 10 epoch of ECG are selected randomly and high resolution alignment [16] is applied on them; then the average of the aligned epoch is calculated as noise-free epoch. The difference of noise-free epoch and noisy epoch is calculated, and the SNR value is estimated. The SNR value of the original signal is 18.6 ± 8.4 dB.

Two types of noise are added to single channel signal. The first noise is a synthetic noise with colored Gaussian zero-mean and signal to noise ratio of -20 dB, -10 dB and 0 dB are added to channel. The bandwidth of the noise is between 1 to 100 Hz. The second noise is a surface EMG signal which is recorded in 24-hour using ME6000 device with frequency sample 1000 Hz. This database is called Cerebral Vasoregulation in Elderly with Stroke and it is available in Physionet website. Some parts of EMG signal are resampled to be same as input signal and its gain changes for creating a noisy signal with different SNR. The denoising algorithm should not distort the arrhythmia of ECG signal which is one the reason that why this database is selected in order to test and verify the performance of the proposed algorithm.

In addition, a non-invasive fetal ECG (NI-FECG) database [17] is also used in this study order to verify the validity of the proposed algorithm for extracting Fetal ECG signals in a single-channel. The data contained in this database were obtained from single subjects which ranged between 21 to 40 weeks of pregnancy from thoracic and abdominal region. These data were sampled at 1 kHz and consists of a set of one-minute, four-channel FECG signals. The recordings were of varying durations and were taken weekly (sometimes two or more recordings were also acquired). These recordings can be used in testing algorithms for signal separation. Although researchers have used various techniques for extracting fetal ECG signals, a more accurate and improved algorithm for extraction of FECG signal is still required. Hence in this work, 14 recordings were randomly selected for testing. A single thoracic channel is also utilized in this study for QRS complex decomposition from fetal ECG.

2.2.2 Preprocessing

In the first stage, the ideal sliding window is applied on the ECG signal. Each window is zero centered by subtracting the average of the signal from the window. The matrix $\boldsymbol{X}$ is referred to the N×M zero-mean extended ECG window signal matrix in which each row is a delayed repetition of the window, and each column corresponds to a time sample. The number of delayed repetitions is dependent on the sampling frequency, and it was fixed to 5. The whitening referred to as 'convolutive sphering' [17] is used, and matrix W could be obtained, provided that the covariance matrix of $\mathbf{Z}$ at time lag zero is equal to the identity matrix.

$$\boldsymbol{E}\{\boldsymbol{X}\boldsymbol{X}^{\boldsymbol{T}}\} = \boldsymbol{U}\boldsymbol{D}\boldsymbol{U}^{\boldsymbol{T}} \qquad (2.1)$$

$$\boldsymbol{W} = \boldsymbol{U}\boldsymbol{D}^{-\frac{\mathbf{1}}{\mathbf{2}}}\boldsymbol{U}^{\boldsymbol{T}} \qquad (\mathbf{2.2})$$

$$\boldsymbol{Z} = \boldsymbol{W}\boldsymbol{X} \qquad (\mathbf{2.3})$$

Where D is a diagonal matrix obtained by the eigenvalue decomposition of the covariance matrix $\boldsymbol{X}$, $\boldsymbol{U}$ is the modal matrix which is calculated by singular value decomposition of $\boldsymbol{X}\boldsymbol{X}^{\boldsymbol{T}}$, $\boldsymbol{T}$ is transpose operation and $E\{\boldsymbol{X}\boldsymbol{X}^{T}\}$ is denoting the covariance matrix of $\boldsymbol{X}$.

2.2.3 Fixed-Point Convolution Kernel Compensation (FP-CKC)

The FP-CKC is mainly used for neural decoding in muscle from the surface electromyogram and is used by Zazula *et al.* [18] for blind source separation in surface electromyogram (sEMG) and image decomposition. The primary goal of this step is to find a noise model for using an adaptive filter as the next step. Therefore, we intend to find the matrix $\widehat{\boldsymbol{d}}$ as the estimated noise component to minimize Equation 2.4, in which $\boldsymbol{d}$ is the ground truth matrix of the noise

component. Note that $\boldsymbol{d(n)}$ denotes the n-th column of matrix $\boldsymbol{d}$ and each row in matrix $\boldsymbol{d}$ can be a component of the signal.

$$\boldsymbol{e(n) = d(n) - \widehat{d(n)}} \qquad \textbf{(2.4)}$$

In other words, the optimization problem can be defined as finding filter coefficients like Equation 2.5 to minimize Equation 2.4.

$$\boldsymbol{\widehat{d(n)} = W_n^T X} \qquad \textbf{(2.5)}$$

By rewriting equation 2.4 and using Equation 2.5:

$$\boldsymbol{e(n) = \widehat{d(n)} - \sum_{n=0}^{N-p} \sum_{k=0}^{p-1} w_n(k) x(n+k)} \qquad \textbf{(2.6)}$$

where $\boldsymbol{p}$ is the order of the filter. Now by rewriting the error in the form of Least Minimum Mean Square Error optimization formulation with the assumption that N is the length of the window and calculating the partial derivation with respect to *w* and setting the result to the zero, the following equation is derived:

$$\boldsymbol{W_n = R_{XX}^{-1} P_{X\widehat{d(n)}}} \qquad \textbf{(2.7)}$$

where, $\boldsymbol{P_{X\widehat{d(n)}}}$ is the cross correlation between input and the desired signal and $\mathbf{R_{XX}^{-1}}$ is the auto correlation of matrix X which is approximately equal to identity because of the whitening, however since we need to elaborate method with RLS in the next section we do not approximate it. Now, by substituting Equation 2.7 in Equation 2.5, we can write Equation 2.8.

$$\boldsymbol{\widehat{d(n)} = P_{X\widehat{d(n)}}^T R_{XX}^{-1} X} \qquad \textbf{(2.8)}$$

The cross-correlation $\boldsymbol{P_{X\widehat{d(n)}}^T}$ is unknown, however it can be estimated by FP-CKC. In this work, we used every sample in a window as initial point of $\boldsymbol{P_{X\widehat{d(n)}}^T}$. In other words, $\boldsymbol{X(0)}$ is chosen as $\boldsymbol{P_{X\widehat{d(n)}}^T}$ for first iteration. Then, the Equation 2.9 runs until termination criteria is met. In this work, the termination criteria is set the number of iteration which is set to 3 due to high convergence rate of the algorithm. We used average of estimated $\boldsymbol{\widehat{d}}$ for finding the main noise model. For extracting the fetal ECG, one of the decomposed signal is highly correlated with maternal ECG, however, since we do not have any prior information about signals and have to continue blindly, we used average of the decomposed components.

2.2.4 Recursive Least Square (RLS)

By assuming that the signal input matrix is zero mean, the autocorrelation input matrix $\boldsymbol{X}$ can be called $\mathbf{R_k^{-1}}$ is updated by Equation 9 in which k is the iteration number and $\mathbf{X(k)}$ is the k-th column of matrix $\boldsymbol{X}$. Hence, for every sample in the window the RLS algorithm should be run.

$$\mathbf{R_k^{-1}} = \frac{1}{\gamma}\left[\mathbf{R_{k-1}^{-1}} - \frac{\mathbf{R_{k-1}^{-1}X(k)X^T(k)R_{k-1}^{-1}}}{\gamma+\mathbf{X(k)R_{k-1}^{-1}X(k)}}\right] \qquad (2.9)$$

Where γ is forgetting factor and initialization is done by assuming $\mathbf{R_k^{-1}} = \boldsymbol{\delta I}$; which $\boldsymbol{I}$ is the identity matrix and δ is the inverse of the input signal power. The $\Delta\boldsymbol{\omega_k}$ in RLS is calculated by Equation 2.10.

$$\Delta\boldsymbol{\omega_k} = \mathbf{R_k^{-1}}\boldsymbol{\alpha_k}\mathbf{X(k)} \qquad (2.10)$$

The error is defined in Equation 2.11.

$$\boldsymbol{\alpha_k} = \widehat{\boldsymbol{d(k)}} - \widehat{\widehat{\boldsymbol{d(k)}}} \qquad (2.11)$$

$$\widehat{\widehat{\boldsymbol{d(k)}}} = \mathbf{X(k)}\boldsymbol{\omega_k} \qquad (2.12)$$

where, $\widehat{\widehat{\boldsymbol{d(k)}}}$ is the desired signal and the main difference between it and $\widehat{\boldsymbol{d(k)}}$, which is calculated by FP-CKC, is that $\widehat{\boldsymbol{d(k)}}$ is an approximation of the noise model and need to be adapted by RLS algorithm on the signal window. The recursion for $\mathbf{R_k^{-1}}$ follows an Algebraic Riccati equation; therefore, it draws parallel to the Kalman Filter. The initial value of $\boldsymbol{\omega_0}$ is selected by particle swarm optimization (PSO) algorithm.

2.2.5 Particle swarm optimization

Since the 1970s, meta-heuristic algorithms which imitating natural phenomena have been devised for optimization problems. PSO is inspired by flocking birds [19]. It uses particles for generating solutions. Each particle has its position and velocity that enables it to search problem space. This algorithm is used for designing IIR filters. For FIR filters, also a review on a combination of PSO and LMS method have been done by Najjarzadeh et al. [20]. This study showed that LMS has good convergence rate, when it is combined with meta-heuristic algorithms, such as particle swarm optimization. This method is used as stochastic optimization with the same internal parameters and topology that Mohebbian et al. used in another approach [21]; except the number of iteration is set to 50 and the cost function which is Equation 2.11. In this regard, the proposed algorithm just tries to find optimized initial weights of $\boldsymbol{\omega_0}$ for adaptive filter.

2.3 Results

2.3.1 Results on denoising

For measuring denoising quality, we used three types of validation parameters. The signal to error ratio (SER) is described in Equation 2.13 [22] in which, $\boldsymbol{x(t)}$ and $\bar{\boldsymbol{x}}\boldsymbol{(t)}$ are original and reconstructed signal respectively and $\boldsymbol{L}$ is the length of the signal.

$$\boldsymbol{SER}(\boldsymbol{x},\bar{\boldsymbol{x}}) = \frac{\sum_{t=0}^{L-1} x^2(t)}{\sum_{t=0}^{L-1}(x(t)-\bar{x}(t))^2} \qquad (2.13)$$

Note that $\boldsymbol{SER}$ is calculated by using original ECG and as an instance when we calculate $\boldsymbol{SER}$ for noisy signal, it means that $\bar{\boldsymbol{x}}\boldsymbol{(t)}$ in Equation 2.13 is set to noisy signal and the similarity of signals

are evaluated. Moreover the root mean square error (RMSE) and Signal to Noise Ratio (SNR) are used as another validators [23]. For evaluating SNR, we calculated the SNR of denoised signal same as we estimate SNR of original signal. It is important to note that The SNR of the original signals is 18.6 ± 8.4 dB

2.3.1.1 Gaussian noise

The 20 series of ECG signals which are mixed with synthesis noise in different SNR from MIT-BIH Arrhythmia dataset is given as the input to the algorithms, then, the ***RMSE***, ***SER*** and ***SNR*** of denoised signal is assessed. Figure 2.2 shows the original signal, noisy signal and denoised signal.

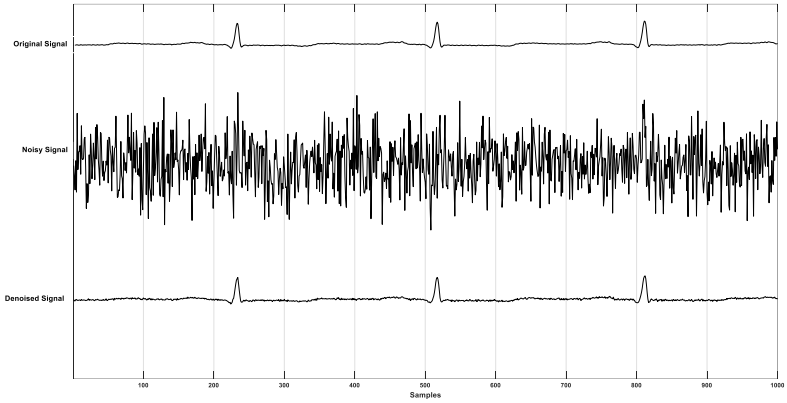

Figure 2-2. ECG noise removal. From top to bottom, original signal, noisy signal is generated using Gaussian noise generator with -20 dB SNR, and denoised signal.

The boxplot of the SNR, RMSE and SER are depicted in Figures 2.3, 2.4 and 2.5, respectively.

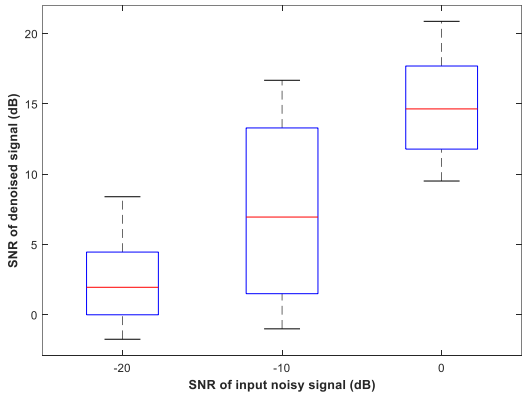

Figure 2-3. The boxplot of the SNR of denoised signal for 20 series of signals; noisy signal is generated using Gaussian noise generator

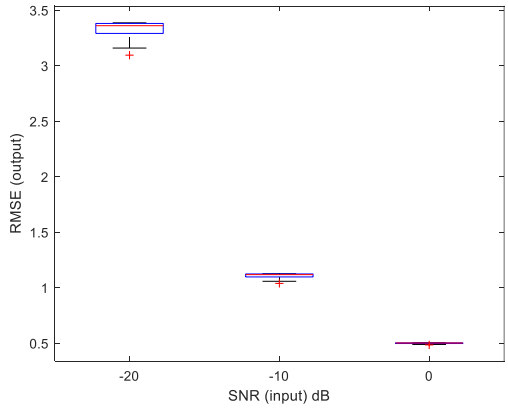

Figure 2-4. The boxplot of the RMSE of denoised signal for 20 series of signals; noisy signal is generated using Gaussian noise generator.

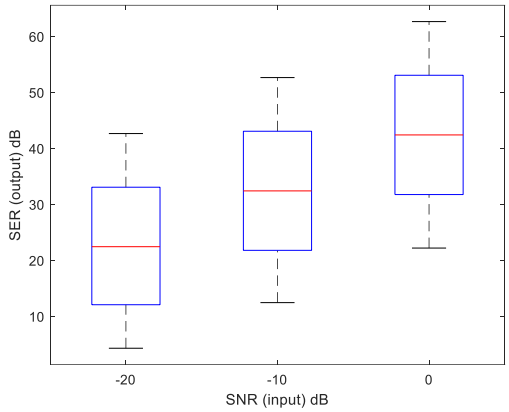

Figure 2-5. The boxplot of the SER of the denoised signal for 20 series of signals; noisy signal is generated using Gaussian noise generator.

The median, minimum and maximum of the RMSE between the desired signal and extracted one in -20 dB SNR, are 3.39, 3.09 and 3.38 respectively. These results are 1.11, 1.03 and 1.12 for -10 dB SNR and 0.49, 0.48 and 0.50 for 0 dB SNR. Furthermore, Figure 2.4 described the SER respect to the SNR and the median, minimum and maximum of the SER between the desired signal and extracted one are 22.42, 4.28 and 42.63 dB for -20 dB SNR. For -10 dB, 32.39, 12.43 and 52.63 dB are acquired, also, for 0 dB, 42.38, 22.18 and 62.63 dB are obtained. The median, minimum and maximum of SNR for denoised signal in -20 dB are 2.43, -1.87 and 8.01. The same parameters for -10 dB are 6.63, -0.98 and 14.09 and are 14.93, 9.81 and 21.78 for 0 dB.

2.3.1.2 The EMG noises

The 20 series of ECG signals are mixed with EMG noise in different SNR same as previous section. Figures 2.6, 2.7 and 2.8 show the ***RMSE***, ***SER*** and ***SNR*** of denoised signal.

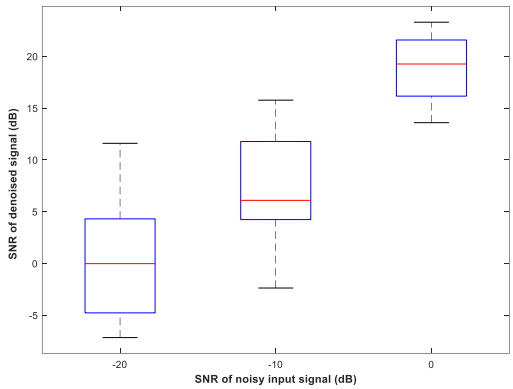

Figure 2-6. The boxplot of the SNR of denoised signal for 20 series of signals; noisy signal is generated by adding surface EMG to signal.

The median, minimum and maximum of the SNR between the original signal and extracted in -20 dB SNR, are -0.03, -7.17, and 11.58 respectively. The same parameter for SNR in -10 dB, are 6.07, 1.03 and -238 and in 0 dB are 19.24, 13.58 and 23.28 dB.

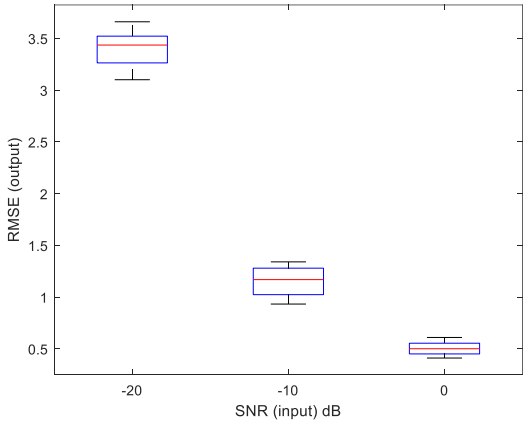

Figure 2-7 .The boxplot of the RMSE of the denoised signal for 20 series of signals; noisy signal is generated by adding surface EMG to signal.

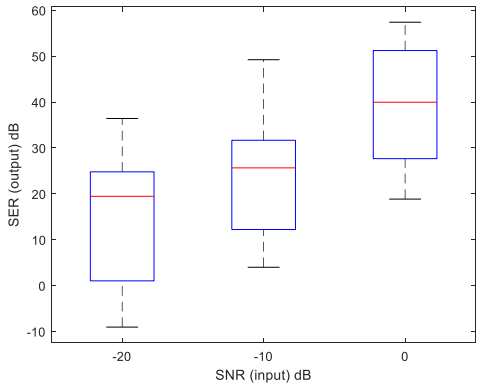

Figure 2-8. The boxplot of the SER of the denoised signal for 20 series of signals; noisy signal is generated by adding surface EMG to signal.

The median, minimum and maximum of the SER between the desired signal and extracted one are 19.64, -9.11 and 37.83 dB for -20 dB SNR. For -10 dB, 26.03, 3.76 and 49.89 dB are acquired. Finally, for 0 dB input signal, 40.82, 19.21 and 57.12 dB are obtained. When input signal is in 0 dB, the median, minimum and maximum of the RMSE are 3.43, 3.10 and 3.66. The same parameters are 1.16, 0.93 and 1.34 for -10 dB and are 0.50, 0.41 and 0.60 for 0 dB.

2.3.2 Results on extracting fetal QRS complex

Fourteen series of the NI-FECG database is selected randomly, and the algorithm is applied to it. A single channel thoracic signal for extracting QRS complex of fetal ECG is used. Figure 2.9 depicts the one of the outputs of proposed algorithm.

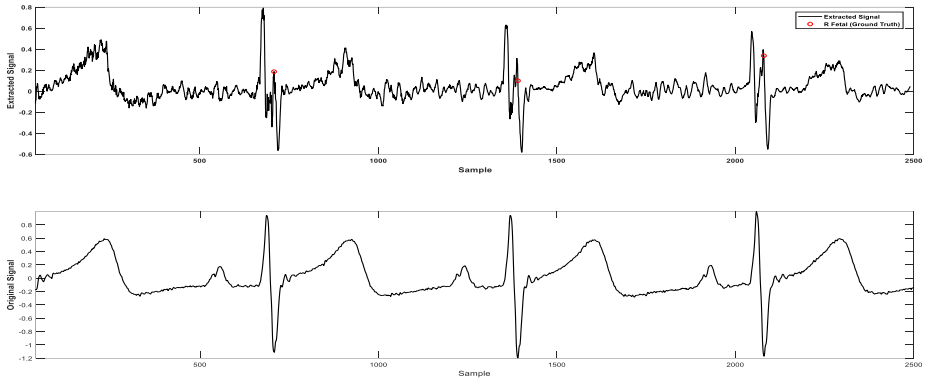

Figure 2-9. The output of the proposed method for extracting fetal ECG from the thoracic signal of mother after one iteration of PSO. The top plot is extracted signal after one iteration and the bottom plot is input thoracic signal.

According to Equation 2.8, the FP-CKC algorithm extract components of signal based on auto and cross correlation. In this regard, waves which are repeated in signal, such as QRS complex of maternal ECG and R wave of fetal ECG, will be compensated and extracted in a component. However, the noise level is high and FP-CKC is not enough for original signal extraction. Therefore, the average of components is calculated for having a noise model and adaptive filter is applied on noisy signal. Recording the maternal ECG is traditional and easy for clinical usage, while, recording the fetal ECG is a clinical issue. The proposed algorithm can extract the fetal ECG from thoracic signal and no need to extra configuration. According to Figure 2.9, a post-processing method is required for extracting fetal R waves. We subtracted extracted signal by the original signal and used a simple threshold method. More example of extracted fetal ECG is provided in supplementary material. The evaluation of the results is obtained using both classical sensitivity and positive predictive accuracy. For calculating predictive accuracy or positive predictive value (PPV) and sensitivity, a matching window of 50 ms is employed, since this matching window is applied by Guerrero-Martinez et al. [24] and Zaunseder et al. [25] is used. The F1-score (F-score) can be defined alternatively as a measure of an algorithm's accuracy [26]. Equation 2.14, 2.15 and 2.16 explain the sensitivity, PPV, and F-score respectively.

$$\textbf{Sensitivity} = \frac{\textbf{TP}}{\textbf{TP+FN}} \qquad (2.14)$$

$$\textbf{PPV} = \frac{\textbf{TP}}{\textbf{TP+FP}} \qquad (2.15)$$

$$\textbf{Fscore} = \frac{\textbf{2} \times \textbf{PPV} \times \textbf{Sensitivity}}{\textbf{PPV+Sensitivity}} \qquad (2.16)$$

Where, TP and FN refer to true positive and false negative respectively. Therefore, the sensitivity, PPV and F-score on the 14 record subsets were 95.3 ± 4.1, 97.1 ± 2.3 and 96.1 ± 3.7 % respectively.

2.4 Discussion and Conclusion

2.4.1 State-of-the-art

One of the crucial issues is the importance of using an adaptive filter after FP-CKC. The modified versions of FP-CKC is used by other researches for blind source separation purposes, especially in neural decoding. However, in these applications, extracting firing times has more critical than finding exact shape of spikes and due to the number of recorded channels, the shape of spikes can be extracted by some simple post-processing. Furthermore, finding appropriate initial points for this application is important, while, in the proposed method every point of the signal is used in FP-CKC. The results of applying FP-CKC to the one of the ECG windows is shown in Figure 2.10.

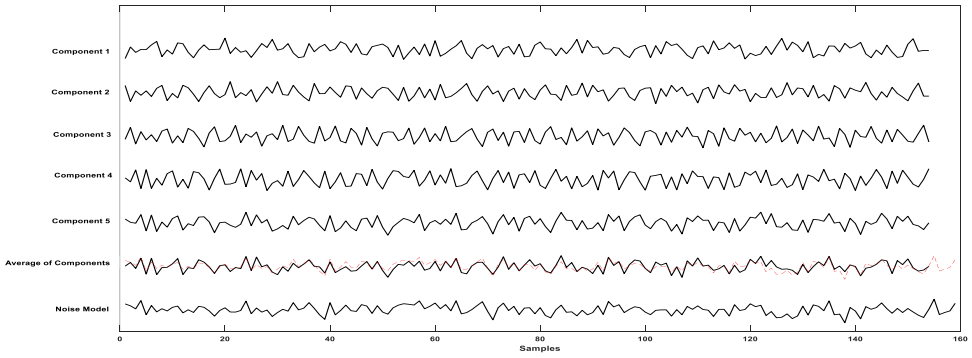

Figure 2-10. The results of the FP-CKC by setting delay to 5. The dash line denotes to the original noise model.

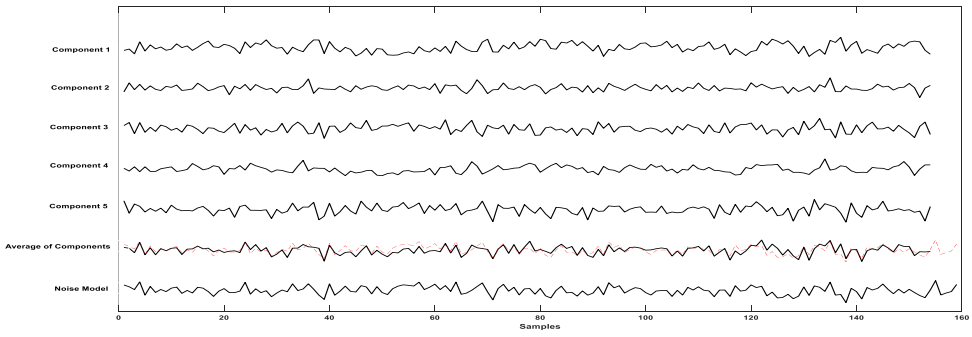

Figure 2-11. The results of the ICA by setting the delay to 5. The dashed line denotes to the original noise model.

As shown in Figure 2.10, the noise model is similar to the average of the component. Using one of the components instead of the averaging is sensible. However, there is no clue for choosing the best one.

Moreover, using another blind source separation methods, like ICA [12], is plausible. However, there are some disadvantages. First, selecting the appropriate kernel for ICA needs trial and error. Moreover, The FP-CKC algorithm can find the noise model more precise than ICA. In this regard, Figure 2.11 is presented for comparing the result of ICA and FP-CKC.

The RMSE of the calculated noise model respect to the original noise model by FP-CKC algorithm is 0.23, while the RMSE by ICA is 0.53. Therefore, the FP-CKC can estimate the noise model more accurate than ICA method.

2.4.2 Base line wandering removal

The baseline of the signal is reduced by zero-mean filtering which is applied on signal window before whitening process. A window is broken to small parts and average of each part is removed from it. Figure 2.12 depicts the result of this process.

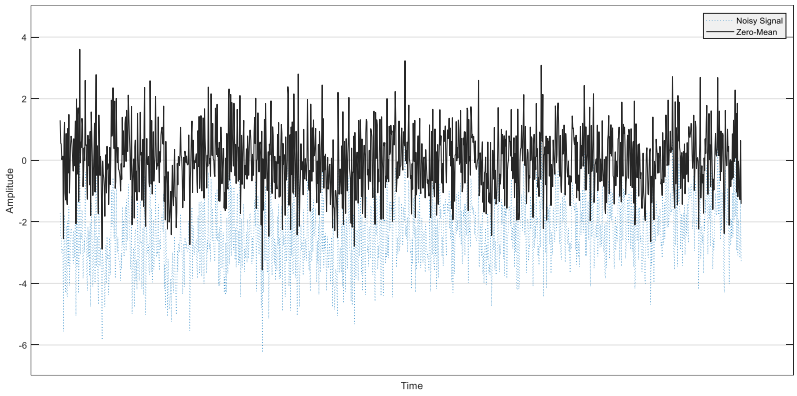

Figure 2-12. The effect of zero-mean on signal windows on baseline wandering

The next steps, including extracting noise model and applying adaptive filter, are based on zero-mean signal; hence, the baseline wandering effect will be reduced in denoised signal. Figure 2.13 shows the denoised and noisy signal and original signal before adding noise.

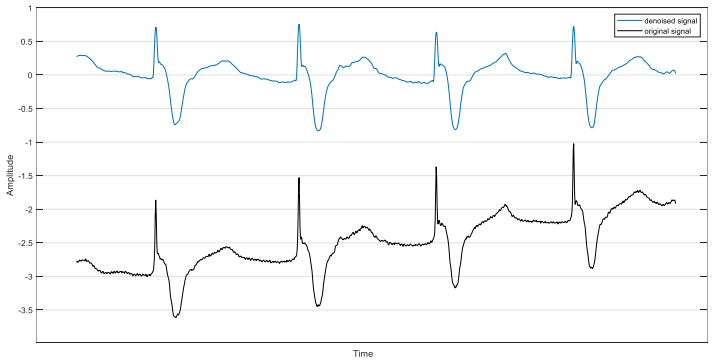

Figure 2-13 . Comparison between baseline of original ECG (before adding noise) and denoised signal using the proposed method.

The zero-mean process cannot remove baselines which are sharp. In other words, if the baseline of signal change fast, the proposed method cannot remove the baseline and this artifact will be reconstructed in denoised signal. Figure 2.14 shows the inability of removing baseline in a specific situation.

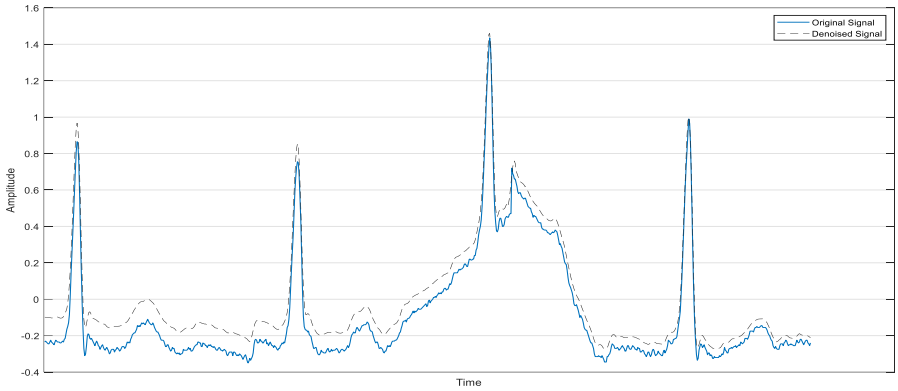

Figure 2-14. Inability of removing baseline wandering when the variation is high

2.4.3 Tuning parameters

Suitable tuning helps to use such deconvolution algorithm in a variety of denoising and blind source separation applications, including speech denoising, detecting seizure in EEG signals, EMG decomposition and extracting fetal from maternal ECG. Neverthelss, some of the parametrs do not have wide effect on the final result of the algorithm. Parameters such as the length of the window which is used for processing, the length of the adaptive filter weights, learning rate in the adaptive filter, number of population in PSO, number of iteration of PSO and number of iteration in FP-CKC should be tuned. Among the mentioned parameters, the length of the adaptive filter and the length of the window are paramount and should be selected wisely. By trial and error the optimized length of the window for ECG signals is selected to be between 1.5 to 3.5 seconds. Also the length of the adaptive filter is selected according to the number of convoluted components. The grid search or exhaustive search can be used for tuning parameters.

Moreover, the PSO algorithm can be utilized for tuning parameters. However, this procedure would widen the searching space and is not efficient in aspect of time consuming and computational cost. In this work, we used 5 delays and therefore a filter with length 5 is used as an adaptive filter for denoising and extracting fetal ECG accordingly.

The number of delayed repetitions affects the performance of the algorithm. Technically, any of these delayed signals can be reconstructed by FP-CKC and eventually, reconstructed signals can have different delay. This happens at relatively large delays. Furthermore, FP-CKC algorithm works based on correlation concept and delays should not be greater than the smallest part in ECG, for example P wave. The larger delay decreases the chance of decomposing signal from noise. The large delay also increases the computational cost

2.4.4 Comparing with other algorithms for denoising ECG

One of the circumstances that ECG signal has noise level is when ECG is contaminated with EMG signal. There are various studies in the literature which reported contamination ECG with EMG. The Table 2.1 is provided for comparing the proposed method with recent methods in literature.

Table 2-1. Comparing the result of the noise removal algorithm.

Method	Method	The worst SNR of noisy input signal (dB)	The best SNR of denoised signal (dB)	Improved SNR (dB)
Lu *et al.* [27]	Adaptive filter	-15	-12	3
Liu *et al.* [22]	Empirical mode decomposition	-5	8	13
Lin *et al.* [28]	Discrete wavelets transform	-15	1	16
Proposed method	FP-CKC combined with adaptive filter	-20	11	31

Lu et al. [27] used a modified adaptive filter for removing ECG noise in EMG signals. The minimum SNR of the noisy signal which they applied to their system is -15.17 dB and their system could improve the SNR of signal 3dB. Liu et al. [22] investigated the empirical mode decomposition algorithm on removing EMG noise for ECG signals and they could improve a noisy signal with -5 dB SNR to 8 dB which means 13 dB improvement. For removing EMG noise form ECG signal, the discrete wavelet transform is used by Lin et al. [28] and they could improve the noisy signal SNR from -15 dB to 1 dB. The proposed algorithm improves the SNR of a noisy ECG signal, contaminated with EMG, from -20 dB to 11 dB which means 31 dB improvement.

2.4.5 Comparing with other algorithms for fetal ECG decomposition

Although many computational techniques have been widely developed in recent years to analyze ECG signals, these techniques still have limitations which hinders its application for the analysis of fetal ECG and prohibits it to be a valid alternative to the commonly used Doppler ultrasound monitoring technique. Fetal ECG signal is commonly affected by low SNR, various noises (baseline drifts, power line, motion artifacts, mother respiration, and electrode contact), low amplitude, and EMG. Although fetal QRS detection looks simple, it is a very challenging and complex task to obtain noise-free accurate results in real clinical practice. The comparative result from using various method for decomposing fetal QRS complex is shown in Table 2.2 and 2.3. All of the methods in Table 2.2 use same dataset. It can also be seen from the Table 2.1 that we used single thoracic signal for extracting QRS complex of fetal ECG, unlike other works.

Table 2-2. Comparing the result of the different method for decomposing fetal ECG with single channel.

Method	F1-Score	Number of channels	Number of tested signals
TS and ES-RNN [26]	97.2	Single-Abdominal channel	14
TS and PCA [26]	95.4	Single-Abdominal channel	14
LMS [26]	95.4	Single-Abdominal channel	14
RLS [26]	95.9	Single-Abdominal channel	14
Proposed method	99.2	Single-Abdominal channel	14
Proposed method	96.1	Single-Thoracic channel	14

TS: Template subtraction, ES-RNN: echo state for the recurrent neural network, PCA: principal component analysis, LMS: Least Mean Square, RLS: Recursive Least Square, ICA: independent component analysis

Table 2-3. Comparing the result of the proposed method with single channel for decomposing fetal ECG with multi-channel approaches.

Method	F1-Score	Number of channels	Number of tested signals
Multi-Step approach [13]	99.2	Four-Abdominal channel	100
ICA [29]	98.9	Four-Abdominal channel	69
Proposed method	96.1	Single-Thoracic channel	14
Proposed method	99.2	Single-Abdominal channel	14

TS: Template subtraction, ES-RNN: echo state for the recurrent neural network, PCA: principal component analysis, LMS: Least Mean Square, RLS: Recursive Least Square, ICA: independent component analysis

Although it seems that F1-Score of the proposed method does not outperform some methods, it is remarkable, since it is applied on the single-Thoracic channel. Applying the proposed algorithm on single-abdominal channel is also tested and gives the 99.2 F1-score; while the maximum F1-Score reported for single-channel configuration is 97.2.

Although reliable, this algorithm demands high computational cost. One of the solutions for decreasing the computational cost is using alternative adaptive filter which are faster than RLS or using fast recursive least square which is introduced by Kazemi *et al*. [30]. Since, each window of signal can be run separately, using GPU for parallel computation can increase the speed. In future, further experiment can be performed on other databases to test its feasibility and effectiveness in removing noises from various kinds of signals.

In conclusion, we proposed a robust algorithm for ECG deconvolution. The proposed algorithm starts with windowing the ECG signal and creating a matrix of delayed window in each row. Then, whitening is performed on input matrix and fixed-point convolution kernel compensation estimate a model of noise in that window. Finally, the noise model is used in adaptive filter using recursive least square which is combined with particle swarm optimization for finding initial vector of adaptive filter. This study shows that the proposed algorithm works in a situation where SNR is very low such as -20 dB or when the ECG signal is not detectable by the naked eye. In these situations, the algorithm can improve the SNR about 31 dB step. This algorithm can also be used for blind source separation approaches such as EMG decomposition and image deconvolution. The developed program is available upon request.

2.5 References

[1] V. P. Rachim and W.-Y. Chung, "Wearable Noncontact Armband for Mobile ECG Monitoring System," *IEEE Trans. Biomed. Circuits Syst.*, vol. 10, no. 6, pp. 1112–1118, Dec. 2016.

[2] A. Milenković, C. Otto, and E. Jovanov, "Wireless sensor networks for personal health monitoring: Issues and an implementation," *Comput. Commun.*, 2006.

[3] G. M. Friesen, T. C. Jannett, M. A. Jadallah, S. L. Yates, S. R. Quint, and H. T. Nagle, "A comparison of the noise sensitivity of nine QRS detection algorithms," *IEEE Trans. Biomed. Eng.*, vol. 37, no. 1, pp. 85–98, 1990.

[4] W. Zong, L. Nielsen, B. Gross, J. Brea, and J. Frassica, "A practical algorithm to reduce false critical ECG alarms using arterial blood pressure and/or photoplethysmogram waveforms," *Physiol. Meas.*, vol. 37, no. 8, pp. 1355–1369, Aug. 2016.

[5] S.-K. Teo *et al.*, "Reducing false arrhythmia alarms in the ICU," in *2015 Computing in Cardiology Conference (CinC)*, 2015, pp. 1177–1180.

[6] J. A. Van Alsté and T. S. Schilder, "Removal of Base-Line Wander and Power-Line Interference from the ECG by an Efficient FIR Filter with a Reduced Number of Taps," *IEEE Trans. Biomed. Eng.*, 1985.

[7] D. Ricciardi *et al.*, "Impact of the high-frequency cutoff of bandpass filtering on ECG quality and clinical interpretation: A comparison between 40 Hz and 150 Hz cutoff in a surgical preoperative adult outpatient population," *J. Electrocardiol.*, vol. 49, no. 5, pp. 691–695, 2016.

[8] S. L. Joshi, R. A. Vatti, and R. V. Tornekar, "A survey on ECG signal denoisingtechniques," in *Proceedings - 2013 International Conference on Communication Systems and Network Technologies, CSNT 2013*, 2013.

[9] K. Bartyzel, "Adaptive Kuwahara filter," *Signal, Image Video Process.*, 2016.

[10] J. Dhiman, S. Ahmad, K. Gulia, and A. Professor, "Comparison between Adaptive filter Algorithms (LMS, NLMS and RLS)," 2013.

[11] E. Ebrahimzadeh, M. Pooyan, S. Jahani, A. Bijar, and S. K. Setaredan, "ECG SIGNALS NOISE REMOVAL: SELECTION AND OPTIMIZATION OF THE BEST ADAPTIVE FILTERING ALGORITHM BASED ON VARIOUS ALGORITHMS COMPARISON," *Biomed. Eng. Appl. Basis Commun.*, 2015.

[12] A. Karimi Rahmati, S. K. Setarehdan, and B. N. Araabi, "A PCA/ICA based Fetal ECG Extraction from Mother Abdominal Recordings by Means of a Novel Data-driven Approach to Fetal ECG Quality Assessment.," *J. Biomed. Phys. Eng.*, 2017.

[13] M. Varanini, G. Tartarisco, L. Billeci, A. Macerata, G. Pioggia, and R. Balocchi, "A multi-step

approach for non-invasive fetal ECG analysis," *Proc. 40th Comput. Cardiol. Conf.*, 2013.

[14] A. Gupta, M. C. Srivastava, V. Khandelwal, and A. Gupta, "A novel approach to fetal ECG extraction and enhancement using Blind Source Separation (BSS-ICA) and adaptive fetal ECG enhancer (AFE)," in *2007 6th International Conference on Information, Communications and Signal Processing, ICICS*, 2007.

[15] R. Martinek *et al.*, "Comparative effectiveness of ICA and PCA in extraction of fetal ECG from abdominal signals: Toward non-invasive fetal monitoring," *Front. Physiol.*, 2018.

[16] K. C. McGill and L. J. Dorfman, "High-resolution alignment of sampled waveforms," *IEEE Trans. Biomed. Eng.*, no. 6, pp. 462–468, 1984.

[17] F. Negro, S. Muceli, A. M. Castronovo, A. Holobar, and D. Farina, "Multi-channel intramuscular and surface EMG decomposition by convolutive blind source separation," *J. Neural Eng.*, 2016.

[18] D. Zazula and A. Holobar, "Multichannel Blind Source Separation Using Convolution Kernel Compensation," *IEEE Trans. SIGNAL Process.*, 2007.

[19] R. Eberhart and J. Kennedy, "A new optimizer using particle swarm theory," in *Micro Machine and Human Science, 1995. MHS'95., Proceedings of the Sixth International Symposium on*, 1995, pp. 39–43.

[20] M. Najjarzadeh and A. Ayatollahi, "FIR digital filters design: Particle swarm optimization utilizing LMS and minimax strategies," in *Proceedings of the 8th IEEE International Symposium on Signal Processing and Information Technology, ISSPIT 2008*, 2008.

[21] M. R. Mohebian, H. R. Marateb, M. Mansourian, M. A. Mañanas, and F. Mokarian, "A hybrid computer-aided-diagnosis system for prediction of breast cancer recurrence (HPBCR) using optimized ensemble learning," *Comput. Struct. Biotechnol. J.*, vol. 15, pp. 75–85, 2017.

[22] S. Sonali, O. Singh, and R. K. Sunkaria, "ECG signal denoising based on Empirical Mode Decomposition and moving average filter," in *2013 IEEE International Conference on Signal Processing, Computing and Control, ISPCC 2013*, 2013.

[23] T. Chai and R. R. Draxler, "Root mean square error (RMSE) or mean absolute error (MAE)? - Arguments against avoiding RMSE in the literature," *Geosci. Model Dev.*, 2014.

[24] J. F. Guerrero-martínez, J. R. Magdalena-benedito, and U. De Valencia, "New Algorithm for Fetal QRS Detection in Surface Abdominal Records Fetal QRS detection," in *Computers in Cardiology, 2006*, 2006.

[25] M. Akhbari, M. Niknazar, C. Jutten, M. B. Shamsollahi, and B. Rivet, "Fetal Electrocardiogram R-peak Detection using Robust Tensor Decomposition and Extended Kalman Filtering," *Comput. Cardiol. 2013*, 2013.

[26] J. Behar, A. Johnson, G. D. Clifford, and J. Oster, "A comparison of single channel fetal ecg extraction methods," *Ann. Biomed. Eng.*, 2014.

[27] G. Lu *et al.*, "Removing ECG noise from surface EMG signals using adaptive filtering," *Neurosci. Lett.*, vol. 462, no. 1, pp. 14–19, Sep. 2009.

[28] H.-Y. Lin, S.-Y. Liang, Y.-L. Ho, Y.-H. Lin, and H.-P. Ma, "Discrete-wavelet-transform-based noise removal and feature extraction for ECG signals," *IRBM*, vol. 35, no. 6, pp. 351–361, Dec. 2014.

[29] M. Varanini, G. Tartarisco, L. Billeci, A. Macerata, G. Pioggia, and R. Balocchi, "An efficient unsupervised fetal QRS complex detection from abdominal maternal ECG," *Physiol. Meas.*, 2014.

[30] M. Kazemi and M. M. Arefi, "A fast iterative recursive least squares algorithm for Wiener model identification of highly nonlinear systems," *ISA Trans.*, vol. 67, pp. 382–388, 2017.

3 FETAL ECG EXTRACTION FROM MATERNAL ECG USING ATTENTION-BASED CYCLEGAN

To monitor and analyze cardiac status of fetal, extracting FECG signal is necessary. There are two ways of recording a fetal electrocardiogram (FECG). In invasive recording FECG, electrodes are attached to the fetal scalp during delivery. In this way, the risk of infection exists; however, the signal quality is excellent. In non-invasive FECG recording, maternal abdominal ECG can be utilized for FECG extraction. Emerging these extraction techniques, which use decomposition, have revolutionized fetus healthcare, and enabled the clinician to monitor fetal heart activities continuously. Most of the decomposition approaches attempt to extract FECG's QRS waves, however, FECG has other essential components, which can allow extensive analysis. The most recognizable parts in FECG are P waves (the depolarization wave from the SA node that traverses the atria), QRS complex (ventricle depolarization), ST segments (both ventricles are depolarized completely), and T wave (ventricular repolarization).

For mapping between a MECG and an FECG, the attention-based Cycle Generative Adversarial Network (CycleGAN) is introduced in this study. We modified the CycleGAN to use attention and sine activation to find a map between maternal and fetal ECGs using adversarial loss. Convolution layer performance is hampered by the strong correlation between maternal and fetal ECG segments. As a result, the attention mechanism masked the region of interest in order to increase the signal generators' accuracy. The proposed algorithm is trained and evaluated using three datasets provided by Physionet and it showed that it can be used in various fetal and maternal heart rate variations. Moreover, because of using CycleGAN adversarial training, the proposed method eliminates the requirement of having paired ECG and FECG signal for training. This feature enables the algorithm to train with a small dataset and more publicly available dataset can be utilized with less effort which finally can lead to a better generalization of the model.

The analysis and findings of this chapter is reported in the below mentioned published journal manuscript. The student contributed to implementing python code, writing tests, writing the original draft, evaluation, calibration and revision of the manuscript.

M. R. Mohebian, S. s. Vedaei, K. A. Wahid, A. Dinh, H. R. Marateb and K. Tavakolian, "Fetal ECG Extraction from Maternal ECG using Attention-based CycleGAN," in *IEEE Journal of Biomedical and Health Informatics*, doi: 10.1109/JBHI.2021.3111873.

Fetal ECG Extraction from Maternal ECG using Attention-based CycleGAN

Mohammad Reza Mohebbian, Seyed Shahim Vedaei, Khan A. Wahid, Member, IEEE, Anh Dinh, Member, IEEE, Hamid Reza Marateb*, Senior Member, IEEE, *and* Kouhyar Tavakolian, Senior Member, IEEE

Abstract

A non-invasive fetal electrocardiogram (FECG) is used to monitor the electrical pulse of the fetal heart. Decomposing the FECG signal from the maternal ECG (MECG) is a blind source separation problem, which is hard due to the low amplitude of the FECG, the overlap of R waves, and the potential exposure to noise from different sources. Traditional decomposition techniques, such as adaptive filters, require tuning, alignment, or pre-configuration, such as modeling the noise or desired signal to map the MECG to the FECG. The high correlation between maternal and fetal ECG fragments decreases the performance of convolution layers. Therefore, the masking region of interest based on the attention mechanism was performed to improve the signal generators' precision. The sine activation function was also used to retain more details when converting two signal domains. Three available datasets from the Physionet, including the A&D FECG, NI-FECG, and NI-FECG challenge, and one synthetic dataset using FECGSYN toolbox, were used to evaluate the performance. The proposed method could map an abdominal MECG to a scalp FECG with an average of 98% R-Square [CI 95%: 97%, 99%] as the goodness of fit on the A&D FECG dataset. Moreover, it achieved 99.7 % F1-score [CI 95%: 97.8-99.9], 99.6% F1-score [CI 95%: 98.2%, 99.9%] and 99.3% F1-score [CI 95%: 95.3%, 99.9%] for fetal QRS detection on the A&D FECG, NI-FECG and NI-FECG challenge datasets, respectively. Also, the distortion was in the “very good” and “good” ranges. These results are comparable to the state-of-the-art results; thus, the proposed algorithm has the potential to be used for high-performance signal-to-signal conversion.

Index Terms—Fetal ECG, CycleGAN, Blind source separation, Attention layer

3.1 Introduction

The electrocardiogram (ECG) signal is used as a non-invasive method for heart disorder diagnosis. Connecting electrodes on the chest, arms, hands, or legs is the traditional way of recording an ECG [1]. In addition, ECG is used for fetal heart monitoring [2].

There are two ways of recording a fetal electrocardiogram (FECG). In invasive recording FECG, electrodes are attached to the fetal scalp during delivery. There is a risk of infection in this way; however, the signal quality is excellent. In non-invasive FECG recording, maternal abdominal ECG can be utilized for FECG extraction. These emerging extraction techniques have revolutionized fetal healthcare and enabled clinicians to monitor fetal heart activities continuously. A proper fetal heart rate involves normal mother oxygenation and transferring

oxygen to the fetus. Any mechanism that induces an oxygen channel breakage may cause disturbances in the fetal heart rate.

The obtained MECG signal may be distorted with noise (e.g., baseline drift and motion artifacts) [2]. These noise sources could contribute to measurement and instrumentation failures, such as power-line disturbance, white noise, electrode connection noise, muscle contraction, electrosurgical noise, baseline wandering, and motion anomalies [3]. Slight distortion in the MECG waveform can impair the FECG extraction [4]. Therefore, using a robust decomposition strategy against noise helps extract and represent the fetus's heart functionality. The majority of the decomposition approaches attempt to extract the FECG's QRS waves [5], [6]; however, the FECG has other essential components, which can allow extensive analysis [7]. The most recognizable parts in the FECG are P waves (the depolarization wave from the SA node that traverses the atria), QRS complex (ventricle depolarization), ST segments (both ventricles are depolarized completely), and T waves (ventricular repolarization) [8].

Adaptive filters are essential methods for extracting FECG components, where coefficients are adapted according to the signal changes in time. However, the power spectral density of the input signal affects the convergence rate of the algorithms [9]. Since the minimum mean-square error is mostly used in adaptive filters' objective function, they require a flat and uniform power spectrum to have excellent convergence. However, real-world problems include colored noise rather than white noise [10], and colored noise can drop the efficiency of adaptive filters. The least mean squares (LMS) and recursive least square (RLS), adapted like the Weiner optimal solution, are designed to work with narrowband frequencies [9]. In RLS and LMS methods, a reference signal that is morphologically akin to the abdominal MECG waveform is usually required. Methods relying on temporal features, like template based and conventional Kalman filters, are also approaches that may be listed as failing when MECG and FECG peaks overlap. The extended state Kalman filter was introduced for robust FECG extraction, which could solve the QRS coincidence issue [11]. Nevertheless, they have high computational complexity and are unable to succeed if they cannot accurately detect R-peaks.

Blind source separation strategies such as principal component analysis (PCA), independent component analysis (ICA), and periodic component analysis are substitutes for adaptive filters [12]. The primary concept of these approaches is a linear stationary mixing matrix between sources and a higher number of abdominal channels for better FECG extraction [13]. However, these methods are not suitable for circumstances with insufficient Signal to Noise Ratio (SNR) and usually require a specific electrode configuration and further post-processing [14].

Some researchers attempted to overcome adaptive filter or blind source separation (BSS) drawbacks using novel techniques. Mohebbian et al. [14] used a BSS technique to estimate the reference signal on the adaptive filter and decomposed FECG using one channel with an F1-Score of 96%. Zhang et al. [15] used singular value decomposition and a smooth window to decompose QRS waves of the FECG with an F1-Score of 99%. A convolutional neural network was utilized by Zhong et al. [5] and could achieve a F1-Score of 77% for QRS wave

extraction. QRS detection was also performed by Zhong et al. [16] using the prefix tree-based model and could achieve a F1-Score of 95%. Many methods tried to extract QRS waves; however, in decomposing the FECG, other parts should also be taken into consideration. Moreover, using a general model that can be used for different subjects with different electrode displacement requires more investigation.

Simulating the MECG tries to cover all artifacts in synthetic signals to enable algorithms to be tested on different scenarios, such as various noise sources, gestational ages, and assorted artifacts [17]. One of the famous libraries for generating synthetic MECGs is fecgsyn [18], which uses realistic noise, a heart rate variability probability model, rotation maternal and fetal heart axes, fetal movement, and physiological features. The generation of FECG signals based on physiological and mathematical models needs a systematic understanding of the factors involved in producing the FECG signal. However, evolving generative adversarial approaches recently provided new perspectives for latent vector-based data generation as they learn the system's nature without prior information [19].

In this work, the attention-based Cycle Generative Adversarial Network (CycleGAN) is introduced for mapping between a MECG and a FECG. The idea of the CycleGAN is from Hertzmann et al. [20], who utilized a non-parametric texture model for mapping two images. Using the weight-sharing technique for representing across domains was used by Aytar et al. [21] and was extended by Liu et al. [22] by adopting variational autoencoders and generative adversarial networks. Recently, the CycleGAN has been used for non-parallel voice conversion [23], adapting image emotion [24], and style transfer in x-ray angiography [25]. Also, using deep neural networks for ECG analysis has been investigated in recent studies [26]–[28]. We modified the CycleGAN to use attention and sine activation to find a map between maternal and fetal ECGs using adversarial loss. The proposed algorithm is trained and evaluated using three datasets provided by Physionet. The paper is organized as follows: information about the proposed method and the datasets are presented in the next section. The results of the proposed approach are described in section 3. Sections 4 and 5 include the comparison with the state-of-the-art results, followed by discussion and conclusions.

3.2 Materials and methods

Figure 3.1 shows the proposed method in detail. Briefly, a sliding window is applied to the abdominal MECG and corresponding FECG signals. They are normalized, then bandpass filtered and fed to the CycleGAN network. Two generators are trained to receive two discriminators using an adversarial training strategy. The generators are designed based on one-dimensional signal processing to maintain the smoothness of the signal. The proposed method is evaluated in two different scenarios: FECG signal extraction and fetal QRS detection. In FECG signal extraction, all FECG signal components are extracted, and signal distortion is essential. While in fetal QRS detection, only R-wave positions are extracted, and the accuracy of R-R detection is critical. More specific details regarding each phase are given in the sub-sections below.

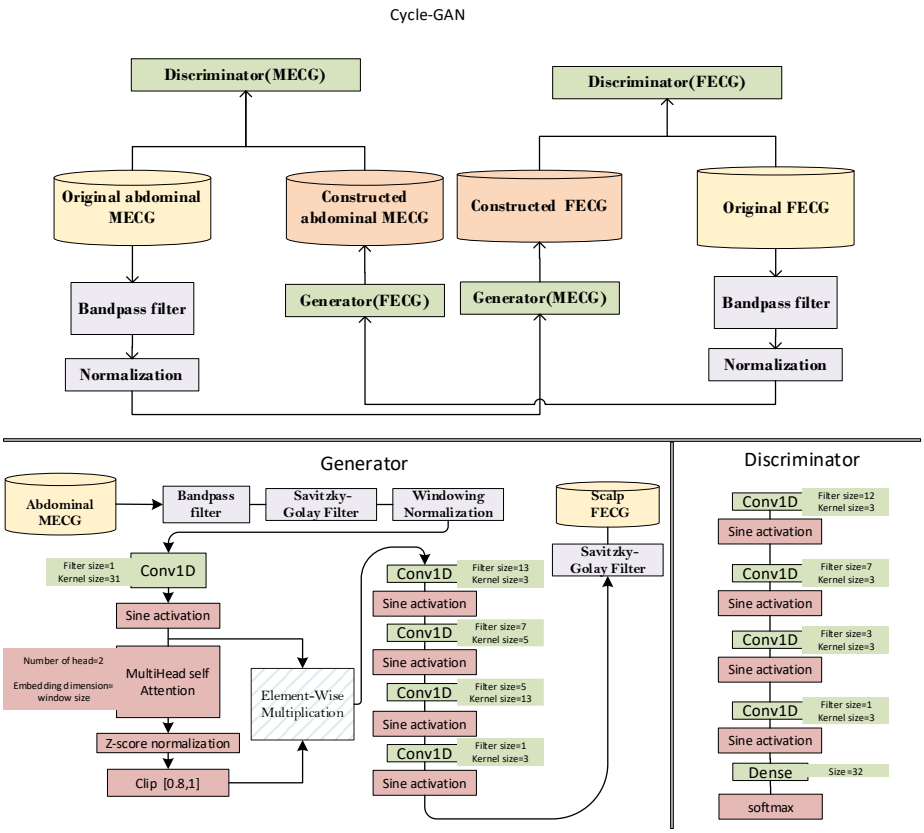

Figure 3-1. The high-level block diagram of the proposed algorithm (top); The generator used in the CycleGAN (bottom left); the discriminator used for the CycleGAN; Kernel size: length of filter; Filter size: number of filters.

3.2.1 Dataset

3.2.1.1 A&D FECG

The abdominal and direct FECG (A&D FECG) [29] dataset from Physionet was used as the main dataset containing FECG recordings. The data contains multichannel fetal electrocardiogram recordings obtained from the fetus scalp of 5 different women between 38 and 41 weeks of gestation (subject 1: record r01, subject 2: record r07, subject 3: record r10, subject 4: record r04, and subject 5: record r08). Each recording consists of five minutes, four abdominal channels, and a corresponding FECG obtained from the fetal head. All signals were sampled at 1 kHz and 16-bit resolution and bandpass filtered during acquisition (0-100 Hz) with digital filtering of the powerline. The abdominal electrode configuration consisted of four electrodes around the belly button, a reference electrode above the symphysis of the pubic, and a common reference electrode on the left leg. These positions were constant during all recordings. Although the FECG is recorded directly from the scalp, it still contaminates the maternal ECG. According to Nurani et al. [30], when the time is closer to delivery due to uterine contractions, the impact of the maternal ECG on the directly recorded FECG can also be higher.

3.2.1.2 NI-FECG and NI-FECG challenge

The non-invasive FECG (NI-FECG) Physionet was also used [31]. This dataset does not contain direct FECG signals from the scalp and only has QRS time samples for the FECG. It contains 55 multichannel abdominal MECGs, taken from a subject between 21 and 40 weeks of pregnancy. The electrodes move sometimes; thus, changing the signal to noise ratio. The data is sampled at 1 kHz and 16-bit resolution and bandpass filtered during acquisition (0-100 Hz). Fourteen sets, including 154, 192, 244, 274, 290, 323, 368, 444, 597, 733, 746, 811, 826, 906, as the benchmark, to facilitate the comparison with the state-of-the-art results [12], [14].

Set-A of the 2013 Physionet/Computing in Cardiology Challenge [32] is also used for benchmarking [32]. The archive consists of 75 abdominal ECG data recorded at a sampling rate of 1 kHz on four channels. The fetal reference R-peaks are provided for Set-A. Due to many incomplete annotations [33], [34], records a33, a38, a52, a54, a71, and a74 were excluded, leaving 69 records for evaluation.

To train the proposed method on the NI-FECG and NI-FECG challenge datasets, a simulated FECG is generated based on the R-R interval provided as ground truth in datasets. More details about simulation, which is based on Daubechies wavelets, are provided in [35]. These simulated signals are mainly used for the training of the proposed system to be used in QRS detection and no further assessment is carried out for the quality of the FECG extraction unlike what is performed on the A&D FECG dataset.

3.2.1.3 Simulated signals:

The FECGSYN toolbox [36] is used, in addition to the available datasets, to model 24 maternal and fetal ECGs at various fetal and maternal heart rates, including 115, 125, 135, 145, 155, 160 bpm [37] and 65, 77, 89, 100 bpm, respectively [38].

3.2.2 Preprocessing

Since the first and last parts of each record have more artifacts and noise, 10 seconds from the first and the last parts are truncated. Signals are resampled to 200 Hz to have less computational cost and the same sample numbers in each second. The clinical ECG has a minimum bandwidth of 100 Hz [39], and according to Sameni and Clifford [40], mostof the ECG's relative power falls under 35 Hz, and the QRS complex has a frequency range of 10-15 Hz for the FECG. Therefore, a bandpass filter with the cut-off frequencies of 1 Hz and 100 Hz is applied to the signals. Since the smoother signal offers better results for the proposed approach and it is not acceptable to select a narrower bandpass filter due to losing information; therefore, the Savitzky-Golay filter [41], [42] was used in our study. The rectangular sliding window is performed on all signals; then, signals are normalized using z-score normalization [43]. The vector x_i refers to the one abdominal MECG channel in size 1×M. Also, i represents the i-th window. Similarly, y_i represents the FECG vector, for i-th window with size the $1\times M$, where M refers to the number of samples, which is set to 200 in this work. The selection of M is investigated in the ablation studies (section 3.3.5).

3.2.3 The proposed method

The goal is to map domains $X = \{x_1, x_2, \dots, x_N\}$ and $Y = \{y_1, y_2, \dots, y_P\}$, while X is $N \times M$ abdominal MECG and Y is the $P \times M$, containing the FECG signal. Like other CycleGAN approaches [23], the model contains two mappings: $G : X \rightarrow Y$ and $F: Y \rightarrow X$. Also, two adversarial discriminators D_x and D_y are defined, where D_x differentiates between X and $F(Y)$ and the objective of D_y is to discriminate between Y and $G(X)$. Concisely, two main objectives follow adversarial loss, trying to fit the representation of the produced signal to represent data in the endpoint domain and cycle consistency loss, which avoids trained mappings G and F from contradicting each other. The final objective cost is defined in Equation (3.1).

$$\arg\min_{G,F}\max_{D_x,D_y}\mathcal{L}(G,F,D_x,D_y)$$

$$\mathcal{L}(G,F,D_x,D_y) = \mathcal{L}_{GAN}(G,D_y,X,Y) + \mathcal{L}_{GAN}(F,D_x,Y,X) + \lambda\,\mathcal{L}_{cyc}(G,F) \qquad (3.1)$$

Wherein,

$$\mathcal{L}_{GAN}(G,D_y,X,Y) = E_y[\log D_y(y)] + E_x[\log(1 - D_y(G(x))] \qquad (3.2)$$

$$\mathcal{L}_{GAN}(F,D_x,Y,X) = E_x[\log D_x(x)] + E_y[\log(1 - D_x(F(y))] \qquad (3.3)$$

$$\mathcal{L}_{cyc}(G,F) = E_x\left[\|F(G(x)) - x\|_1\right] + E_y[\|G(F(y)) - y\|_1] \qquad (3.4)$$

where λ controls the relative objectives, which are set to 3.4 to give more weight to cyclic consistency. Equations 3.2 and 3.3 represent the adversarial objective, which trains G and F to produce outputs identically as targets. On the other hand, objective 3.4 has two terms of forward and backward cycle consistency that guarantees the learned models can map individual input to a specific output. Using greater λ reduces identity mapping.

Former GAN methods depend on one-to-one examples for training; however, the CycleGAN can learn these transformations without the need to map one-to-one between the training data in source and target domains [23]. A coupled signal requirement in the target domain is removed by having a two-step transition: first attempting to convert it to the target domain and then back to the main signal. The generator is applied to the signal to map it to the target domain, then the quality of the generated signal is improved by performing the generator against a discriminator. This feature enables the algorithm to train with a small dataset.

The network architecture contains two main parts, generator and discriminator. Both the generator and discriminator architectures are depicted in Figure 3.1. The purpose of the

generator is to intensify waves related to the target signal and to reduce the influence of waves from the input signals. However, based on the analysis, we observed that the convolutional kernels, which could increase the amplitude of the FECG waves, could also boost the MECG waves. In other words, instead of suppressing the maternal R wave, it may amplify it along with enhancing the R wave of the fetus. To solve this problem, an attention layer [44] is used to provide a mask to certain parts of the signal and avoid processing parts that can increase errors. Instead of using the softmax layer, which is usual after attention, the output of the attention layer is normalized and weights between 0.8 and 1 are selected for masking. The mask is multiplied by the signal to extract the region of interest. Next, three one-dimensional convolution layers (Conv1D) are applied with the sine activation function [45]. The sine activation function has shown significant results for representing signals, such as audio [45], video, and images [46], [47], and can retain details better than other popular activation functions like LeakyRelu. The three Conv1D layers aim to enhance the FECG and smooth signals using stride two and bigger kernel size parameters [48]. The discriminator contains four Conv1D layers with a sine activation function that tries to classify the input as fake or real using a dense layer and a softmax layer as classification. The generator is trained to produce signals that the discriminator identifies as actual. The algorithm ran for 50 epochs with the loss function $\log(\cosh)$ and the Nesterov Adam optimizer [49].

3.2.4 Validation

The performance of the proposed method is evaluated in two ways: quality of extracted signal and accuracy of QRS detection. In all cases, following the STARD [50] and TRIPOD [51] standards, the CI 95% of the performance indices are reported for showing the reliability of the estimation.

3.2.4.1 Signal extraction quality

In the A&D FECG dataset, the FECG signals are recorded from the fetus's scalp and can be used as continuous ground truth. For the NI-FECG and NI-FECG challenge datasets, there is no recorded FECG, and the simulated FECG based on R information is only used for QRS evaluation. The leave-one-subject-out cross-validation approach was used for performance assessment. All the signals except for one subject are used for the training, and the remaining signal is used for tests. This approach is repeated five times to test all subjects. The R-squared goodness of fit [52], intra-class correlation (ICC) [53], and Bland-Altman plots or Tukey's Mean Difference Map [54] are used for reporting the performance on each subject. The Tukey's Mean Difference Map is a statistical tool for evaluating the variations between the two measurement processes. It analyzes the homogeneity and trend of the residual signal, the bias (a.k.a., mean of the residual signal), and the limit of agreement (LoA). The LoA was defined as bias ± 1.96× (standard deviation of the residual signal).

For diagnostic distortion analysis purposes, the mean value of the original signal and the predicted signal are subtracted from the signals. Using Daubechies 9/7 biorthogonal Wavelet

filters up to 5 levels, all signals are decomposed. The QRS complex typically has the highest amplitude and the broadest spectrum. Therefore, the QRS complex is visible on all levels; however, it is more noticeable in the second and third levels. On the first two levels, the P and T waves are not apparent and primarily belong to fourth and fifth levels. The deviation between the original signal's Wavelet coefficients and the reconstructed signal's Wavelet coefficients is determined by the percentage root mean square difference, referred to as the Wavelet PRD (WPRD). Finally, the Wavelet Energy-based Diagnostic Distortion (WEDD) is calculated by the weighted average of the WPRD in all levels [55] as shown in Equation 3.5.

$$\boldsymbol{WEDD} = \sum_{l=1}^{L+1} \boldsymbol{w_l}\ \boldsymbol{WPRD_l} = \sum_{l=1}^{L+1} \boldsymbol{w_l} \sqrt{\frac{\sum_{k=1}^{K_l}[d_l(k)-\widetilde{d_l(k)}]^2}{\sum_{k=1}^{K_l}[d_l(k)]^2}},\ \mathbf{l = 1, 2, 3, \ldots L} \qquad \textbf{(3.5)}$$

where, $WPRD_l$ is the error in $l-th$ subband, and $d_l(k)$ and $\widetilde{d_l(k)}$ are the $k-th$ wavelet coefficient in $l-th$ subband of original and predicted signals, respectively. The WEDD value can be categorized into five quality groups [55]: excellent (0-4.6), very good (4.6-7), good (7-11.2), not bad (11.2-13.6), and bad (>13.6).

The statistical analysis was performed using SPSS Statistics for Windows version 22 (IBM Corp. Released 2013. Armonk, NY: IBM Corp.). The paired-sample t-test was also used to identify whether the reconstructed signals are significantly different from the original signals, especially in terms of bias. Results are reported as mean ± standard deviation, and P-values less than 0.05 were considered significant.

3.2.4.2 QRS detection accuracy

The QRS wave detection was performed using P&T [56] and analyzed using traditional sensitivity, positive predictive value (PPV), F1-Score, and Mathews Correlation Coefficient (MCC) [2], [15], [16], [57]. Smith et al. [58] reviewed seven different fetal ECG datasets and showed that the average of QRS width, and PR and ST intervals are 55 ms, 96 ms, and 195 ms for the fetal ECG. Therefore, from one QRS to the next QRS, there is an average of 291 ms time interval. For calculating the performance of QRS detection, different time precision is used by various researchers. For example, Guerrero-Martinez et al. [59] used a matching window of 50 ms, while Zhang et al. [15] used 30 ms. In this study, every sample in decomposed data belongs to the 5 ms due to down-sampling. Therefore, a window of 6 samples (30 ms) is used for calculating performance indices, which is more precise than in previous works.

3.3 Results

3.3.1 Results for signal extraction

Two examples of mapping the MECG and the FECG for subjects 2 and 4are depicted in Figure 3.2.

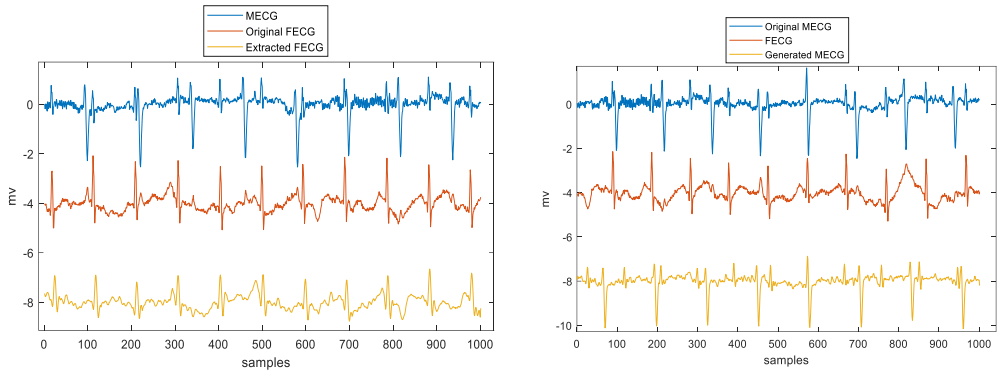

Figure 3-2. Two examples of FECG and MECG generation. The top one is the decomposed FECG using the proposed method on 1000 samples of the MECG test set for subject 4; The bottom one is the generated MECG from the FECG on subject 2 for 1000 samples. All signals are normalized for visualization purposes.

The ICC, R- squared, and WEDD indices are shown in Table 3.1. All parameters suggest that the predicted signals are very similar to the original ones. Moreover, the Tukey/Bland-Altman mean difference plot of the decomposed FECG for each subject is depicted in Figure 3.3. It shows the homogeneity of the residual signal (predicted FECG - original FECG) in low and high values of the FECG signal. Overall, more than 97.3% of samples of the residual signal of the subjects 1-5 lie within the LoA's. Also, the residual signal for each subject was normally distributed.

According to [55] and the WEDD values, the rate of distortions are in "very good" and "good" ranges for all subjects, showing that the main FECG components are retained. Moreover, there were no significant differences between the reconstructed and original signals 1-5 (paired t-test; P-value>0.1).

Although the focus of this work is to extract the FECG from the MECG, both generators are trained together. Similar results are also provided for the MECG generator assessment in the

Table 3-1 The performance of the estimated fecg signal on test set (CI 95% are reported in parenthesis).

Subject	1	2	3	4	5
ICC	0.99 (0.97-0.99)	0.99 (0.97-0.99)	0.98 (0.94-0.99)	0.99 (0.95-0.99)	0.99 (0.97-0.99)
R-squared	0.99 (0.99-1.00)	0.98 (0.97-0.99)	0.96 (0.93-0.97)	0.98 (0.97-0.99)	0.98 (0.97-0.99)
WEDD [55]	7.0 % (6.3–7.3) good	5.7 % (4.7-5.8) very good	9.2% (8.1-9.9) good	6.3% (6.1-6.8) very good	7.2% (6.8-8.0) good

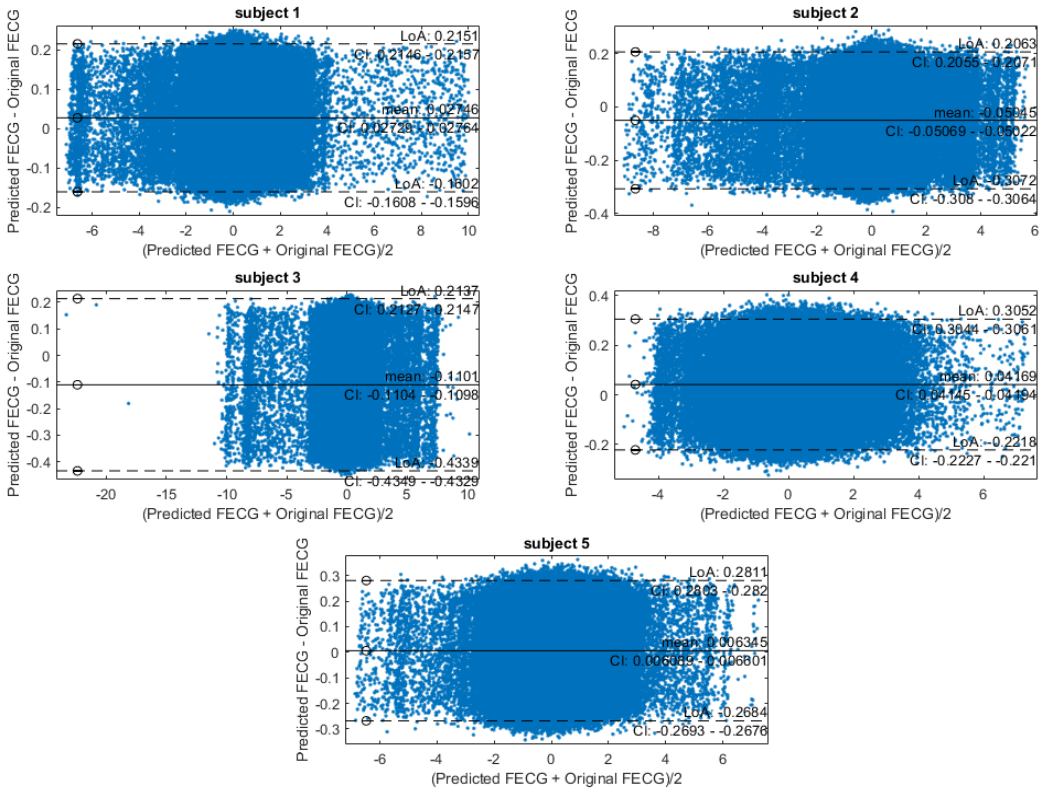

Figure 3-3. The mean difference plots between predicted FECG and original FECG for all subjects in A&D FECG dataset. LoA: Limit of Agreement; CI: Confidence Interval.

supplementary material. Moreover, the supplementary material shows an example of generated MECGs for 4000 samples and depicts a comparison between loss values on the test set during the training of both generators.

Table 3-2. Performance of the qrs detection based on p&t method; mean ± std (CI 95% is reported in parenthesis)

Train	Test	F1-score (%)	MCC (%)	PPV (%)	Sensitivity (%)	# tested signals
A&D FECG	A&D FECG	99.7 ± 0.4 (97.8-99.9)	96.5 ± 2.3 (94.3-98.1)	99.6 ± 0.7 (97.4 - 99.9)	99.4 ± 0.6 (98.8-99.7)	5
	NI-FECG	97.9 (96.5-98.4)	94.2 (93.3-95.7)	97.2 (95.9-97.9)	96.8 (95.4-98.1)	14
	NI-FECG challenge	94.7 (92.6-96.5)	91.0 (90.1-92.4)	93.9 (92.6-95.3)	93.9 (91.6-95.2)	69
NI-FECG	NI-FECG	99.6 ± 1.3 (98.2-99.9)	95.3 ± 2.8 (92.2-97.4)	99.6 ± 0.6 (98.9-99.9)	99.6± 0.9 (98.8-99.9)	14
NI-FECG challenge	NI-FECG challenge	99.3 ± 1.3 (95.3-99.9)	93.8 ± 3.3 (90.1-96.2)	99.1 ± 1.0 (95.3-99.9)	99.2 ± 0.6 (96.1-99.9)	69

Since the training and assessment of the A&D FECG dataset was based on subject-leave-out, not all heart rate values were considered for the trained models. To generalize, a model is trained on all the A&D FECG dataset. This model is used for testing on the NI-FECG and NI-FECG challenge datasets. Moreover, this model is applied on 24 simulated MECG and FECG signals generated by the FECGSYN toolbox. The boxplot for R-Squared and WEDD indices are plotted for different maternal and fetal heart rates in Figure 3.4. This figure shows that the

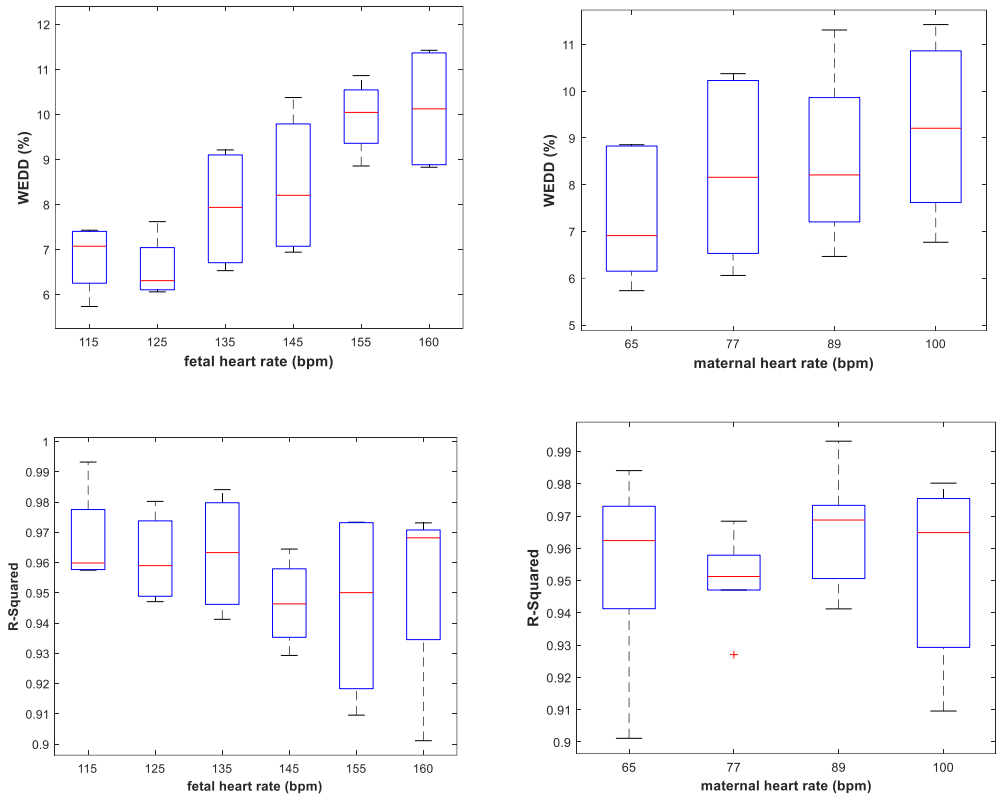

Figure 3-4. Boxplots for R-Squared and WEDD indices computed on simulated FECG and MECG based on trained model using A&D FECG dataset. The trained system can extract fetal signal in different heart rates without considerable decreased performance.

system's performance does not substantially drop if it is trained with data that covers most of the heart rate variabilities. There is no correlation between WEDD and maternal HR (Kendall's τ_b =-0.016; P-value=0.918). However, there is a weakly negative correlation between R-square and maternal HR, but it is not statistically significant (Kendall's τ_b =-0.221; P-value=0.165).

3.3.2 Results for QRS detection

The NI-FECG challenge and NI-FECG dataset are used for QRS detection evaluation. NI-FECG is obtained from a subject at 21 and 40 weeks of pregnancy. Compared to the A&D FECG dataset recorded from women at 38 and 41 weeks, the FECG QRS of these two datasets has less amplitude, and it is more difficult to extract the FECG. First, the trained system on the A&D FECG dataset is tested on 14 signals of the NI-FECG dataset and 69 signals of the NI-FECG challenge. Second, 4-fold cross-validation is performed on the NI-FECG dataset and the NI-FECG challenge datasets, and the average and standard deviation of test sets are reported. As explained earlier, since the original FECG is not provided in these two datasets, a simulated FECG is generated based on Daubechies wavelets and R-R interval values provided as ground truth are used as the parameter. Table 3.2 shows the results a simulated.

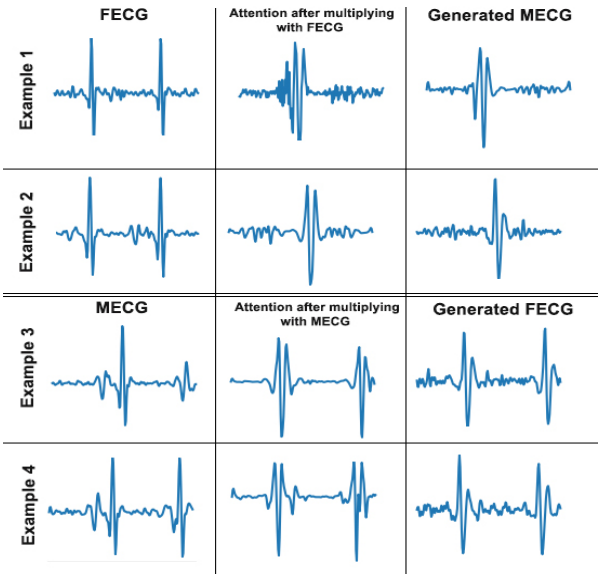

Figure 3-5. Illustrating the output of attention layer which shows it could focus on part of input signals that has high impact on generating target signal. All subplots show 200 samples, and their values are normalized between -1 and 1. In all cases, R-squared between the generated signals and target signal is 99%; therefore, target signal is not depicted.

3.3.3 Ablation studies

Deep learning ablation studies are based on the concept of ablation studies in neuroscience to explore the structure of information embodied by the network [60]. The idea is that certain parameters of a trained network contribute very little or nothing to the network's performance, making them insignificant and, therefore, able to be removed. We want to use this ablation approach not to improve the size and speed of a neural network but to acquire insights into the impact of each step on the performance, resulting in an interpretable model.

3.3.4 Impact of sine activation and attention

A model was trained based on Conv1D layers along with the LeakyRelu activation function and normalization without attention. The structure of the discriminator and all other parameters remained the same. The R-Squared index for five subjects of the A&D FECG dataset was dropped to 0.79, 0.80, 0.77, 0.82, and 0.81. Replacing the Sine activation instead of the LeakyRelu meant that the R-Squared increased to 0.80, 0.81, 0.78, 0.83, and 0.81, respectively.

Without using the attention layer, the proposed method does not perform well. The CNN can help to amplify R waves; however, it amplifies maternal R waves along with enhancing the fetal R waves. Figure 3.5 shows outputs of the attention masks after the element-wise multiplication layer for four epochs from using subject 1 in the A&D FECG dataset as a test set. It is clear that attention performs a significant role for finding segments that have more relevancy with the target signal. High correlation between the generated signal and the attention output shows its impact on the process.

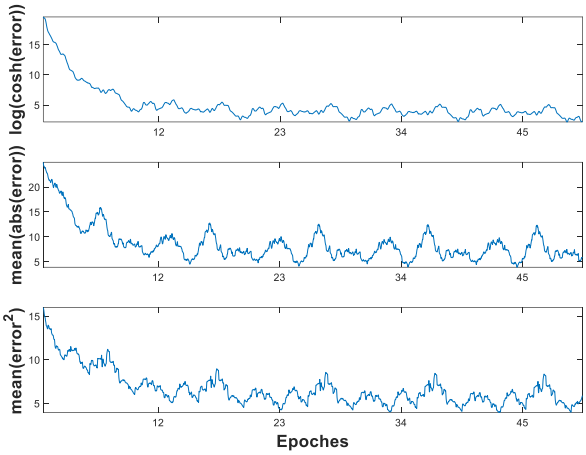

Figure 3-6. The loss obtained from a test set (subject 1) during training on subjects 2 to 5 in the A&D FECG dataset. The log(cosh) results in smoother loss function and has fewer local optima. The R-squared on the test set is depicted in the top right of each subplot.

3.3.5 Impact of loss function

For the loss function, the use of $l_1 = mean\ absoulute\ error$, log(cosh) and $l_2 = mean\ square\ error$ is tested. The l_1 loss had a better performance than l_2 and log(cosh) had a better performance than l_1.

Using l_2 norm induces unnecessary smoothing, which causes less efficiency. Since most of the ECG signal contains low-frequency parts, l_2 norm may even converge to constant zero values. However, signal fluctuations are preserved by the standard l_1. The smoothing effect of l_2 was also observed for an electrocardiographic inverse problem for epicardial potential [61]. The log(cosh), on the other hand, gives smooth results and preserves signal details. It has also been shown to improve the reconstruction without damaging the latent space optimization [62]. Figure 3.6 shows the loss on a test set (subject 1) during training on subjects 2 to 5 of the A&D FECG dataset. Smoother loss for log(cosh) shows that it is more stable and has fewer local optima.

The variation of ג coefficient, which is in the objective function of the CycleGAN in Equation 3.1, is assessed by adjusting it from 0.1 to 40, and the sensitivity analysis plot is depicted in Figure 3.7.

Concisely, the cycle and identity of the system could be preserved in $2 <$ ג <10. The higher ג, the less precision in the FECG retrieval. In comparison, using smaller ג does not allow the algorithm to converge due to extra focus on identity. According to Equation 3.1, using a higher value of ג is equal to not using a discriminator. Empirically, a discriminator helped the network to be more stable and to generate signals that are similar to the ECG, while signals generated without using a discriminator are similar to a noisy signal with high variations, even though their L1 loss is reduced during training.

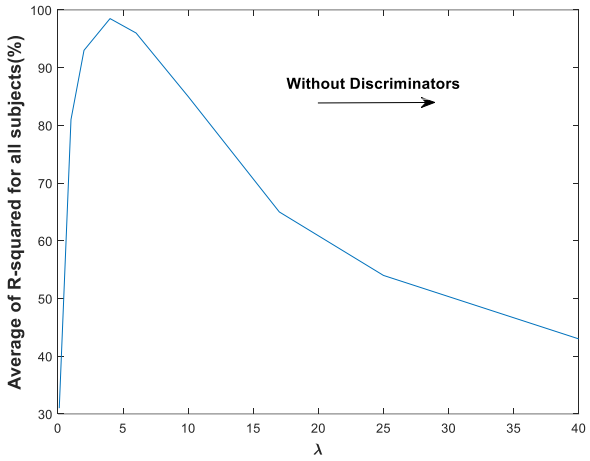

Figure 3-7. Sensitivity analysis of ג for all subjects in the A&D FECG dataset.

3.3.6 Impact of network parameters

Other network parameters are also analyzed by utilizing sensitivity analysis. In different steps, kernel size for each layer is changed. The selected kernel size for the proposed method was based on whether the signal needs more smoothing (bigger kernel size) or needs more details retrieved (smaller kernel size). Sensitivity analysis showed that changing kernel sizes can decrease the performance; however, if their ratio in respect to each other remained the same, similar performance is achieved.

Finally, the number of Conv1D layers in the generator network after the attention step is decreased from four to three (first Conv1D layer after the attention layer is removed) and resulted in the average R-Squared performance dropping by 5%. The performance of the proposed method is also evaluated by changing the number of Conv1D layers in the discriminator and results showed that the system is rather insensitive to the number of layers in the discriminator. Nevertheless, four layers of Conv1D are used, since it achieved a slightly better result. Figure 3.8 shows the R-squared acquired for subject 1 from the A&D FECG dataset with various numbers of Conv1D layers of the discriminator.

3.3.7 Impact of noise

Cerebral Vasoregulation in Elderly with Stroke is a database [63], available on the Physionet website, containing 24-hour surface electromyographic (EMG) signals collected using the ME6000 device with a sampling frequency of 1000 Hz. Some portions of the EMG signal are resampled and scaled to generate a noisy signal with a varied SNR. The effect of noise on the proposed method is evaluated by adding EMG noise with different amplitudes to the MECG signal to evaluate FECG generation. Figure 3.9 depicts the SNR of signals and the R-square acquired for subject 1 in the A&D FECG dataset based on training on other subjects with noisy signals.

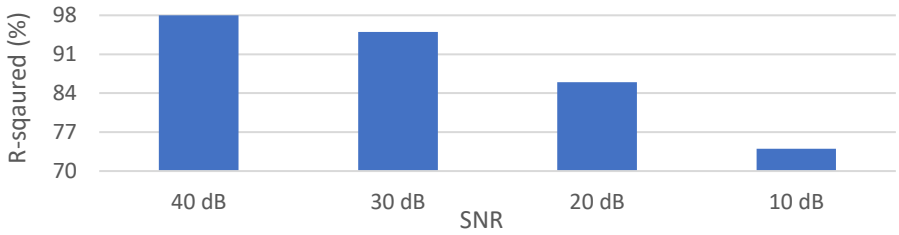

Figure 3-8. The relation between SNR and R-square for subject 1 in the A&D FECG dataset.

3.3.8 Impact of sliding window length

To decrease the computational cost, especially for the attention mechanism, which is in complexity of $O(n^2)$ [44], signals are down sampled to 200 sample/second. The effect of changing sliding window length is evaluated by setting M to 50, 200, and 400. Figure 3.10 depicts the R-square acquired for subject 1 in the A&D FECG dataset based on training on other subjects. To ensure that at least one cycle of ECG pattern (QRST) is present in each training sample, M is set to 200. The smaller window length does not allow the network to

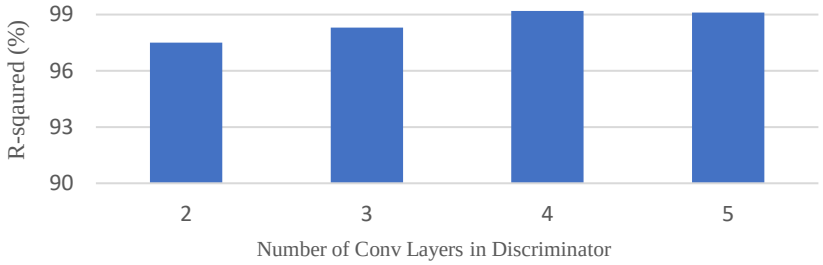

Figure 3-9. The impact of number of Conv1D layers of the discriminator on the performance of subject 1 in A&D FECG dataset.

capture attention between a cycle of the FECG and the MECG. On the other hand, the wider window can introduce unnecessary attention and increase the complexity of the algorithm.

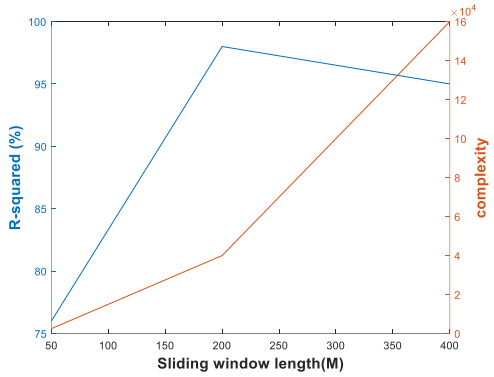

Figure 3-10. The relation of sliding window length with R-square and the complexity of the algorithm, acquired for subject 1 in the A&D FECG dataset.

3.3.9 Probability calibration

Assessing the uncertainty is as important as model accuracy. Recently Gal et al.[64] , and Lakshminarayann et al. [65] presented uncertainty estimating approaches for deep neural networks, which included ensemble methods, heteroscedastic regression, and concrete dropout. We adopted the recent method proposed by Kuleshov et al. [66] that is an extend calibration for classification to regression in model agnostic approach. Regression calibration was used in a way that predicted value should fall in a 90% confidence interval in 90% of the times. For calibration, an isotonic regression is applied on predicted values to fit on target data to calculate the actual probability of any quantile. To avoid overfitting, the calibration model should ideally be fitted on a separate set.

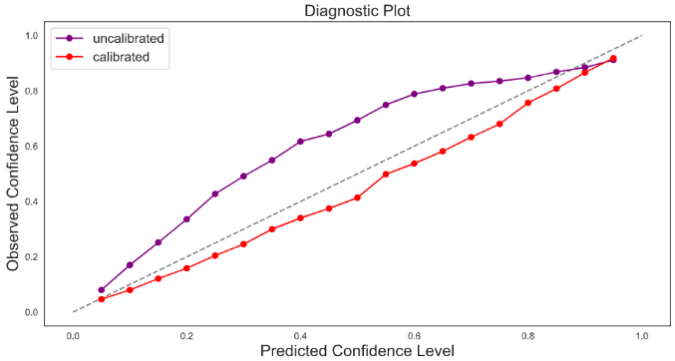

Figure 3-11. Successfully calibrated model on the subject 1 of the A&D FECG dataset which is well generalized on other data in the A&D FECG dataset. In entire cases, the calibrated model achieved 0.5% and 0.1% average reduction for R-squared and WEDD, respectively; however, the uncertainties were reduced. As a result, the actual percentage of the test set points in the 90% interval is much closer to 90%.

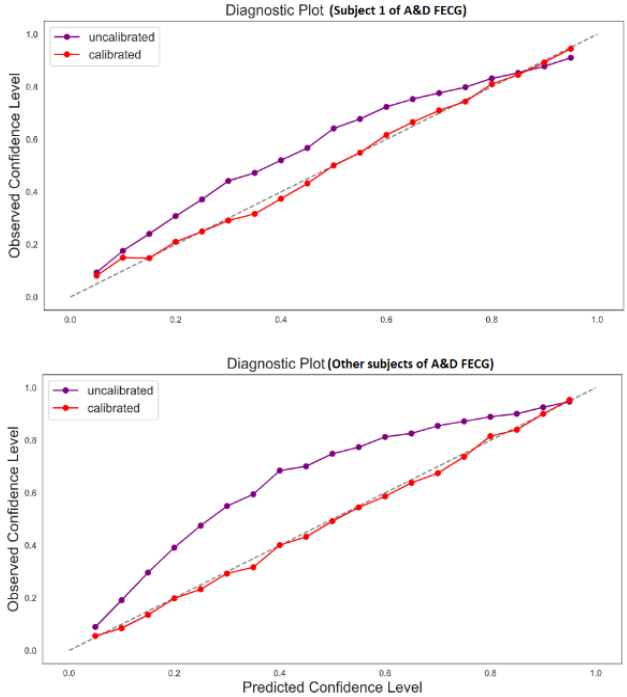

Figure 3-12. Result of calibration on NI-FECG dataset when trained on A&D FECG dataset.

Here, we calibrated the CycleGAN model trained on the subject 1 of A&D FECG dataset and evaluated the performance on the entire subjects. Result of the calibration is shown in Figure 3.11. Noted that the performance metrics of the model, such as average of WEDD and R-squared are decreased 0.5% and 0.1%, respectively, to the cases without calibration which is negligible. However, the certainty is increased.

Furthermore, we used the previous calibration on NI-FECG dataset as another test set whose result is shown in Figure 3.12. Although the dataset shift is one of the challenges in the proposed calibration scheme [66] and calibration results are better when it is applied on test set in the same dataset, the calibrated model is also acceptable when it is performed on another dataset.

3.4 Discussion

3.4.1 Performance and properties of the proposed method

A signal-to-signal model is trained for extracting the FECG signal from the abdominal MECG. The novelty of this algorithm was using the attention mechanism as a filtering mask for focusing on the signal region of interest. Furthermore, using sine activation function and log(cosh) loss were important parts that also had a significant effect on the results.

The validation of the proposed method had two main phases: FECG extraction and QRS detection. Table 3.3 compares different approaches for fetal QRS complex detection. External validation shows whether the models are robust enough to work with similar though not identical data. Being in different weeks of gestation for training and test sets results in both different quality and different intensity of fetal cardiac activity, which can be considered the critical factor for decreased accuracy.

The performance of the proposed method does not decrease significantly by electrode configuration and varying calibration. For instance, the A&D FECG dataset is recorded by four electrodes around the navel, a reference electrode above the pubic symphysis, and a common mode reference electrode. While in NI-FECG dataset, to achieve better SNRs, electrode placement was changed during each record. Table 3.2 shows that the performance of the proposed method is not dropped in such conditions.

The average performance of the proposed method on the NI-FECG challenge dataset is less when it is performed on other datasets. In some noisy abdominal records with small FECG amplitude, like a29, a38, a40, a42, a52, a53, a54, a56, a61, and a65, performance deteriorated considerably, which affects the overall performance.

Behar *et al.* [12] evaluated recurrent neural network (RNN), PCA, LMS, and RLS, and template subtraction for QRS detection based on the P&T method [56]. They trained on 30 seconds of the NI-FECG dataset and used a 50 ms matching window. They also reported the results of the trained model on a single dataset as external validation. However, the proposed method could achieve better results. It also gave higher accuracy on the A&D FECG dataset compared to the Encoder-Decoder method [67], and SVD-SW [15] approaches when tested on more signals. The proposed method outperformed Behar et al. [34], who used a combination

of template subtraction and ICA. The proposed method also outperformed Varanini *et al.*'s [33] QRS detection algorithm. They proposed a signal extraction technique based on ICA and a post-processing method specialized for detecting the QRS on the NI-FECG challenge dataset. Warmerdam *et al*. [68] used a multichannel hierarchical probabilistic system, which incorporates ECG waveform and heart rate predictive models, to detect fetal R peaks in the NI-FECG challenge dataset. They reported only 99.6% accuracy defined as TP/(TP+FP+FN) and did not provide the sensitivity or F1-Score for better comparison. However, their accuracy outperformed the method of Varanini *et al* [33] with an accuracy of 98.6%. The accuracy of our proposed method was 99.6% on QRS detection, which is similar to Warmerdam. Nevertheless, better comparison requires more performance indices and analysis.

3.4.2 Future works and limitations

The QRS detection is not the primary task supported by the proposed method. The proposed method can extract the complete FECG signal. A QRS detection algorithm is added on top of it to demonstrate one of the capabilities of the proposed method. The WEDD index, which shows distortion between the predicted FECG and the original FECG, showed that the proposed method can extract important waveforms (Table 3.1 and Figure 3.4). This capability can stimulate the idea that a similar attention mechanism can also be used for ECG wave analysis or to map other signals, such as ECG to PPG or vice versa [69].

Table 3.3. Comparing the result of the different methods for decomposing fetal ECG

Method	F1-score (%)	Dataset	QRS detection method	Number of channels	Matching window length (ms)	Number of tested signals
TS and ES-RNN [12]	97.2	NI-FECG	P&T	1 Abdominal	50	14
	90.2	Train on NI-FECG and test on private dataset				
TS and PCA [12]	95.4	NI-FECG				
	89.3	Train on NI-FECG and test on private dataset				
LMS [12]	95.4	NI-FECG				
	87.9	Train on NI-FECG and test on private dataset				
RLS [12]	95.9	NI-FECG				
	88.2	Train on NI-FECG and test on private dataset				
OBACKC [14]	95.6	NI-FECG	Thresholding	1 Thoracic		
SVD-SW [15]	99.4	A&D FECG	P&T	1 Abdominal		2
Encoder-Decoder [64]	94.1	A&D FECG		1 Abdominal		5
Behar *et al.* [34]	95.9	NI-FECG challenge		4 Abdominal		69
Varanini *et al.* [33]	99.0	NI-FECG challenge	Customized	4 Abdominal		69
Proposed Method	99.6	NI-FECG	P&T	1 Abdominal	30	14
	99.7	A&D FECG				5
	99.3	NI-FECG challenge				69
	94.7	Train on A&D FECG and test on NI-FECG challenge				69
	97.9	Train on A&D FECG and test on NI-FECG				14

TS: Template subtraction, ES-RNN: echo state for the recurrent neural network, PCA: principal component analysis, LMS: Least Mean Square, RLS: Recursive Least Square, ICA: independent component analysis; OBACKC: optimized blind adaptive filtering using convolution kernel compensation; SVD-SW: singular value decomposition and smooth windowing.

One of the future works is using new versions of transformers, such as reformer [70], which could be used to reduce the complexity of the attention mechanism and may also improve the performance. Furthermore, neural architecture search [71] can be used for designing the optimal architecture for the generator and the discriminator.

The proposed method is trained based on abdominal MECGs. However, using only maternal thoracic for converting the MECG to the FECG, as performed by Mohebbian *et al.* [14], is not investigated and could be done in future work.

One of the limitations of this study is the complexity of the model, which is common in deep learning algorithms. This complexity may increase the computational cost and might be a burden for embedded systems, which can be eliminated by advances in hardware technology and using GPUs with less power consumption. Two systems are utilized to calculate computing time on the training and test steps. The first machine is a PC with a Core i9 processor, 16 GB of RAM, and a 6GB Nvidia GeForce GTX 1060 graphics card. The second machine is a laptop with a Core-i7 processor, 16 GB of RAM, and no graphics card. On the PC, we trained the model on subjects 2 to 5 from the A&D FECG dataset and applied trained model for one minute of abdominal, once with GPU (batch size 8) and once without it, and then on the laptop we ran the test step only with the CPU. We repeated the test procedure for 5 times. The training time using GPU and CPU on the PC was 10400 seconds and 43910 seconds, respectively. After training, the processing of one minute requires a total of 1.9 ± 0.4 seconds on GPU and 2.5 ± 0.2 seconds and 2.6 ± 0.3 seconds with CPU on PC and laptop, respectively. Additionally, a larger sample size is required to show whether this approach can operate efficiently in all circumstances.

3.5 Conclusion

A novel architecture based on the attention layer, sine activation function, and cycle generative adversarial neural network is investigated to map maternal and fetal ECGs. The proposed method is evaluated in two forms. First, the quality of the FECG extracted from the MECG was evaluated. Second, the fetal QRS detection from the MECG was assessed. On the abdominal and direct FECG (A&D FECG) dataset, an average 98% of R-Square [CI 95%: 97%, 99%] as the goodness of fit and 99.7% for the F1-score [CI 95%: 97.8%, 99.9%] for QRS estimation achieved based on subject-leave-out validation. Besides the A&D FECG dataset, the non-invasive FECG (NI-FECG) and NI-FECG challenge datasets were also used for fetal QRS estimation and achieved 99.7 % for the F1-score [CI 95%: 97.8-99.9], 99.6% for the F1-score [CI 95%: 98.2%, 99.9%] and 99.3% for the F1-score [CI 95%: 95.3%, 99.9%], respectively. A synthetic dataset was generated to investigate the effect of maternal and fetal heart rates. The proposed method could be used in various fetal and maternal heart rate variations. Such results were comparable and superior to the-state-of-the-art results and therefore the proposed method is promising for FECG extraction.

3.6 References

[1] P. R. Jeffries, S. Woolf, and B. Linde, "Technology-based vs. traditional instruction: A comparison of two methodsfor teaching the skill of performing a 12-lead ecg," *Nurs. Educ. Perspect.*, vol. 24, no. 2, pp. 70–74, 2003.

[2] M. A. Hasan, M. I. Ibrahimy, and M. B. I. Reaz, "Techniques of FECG signal analysis: detection and processing for fetal monitoring," *WIT Trans. Biomed. Health*, vol. 12, pp. 295–305, 2007.

[3] G. D. Clifford, F. Azuaje, and P. Mcsharry, "ECG statistics, noise, artifacts, and missing data," *Adv. Methods Tools ECG Data Anal.*, vol. 6, p. 18, 2006.

[4] E. R. Ferrara and B. Widraw, "Fetal electrocardiogram enhancement by time-sequenced adaptive filtering," *IEEE Trans. Biomed. Eng.*, no. 6, pp. 458–460, 1982.

[5] W. Zhong, L. Liao, X. Guo, and G. Wang, "A deep learning approach for fetal QRS complex detection," *Physiol. Meas.*, vol. 39, no. 4, p. 045004, 2018.

[6] M. Varanini, G. Tartarisco, R. Balocchi, A. Macerata, G. Pioggia, and L. Billeci, "A new method for QRS complex detection in multichannel ECG: Application to self-monitoring of fetal health," *Comput. Biol. Med.*, vol. 85, pp. 125–134, 2017.

[7] R. A. Shepoval'nikov, A. P. Nemirko, A. N. Kalinichenko, and V. V. Abramchenko, "Investigation of time, amplitude, and frequency parameters of a direct fetal ECG signal during labor and delivery," *Pattern Recognit. Image Anal.*, vol. 16, no. 1, pp. 74–76, 2006.

[8] G. D. Clifford, I. Silva, J. Behar, and G. B. Moody, "Non-invasive fetal ECG analysis," *Physiol. Meas.*, vol. 35, no. 8, p. 1521, 2014.

[9] B. Rafaely and S. J. Elliot, "A computationally efficient frequency-domain LMS algorithm with constraints on the adaptive filter," *IEEE Trans. Signal Process.*, vol. 48, no. 6, pp. 1649–1655, 2000.

[10] D. Mumford and A. Desolneux, *Pattern theory: the stochastic analysis of real-world signals*. CRC Press, 2010.

[11] M. Niknazar, B. Rivet, and C. Jutten, "Fetal ECG extraction by extended state Kalman filtering based on single-channel recordings," *IEEE Trans. Biomed. Eng.*, vol. 60, no. 5, pp. 1345–1352, 2013.

[12] J. Behar, A. Johnson, G. D. Clifford, and J. Oster, "A comparison of single channel fetal ECG extraction methods," *Ann. Biomed. Eng.*, vol. 42, no. 6, pp. 1340–1353, 2014.

[13] R. Martinek *et al.*, "Comparative effectiveness of ICA and PCA in extraction of fetal ECG from abdominal signals: Toward non-invasive fetal monitoring," *Front. Physiol.*, vol. 9, p. 648, 2018.

[14] M. R. Mohebbian, M. W. Alam, K. A. Wahid, and A. Dinh, "Single channel high noise level ECG deconvolution using optimized blind adaptive filtering and fixed-point convolution kernel compensation," *Biomed. Signal Process. Control*, vol. 57, p. 101673, 2020.

[15] N. Zhang *et al.*, "A novel technique for fetal ECG extraction using single-channel abdominal recording," *Sensors*, vol. 17, no. 3, p. 457, 2017.

[16] W. Zhong, X. Guo, and G. Wang, "QRStree: A prefix tree-based model to fetal QRS complexes detection," *PloS One*, vol. 14, no. 10, 2019.

[17] A. Josko and R. J. Rak, "Effective simulation of signals for testing ECG analyzer," *IEEE Trans. Instrum. Meas.*, vol. 54, no. 3, pp. 1019–1024, 2005.

[18] J. Behar, F. Andreotti, S. Zaunseder, Q. Li, J. Oster, and G. D. Clifford, "An ECG simulator for generating maternal-foetal activity mixtures on abdominal ECG recordings," *Physiol. Meas.*, vol. 35, no. 8, p. 1537, 2014.

[19] M. Frid-Adar, I. Diamant, E. Klang, M. Amitai, J. Goldberger, and H. Greenspan, "GAN-based synthetic medical image augmentation for increased CNN performance in liver lesion classification," *Neurocomputing*, vol. 321, pp. 321–331, 2018.

[20] L. Ying, A. Hertzmann, H. Biermann, and D. Zorin, "Texture and shape synthesis on surfaces," in *Rendering Techniques 2001*, Springer, 2001, pp. 301–312.

[21] Y. Aytar, L. Castrejon, C. Vondrick, H. Pirsiavash, and A. Torralba, "Cross-modal scene networks," *IEEE Trans. Pattern Anal. Mach. Intell.*, vol. 40, no. 10, pp. 2303–2314, 2017.

[22] M.-Y. Liu and O. Tuzel, "Coupled generative adversarial networks," in *Advances in neural information processing systems*, 2016, pp. 469–477.

[23] T. Kaneko, H. Kameoka, K. Tanaka, and N. Hojo, "Cyclegan-vc2: Improved cyclegan-based non-parallel voice conversion," in *ICASSP 2019-2019 IEEE International Conference on Acoustics, Speech and Signal Processing (ICASSP)*, 2019, pp. 6820–6824.

[24] S. Zhao *et al.*, "CycleEmotionGAN: Emotional semantic consistency preserved cycleGAN for adapting image emotions," in *Proceedings of the AAAI Conference on Artificial Intelligence*, 2019, vol. 33, pp. 2620–2627.

[25] O. Tmenova, R. Martin, and L. Duong, "CycleGAN for style transfer in X-ray angiography," *Int. J. Comput. Assist. Radiol. Surg.*, vol. 14, no. 10, pp. 1785–1794, 2019.

[26] B. Hou, J. Yang, P. Wang, and R. Yan, "LSTM-Based Auto-Encoder Model for ECG Arrhythmias Classification," *IEEE Trans. Instrum. Meas.*, vol. 69, no. 4, pp. 1232–1240, 2019.

[27] B. Taji, A. D. Chan, and S. Shirmohammadi, "False alarm reduction in atrial fibrillation detection using deep belief networks," *IEEE Trans. Instrum. Meas.*, vol. 67, no. 5, pp. 1124–1131, 2017.

[28] T. H. Linh, S. Osowski, and M. Stodolski, "On-line heart beat recognition using Hermite polynomials and neuro-fuzzy network," *IEEE Trans. Instrum. Meas.*, vol. 52, no. 4, pp. 1224–1231, 2003.

[29] J. Jezewski, A. Matonia, T. Kupka, D. Roj, and R. Czabanski, "Determination of fetal heart rate from abdominal signals: evaluation of beat-to-beat accuracy in relation to the direct fetal electrocardiogram," *Biomed. Tech. Eng.*, vol. 57, no. 5, pp. 383–394, 2012.

[30] R. Nurani, E. Chandraharan, V. Lowe, A. Ugwumadu, and S. Arulkumaran, "Misidentification of maternal heart rate as fetal on cardiotocography during the second stage of labor: the role of the fetal electrocardiograph," *Acta Obstet. Gynecol. Scand.*, vol. 91, no. 12, pp. 1428–1432, 2012.

[31] A. L. Goldberger *et al.*, "Components of a new research resource for complex physiologic signals," *PhysioBank PhysioToolkit Physionet*, 2000.

[32] I. Silva *et al.*, "Noninvasive fetal ECG: the PhysioNet/computing in cardiology challenge 2013," in *Computing in Cardiology 2013*, 2013, pp. 149–152.

[33] M. Varanini, G. Tartarisco, L. Billeci, A. Macerata, G. Pioggia, and R. Balocchi, "An efficient unsupervised fetal QRS complex detection from abdominal maternal ECG," *Physiol. Meas.*, vol. 35, no. 8, p. 1607, 2014.

[34] J. Behar, J. Oster, and G. D. Clifford, "Combining and benchmarking methods of foetal ECG extraction without maternal or scalp electrode data," *Physiol. Meas.*, vol. 35, no. 8, p. 1569, 2014.

[35] P. E. McSharry, G. D. Clifford, L. Tarassenko, and L. A. Smith, "A dynamical model for generating synthetic electrocardiogram signals," *IEEE Trans. Biomed. Eng.*, vol. 50, no. 3, pp. 289–294, 2003.

[36] E. C. G. An, "model for simulating maternal-foetal activity mixtures on abdominal ECG recordings/Behar J., Andreotti F., Zaunseder S. et al," *Physiol Meas*, vol. 35, no. 8, pp. 1537–1550, 2014.

[37] S. P. Von Steinburg *et al.*, “What is the ‘normal’ fetal heart rate?,” *PeerJ*, vol. 1, p. e82, 2013.

[38] J. Patrick, K. Campbell, L. Carmichael, R. Natale, and B. Richardson, “Daily relationships between fetal and maternal heart rates at 38 to 40 weeks of pregnancy.,” *Can. Med. Assoc. J.*, vol. 124, no. 9, p. 1177, 1981.

[39] J. J. Bailey *et al.*, “Recommendations for standardization and specifications in automated electrocardiography: bandwidth and digital signal processing. A report for health professionals by an ad hoc writing group of the Committee on Electrocardiography and Cardiac Electrophysiology of the Council on Clinical Cardiology, American Heart Association.,” *Circulation*, vol. 81, no. 2, pp. 730–739, 1990.

[40] R. Sameni and G. D. Clifford, “A review of fetal ECG signal processing; issues and promising directions,” *Open Pacing Electrophysiol. Ther. J.*, vol. 3, p. 4, 2010.

[41] S. Das and M. Chakraborty, “QRS detection algorithm using Savitzky-Golay filter,” *ACEEE Int J Signal Image Process.*, vol. 3, no. 01, pp. 55–58, 2012.

[42] N. Rastogi and R. Mehra, “Analysis of Savitzky-Golay filter for baseline wander cancellation in ECG using wavelets,” *Int J Eng Sci Emerg Technol*, vol. 6, no. 1, pp. 15–23, 2013.

[43] S. Patro and K. K. Sahu, “Normalization: A preprocessing stage,” *ArXiv Prepr. ArXiv150306462*, 2015.

[44] A. Vaswani *et al.*, “Attention is all you need,” *ArXiv Prepr. ArXiv170603762*, 2017.

[45] V. Sitzmann, J. Martel, A. Bergman, D. Lindell, and G. Wetzstein, “Implicit neural representations with periodic activation functions,” *Adv. Neural Inf. Process. Syst.*, vol. 33, 2020.

[46] T. E. Ozmermer, “Sinusoidal Neural Networks: Towards ANN that Learns Faster,” *Complex Syst. Inform. Model. Q.*, no. 23, pp. 44–57, 2020.

[47] İ. Atli and O. S. Gedik, “Sine-Net: A fully convolutional deep learning architecture for retinal blood vessel segmentation,” *Eng. Sci. Technol. Int. J.*, vol. 24, no. 2, pp. 271–283, 2021.

[48] X. Fang, M. Wang, A. Shamir, and S.-M. Hu, “Learning Explicit Smoothing Kernels for Joint Image Filtering,” in *Computer Graphics Forum*, 2019, vol. 38, no. 7, pp. 181–190.

[49] D. P. Kingma and J. Ba, “Adam: A method for stochastic optimization,” *ArXiv Prepr. ArXiv14126980*, 2014.

[50] P. M. Bossuyt *et al.*, “STARD 2015: an updated list of essential items for reporting diagnostic accuracy studies,” *Clin. Chem.*, vol. 61, no. 12, pp. 1446–1452, 2015.

[51] G. S. Collins, J. B. Reitsma, D. G. Altman, and K. G. Moons, “Transparent Reporting of a Multivariable Prediction Model for Individual Prognosis or Diagnosis (TRIPOD) The TRIPOD Statement,” *Circulation*, vol. 131, no. 2, pp. 211–219, 2015.

[52] J. Miles, “R squared, adjusted R squared,” *Wiley StatsRef Stat. Ref. Online*, 2014.

[53] S. Mehta *et al.*, “Performance of intraclass correlation coefficient (ICC) as a reliability index under various distributions in scale reliability studies,” *Stat. Med.*, vol. 37, no. 18, pp. 2734–2752, 2018.

[54] J. M. Bland and D. G. Altman, “Statistical methods for assessing agreement between two methods of clinical measurement,” *Int. J. Nurs. Stud.*, vol. 47, no. 8, pp. 931–936, Aug. 2010, doi: 10.1016/j.ijnurstu.2009.10.001.

[55] M. S. Manikandan and S. Dandapat, “Wavelet energy based diagnostic distortion measure for ECG,” *Biomed. Signal Process. Control*, vol. 2, no. 2, pp. 80–96, 2007.

[56] J. Pan and W. J. Tompkins, “A real-time QRS detection algorithm,” *IEEE Trans. Biomed. Eng.*, no. 3, pp. 230–236, 1985.

[57] D. Chicco and G. Jurman, “The advantages of the Matthews correlation coefficient (MCC) over F1 score and accuracy in binary classification evaluation,” *BMC Genomics*, vol. 21, no. 1, pp. 1–13, 2020.

[58] V. Smith, S. Arunthavanathan, A. Nair, D. Ansermet, F. da Silva Costa, and E. M. Wallace, “A systematic review of cardiac time intervals utilising non-invasive fetal electrocardiogram in normal fetuses,” *BMC Pregnancy Childbirth*, vol. 18, no. 1, pp. 1–15, 2018.

[59] J. F. Guerrero-Martinez, M. Martinez-Sober, M. Bataller-Mompean, and J. R. Magdalena-Benedito, “New algorithm for fetal QRS detection in surface abdominal records,” in *2006 Computers in Cardiology*, 2006, pp. 441–444.

[60] R. Meyes, M. Lu, C. W. de Puiseau, and T. Meisen, “Ablation studies in artificial neural networks,” *ArXiv Prepr. ArXiv190108644*, 2019.

[61] S. Ghosh and Y. Rudy, “Application of l1-norm regularization to epicardial potential solution of the inverse electrocardiography problem,” *Ann. Biomed. Eng.*, vol. 37, no. 5, pp. 902–912, 2009.

[62] X. Xu, J. Li, Y. Yang, and F. Shen, “Towards Effective Intrusion Detection Using Log-cosh Conditional Variational AutoEncoder,” *IEEE Internet Things J.*, 2020.

[63] V. Novak *et al.*, “Cerebral flow velocities during daily activities depend on blood pressure in patients with chronic ischemic infarctions,” *Stroke*, vol. 41, no. 1, pp. 61–66, 2010.

[64] Y. Gal, J. Hron, and A. Kendall, “Concrete dropout,” *ArXiv Prepr. ArXiv170507832*, 2017.

[65] B. Lakshminarayanan, A. Pritzel, and C. Blundell, “Simple and scalable predictive uncertainty estimation using deep ensembles,” *ArXiv Prepr. ArXiv161201474*, 2016.

[66] V. Kuleshov, N. Fenner, and S. Ermon, “Accurate uncertainties for deep learning using calibrated regression,” in *International Conference on Machine Learning*, 2018, pp. 2796–2804.

[67] W. Zhong, L. Liao, X. Guo, and G. Wang, “Fetal electrocardiography extraction with residual convolutional encoder–decoder networks,” *Australas. Phys. Eng. Sci. Med.*, vol. 42, no. 4, pp. 1081–1089, 2019.

[68] G. J. Warmerdam, R. Vullings, L. Schmitt, J. O. Van Laar, and J. W. Bergmans, “Hierarchical probabilistic framework for fetal R-peak detection, using ECG waveform and heart rate information,” *IEEE Trans. Signal Process.*, vol. 66, no. 16, pp. 4388–4397, 2018.

[69] P. Sarkar and A. Etemad, “CardioGAN: Attentive Generative Adversarial Network with Dual Discriminators for Synthesis of ECG from PPG,” *ArXiv Prepr. ArXiv201000104*, 2020.

[70] N. Kitaev, Ł. Kaiser, and A. Levskaya, “Reformer: The efficient transformer,” *ArXiv Prepr. ArXiv200104451*, 2020.

[71] T. Elsken, J. H. Metzen, and F. Hutter, “Neural architecture search: A survey.,” *J Mach Learn Res*, vol. 20, no. 55, pp. 1–21, 2019.

4 SEMI-SUPERVISED ACTIVE TRANSFER LEARNING FOR FETAL ECG ARRHYTHMIA DETECTION

Recording clean signal and extracting FECG have been investigated in previous sections. However, the main purpose of denoising, and extracting signal is to detect anomaly and disorders. In this regard, designing an anomaly detection system is one important part in creating a computer-aided system that can ease the monitoring and analyzing the cardiac status of fetus and mother.

Todays, fetal monitoring is only focused on the fetal heart rate. However, detecting the fetal abnormal heartbeat rhythm does not take into account the waveform features of the fetal ECG (FECG), which is the basis of cardiac assessment in both children and adults. Lack of annotated datasets for FECG anomaly detection is one of the reasons that FECG arrhythmia detection needs more research. This is, partly due to absence of comprehensive clinical information about fetal cardiac function and in part, due to low signal to noise ratio of FECG compared to the maternal ECG. In this chapter, we utilized active learning for fine tuning the transfer learning model for FECG arrhythmia detection. In the first step, we used Massachusetts Institute of Technology-Beth Israel Hospital (MIT-BIH) Arrhythmia Database for training a deep learning model to classify adult ECG beats into normal and abnormal categories. Then, we used the trained model as base learner for FECG arrhythmia detection on Non-Invasive Fetal ECG Arrhythmia Database (NIFEA DB). The NIFEA DB is not annotated for FECG beats and it is annotated using active learning by a medical doctor. The sampling process of the proposed active learning is modified to select least number of samples from all data distribution. Moreover, the sampling process select the lowest confidence sample after model calibration, which improve the selection reliability. We evaluated the proposed approach performance by eliminating each important components and comparing the results with and without them. The proposed method could achieve 92% accuracy for FECG anomaly detection using 399 training samples. In contrast, training a model with random weight using active learning required twice annotation data. The annotation effort can even be increased about three times when there is no active learning and transfer-learning. The proposed method has potential to be used in clinical machine learning, where the annotation is costly and hard to achieve. Following are the results from the proposed method.

- The knowledge learned while identifying adult ECG anomalies can be applied to classifying FECG anomalies.

- When the target domain data is low quality and lacks annotation, combining transfer-learning with active learning can enhance model performance.
- Active learning annotation effort can be reduced by sampling from different parts of the data distribution.
- Training an autoencoder on the source and target domains can assist in the coverage of all data distribution in sampling strategy.
- Prior to sampling, calibration of the confidences can decrease the number of samples required for annotation.

The analysis and findings of this chapter is under-review in the *Computer Methods and Programs in Biomedicine Update journal*. The student contributed to designing a software for annotation, training model in each step, reporting results, writing the original draft, and revision of the manuscript.

Semi-Supervised Active Transfer Learning for Fetal ECG Arrhythmia Detection

Mohammad Reza Mohebbian*, Khan A. Wahid

Department of Electrical and Computer Engineering, University of Saskatchewan, Saskatoon, SK S7N 5A9, Canada.

*Corresponding author. Email: mom158@usask.ca

Abstract

Artificial intelligence, such as deep learning methods, has demonstrated excellent results for ECG anomaly detection, wherein majority of approaches used supervised learning. The requirement of thousands of manually annotated samples is a concern for state-of-the-art anomaly detection systems, especially for fetal ECG (FECG) that currently there is not a publicly available FECG dataset annotated for each FECG beat. In this work, we offer a modified active learning technique, based on transfer learning, calibration probability and autoencoder-based sampling, for reducing the need to annotate the majority of the FECG epochs in the dataset. In this regard, we used MIT-BIH Arrhythmia Database for training a deep learning model to detect anomaly on non-fetus subjects. Then we used unlabeled Non-Invasive Fetal ECG Arrhythmia Database (NIFEA DB) to fine-tune the trained model based on active learning to detect anomaly in binary form for fetal. A variational autoencoder is trained on all data (adult and fetal ECG) and clustering is applied on latent features extracted from data after dimension reduction. Then, the sampling process of active learning selected samples from different clusters that has low confidence to cover all data distribution. Moreover, a probability calibration based on mc-dropout and isotonic regression is used to calibrate confidences, helping to select reliable low confidence samples. Various ablation studies performed to show influence of each step, such as autoencoder-based sampling, calibration, and transfer learning, which showed the proposed method could achieve 92% accuracy on FECG arrhythmia detection with less effort in annotation.

***Index Terms*—FECG, Arrhythmia, Transfer learning, Active learning, Anomaly**

4.1 Introduction

About 1% of fetuses are found to have heart arrhythmias. 10% percent of these arrhythmias are thought to be potential causes of morbidity [1]. Obstetricians will be able to make the best decisions before and after delivery if the fetal heart is carefully monitored [2]. The best way to monitor a fetus's cardiac activity is to use magnetocardiography (MCG), however the

expensive cost of MCG makes it expensive for low- and middle-income economies [3]. Cardiotocography (CTG) and Doppler ultrasound are two current methods that have certain drawbacks. CTG, for example, can be used to determine the fetal heart rate (FHR) during the third trimester of pregnancy (after 28 weeks of pregnancy) and solely gives information on ventricular blood flow [4]. The widespread use of CTG monitoring in hospitals has also raised the prevalence of caesarean section deliveries [5]. When compared to CTG diagnosis, the signal quality of electrocardiography (ECG) offers better findings even at 20 weeks of pregnancy[4]. The fetal ECG (FECG) can be measured invasively by placing an electrode on the fetal scalp, but this can only be done after cervical dilation [6], which puts both the fetal and the mother at danger. The FECG signal can also be measured by putting electrodes on the mother's abdomen (AECG) [7].

Fetal and adult hearts have some structural differences [8]. The left ventricle is supposed to pump blood throughout the body after birth, whereas the right ventricle pumps blood to the lungs for oxygenation. On the other hand, in fetal, the placenta provides fetal oxygen; hence blood is no longer pushed to the lungs. Alternatively, both ventricles work together to circulate blood to the body (including the lungs). While the mechanical functionality of fetal heart differs from adult heart, its electrical activity is quite comparable beat to beat [9]. Adults and fetal show comparable ECG patterns morphologically, but the relative amplitudes of the fetal complexes fluctuate throughout pregnancy and even after delivery [10]. As an instance, the T-waves, which are very weak for fetal and infants, undergo the most significant alteration.

Despite of high similarity of adult ECG and FECG, adult ECG processing has made significant advances in modern medicine [11], but FECG processing remains a significant issue [12]. Todays, fetal monitoring is only focused on the fetal heart rate [13]. The abnormal fetal heartbeat usually be categorized as tachy-arrhythmia (faster than 160 beats per minute) or brady-arrhythmia (slower than 120 beats per minute). However, detecting the fetal abnormal heartbeat rhythm does not take into account the waveform features of the FECG, which are the basis of cardiac assessment in both children and adults. The technology to accurately measure FECG is mainly unavailable, which is the fundamental reason for its exclusion from clinical settings. As a result, there hasn't been much study linking ECG features to FECG outcomes on a broad scale. Moreover, lack of gold standard datasets for FECG anomaly detection is another reason that FECG arrhythmia detection needs more research. This is, partly due to absence of comprehensive clinical information about fetal cardiac function and in part, due to low signal to noise ratio of FECG compared to the maternal ECG [12].

Deep learning has been one of the best effective machine learning methodologies in the last decade [14]. A deep learning model requires on the availability of a large dataset for training to learn the dataset's interesting features; accordingly, training the model with a limited dataset typically results in an overfitted model. Transfer learning (TL) is a popular technique for

dealing with data limitation [15] that obtain information in one problem domain and transferring it to a different but similar problem. For example, the knowledge learned while identifying adult ECG anomalies may be applied to classifying FECG anomalies. The transfer learning models usually require to be fine-tuned on small portion of new domain data. This can decrease the effort of labeling large number of datasets, however, manually annotating data is still costly and time-consuming, especially when subject expertise is required. Therefore, utilizing active learning in combination of transfer learning can help to reduce more annotation efforts.

In this work we utilized active learning for fine tuning the transfer learning model for FECG arrhythmia detection. In the first step, we used MIT-BIH Arrhythmia Database for training a deep learning model to classify adult ECG beats into normal and abnormal categories. Then, we used the trained model as base learner for FECG arrhythmia detection on Non-Invasive Fetal ECG Arrhythmia Database (NIFEA DB). The NIFEA DB is not annotated for FECG beats. Therefore, we applied the base learner on the data and beats from various part of data distribution that has less confident than others are sampled for annotation. The data distribution is estimated by training an autoencoder and clustering encoded features. Moreover, the reliability of confidences is improved using probability calibration schemes. Annotated samples are used for fine tuning of the model and this process is continued until all termination criteria is met. The final calibrated model is applied on portion of unlabeled data and result is evaluated by an expert.

The rest of this paper is organized as follows: in the next section, information about signals and formulation of methods used in this study is presented. Section 3 provides the results of the proposed method. The discussion is provided in section 4, and the last section is the conclusion.

4.2 Materials and methods

4.2.1 Dataset

The MIT-BIH Arrhythmia Dataset [16,17] includes 48 half-hour samples of two-channel ambulatory ECG recordings acquired from 47 patients examined by the BIH Arrhythmia Laboratory. Across a 10-mV range, the recordings were collected at 360 samples per second per channel using 11-bit resolution. Each record was separately annotated by two or more cardiologists, and differences addressed in order to get the computer-readable benchmark annotations for each beat. About 110,000 annotations in total is provided in the database. In this research, we used 25000 seconds of annotated data randomly to have balance number of classes. We used four types of anomalies in abnormal samples, including left bundle branch block beat, right bundle branch block beat, atrial premature beat, and premature ventricular contraction. The reason is that these types of anomalies are more popular and can also happen for fetal.

The Non-Invasive Fetal ECG Arrhythmia Database [1] (NIFEA DB) contains a collection of non-invasive FECG recordings of fetal arrhythmias (n=12) and control normal rhythm recordings (n=14) which is available from February 2019. A set of four or five abdominal channels and one chest maternal signal were collected for each record. The dataset comprises 500 recordings that were continuously collected for various times ranging from 7 minutes to 32 minutes. One chest lead and four to five abdominal leads (recorded using five–six abdominal electrodes on the maternal belly and two chest electrodes) are included in the records. The sampling rate was either 500 Hz or 1 kHz. This data is annotated by a medical doctor based on instructions provided by a cardiologist.

4.2.2 Proposed method

The block diagram of the proposed method is depicted in Figure 4.1. In the first step, a deep learning model is trained on the MIT-BIH Arrhythmia Dataset. The trained model is then transferred to active learning process for learning fetal arrhythmia. The FECG signals are extracted from abdominal MECG in NIFEA DB, and a part of the extracted data is used as training set. The training set is fed to the transfer learning model and arrhythmia along with confidence are predicted. The model is calibrated using probability calibration and calibrated predictions are used for sampling step. FECG beats with low confidence from various data distributions, as determined by an autoencoder, are taken in the sampling step. Finally, these beats are annotated by a medical doctor and are added to the training process. This process continue until the termination criteria is met. More details are provided in the next subsections.

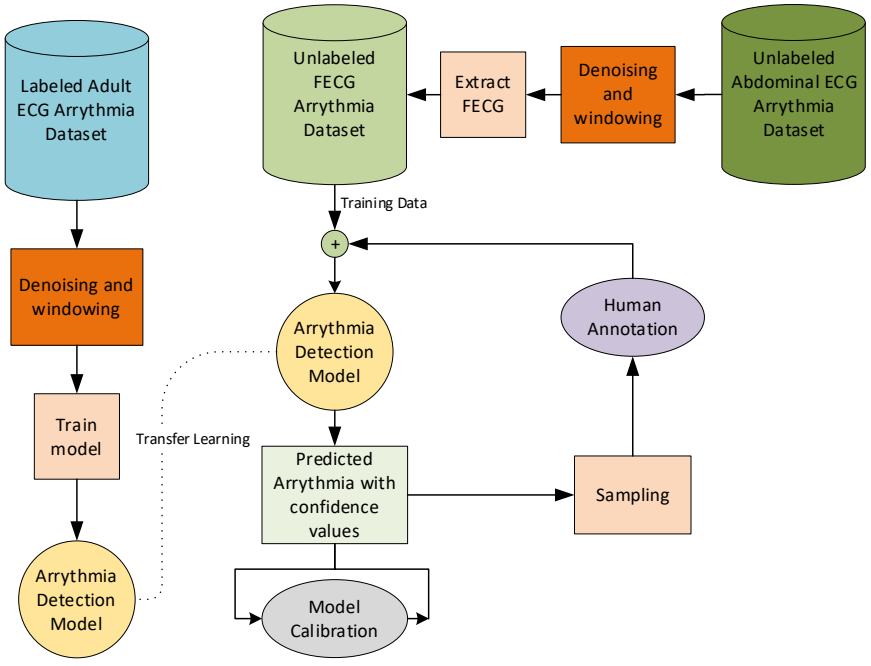

Figure 4-1. The block diagram of the proposed semi-supervised transfer active learning for FECG arrhythmia detection.

4.2.2.1 Data preparation

4.2.2.1.1 Denoising and windowing

ECG signals are commonly contaminated by various noises throughout collecting and transmission in the real world. Multiresolution, a branch of the wavelet transform, has produced excellent results in noise reduction processing in a variety of disciplines, including ECG signal [18], speech signal [19], and images [20]. Multiresolution, on the other hand, is highly dependent on selected wavelet threshold and wavelet function. The best choice for finding maximum decomposition level is stopping decomposition when the signal becomes shorter than the FIR filter length for a specific wavelet [21]. Moreover, many scholars perceived the Symlet wavelet transform to be the best wavelet family for ECG denoising [22,23].

In this regard, we used Sym4 [22–25] for denoising and the threshold for filtering coefficient is selected based on Wang et al. [22] method that use adaptive thresholding for each level. If a consistent global threshold is used, the same frequency band may be removed at different decomposition levels, causing the original signal to deviate from its original shape.

In the next step, signals are normalized using z-score normalization [26] and all signals are resampled to 360 Hz to have less computational cost and be same as MIT-BIH Arrhythmia Dataset sampling rate. Then, the non-overlapped rectangular sliding window is performed on all signals with size 2 second (720 samples) to guarantee that at least one ECG beat present in each window and normal and abnormal rhythms can be annotated.

4.2.2.1.2 Extract FECG

Mohebbian et al. [27] provided a methodology for ECG deconvolution that can be used for FECG extraction from abdominal maternal ECG. The proposed method works based on combination of blind source separation and adaptive filters. Since ECG Signals are non-stationary, adaptive filters are often achieving a good result on them [28]. Because adaptive filters can alter their parameters in response to the signal changes. However, adaptive filters have the drawback of requiring a reference signal. In this regard, blind source separation technique is used to estimate a reference for each iteration of adaptive filter. Although in this research, the described method is used for extracting FECG, any other method that can extract FECG accurately can be used.

4.2.2.2 Arrythmia detection model

The baseline model is used for training consists of four layers. The first and second layers are similar in architecture and have one dimensional convolutional layer (Conv1D) [29], batch normalization and rectified linear unit (ReLU) activation function [30]. In the next, the global max pooling in one dimension is applied on the output of the second layer. Finally, a Dense layer with softmax is used as classification layer. The model is trained using Adam optimizer and categorical cross entropy loss. This architecture is selected because in other works it is also used as one of the best architectures for time series data classification [31]. Figure 4.2 shows the proposed architecture.

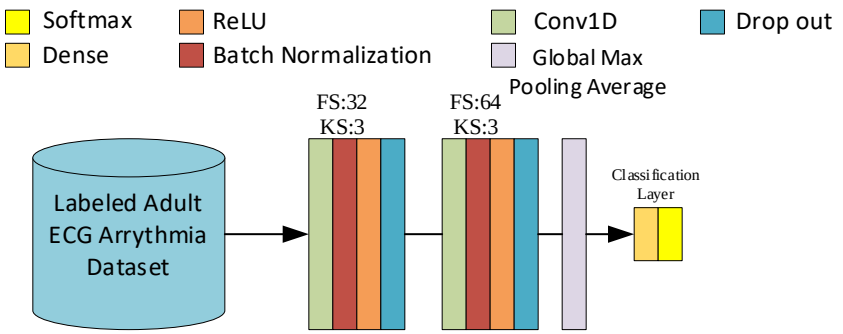

Figure 4-2. Arrhythmia detection model. FS: filter size; KS: kernel size. Kernel size: length of filter; Filter size: number of filters.

The MIT-BIH Arrhythmia Dataset is separated to training (20000 seconds) and test sets (5000 seconds), wherein samples from one subject are not presented in training and test simultaneously. Then, model is trained using training data and is evaluated on test set. This model is used as transfer-learning model for active learning in the next step.

4.2.2.3 Active learning for FECG arrhythmia detection

The aim of active learning is to decide which data must be annotated in order to build the model as rapidly as possible using a source of unlabeled data [32]. This implies that rather than asking experts to annotate all the data, we choose which pieces of information should be annotated. Appropriate sampling of unlabeled data for annotation has two conditions. First, we are willing to annotate samples that cover most of the data distribution [33]. Second, we are interested in annotating samples that model has not enough confidence in predicting their labels.

4.2.2.3.1 Sampling

For meeting the first condition, understanding of underlying data distribution is crucial. One of the solutions for estimating data subspaces is extracting latent features from samples. In this regard, we combined MIT-BIH Arrhythmia Dataset and NIFEA DB and trained a variational autoencoder to extract latent representation of data [34]. Autoencoder works unsupervised and extracts latent features which can represent data distribution. Figure 4.3 shows the proposed autoencoder for extracting latent representation.

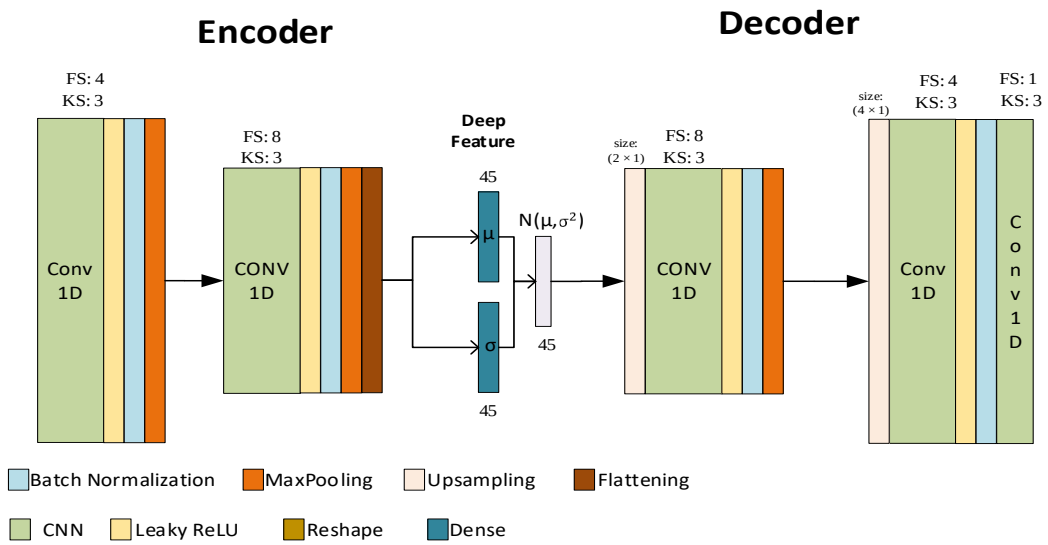

Figure 4-3. Autoencoder model used for extracting latent representation of data. FS: filter size; KS: kernel size.

t-Distributed Stochastic Neighbor Embedding (t-SNE) is a dimensionality reduction technique that is ideally suited for the visualization of high-dimensional data [35]. This technique helps to visualize data distribution and we used it to reduce dimension of latent features (μ) to two. In the next step, we cluster reduced latent features, using Ordering Points to Identify the Clustering Structure (OPTICS) to create clusters that cover different parts of data distributions. OPTICS [36], has been shown to be appropriate for problems that have clusters with different dispersions across various density-based clustering algorithms. It does not require several runs on various pre-defined cluster numbers, unlike K-means or any other aggregative clustering process. There is one parameter required for the OPTICS algorithm, namely MinPts, which show the minimum number of points in the cluster, and we set it to 5 to have clusters covering various data distribution.

After extracting clusters as representation for data distribution, FECG samples in NIFEA DB is split to train and test. The split is performed by choosing 70%, then 30% of FECG random samples from each cluster as training and test, respectively. This helps to split data wisely to have data from different distribution in all sets. The test set is annotated by a medical doctor to evaluate the proposed method.

Next, the trained model in previous step (trained on MIT-BIH Arrhythmia Dataset) is calibrated using MIT-BIH Arrhythmia Dataset and calibrated model is applied on trained set of FECG samples. Then, from each cluster 1 samples with lowest confidence that satisfies <0.5 is selected for annotation. Annotated samples will be added to training data and the model is calibrated based on new training data and the process continues.

It is worth mentioning that sampling has another condition that selected beats should not have high similarity and this condition will be satisfied automatically owing to clustering and autoencoder latent features characteristics. Moreover, the autoencoder and clustering only need

to be performed at first, however, calibration and sampling will continue until termination criteria is met. The termination criteria include not having samples with low confidence (<0.5) in each cluster, or not improving more than a percent accuracy after two iterations on test set. In the next, the probability calibration method is explained.

4.2.2.3.2 Calibration

Assessing the uncertainty is as important as model accuracy. Since calibration change the output probabilities to increase generalization, it would help the sampling of active learning approach to select the most difficult samples for annotation. A general framework for dealing with uncertainty is provided by Bayesian techniques. However, Bayesian uncertainty sometimes fail to estimate the actual data distribution. Recently Gal et al.[37] , and Lakshminarayann et al. [38] presented uncertainty estimating approaches for deep neural networks, which included ensemble methods, heteroscedastic regression, and concrete dropout. We adopted the recent method proposed by Kuleshov et al. [39] that is a model agnostic approach and combined it with Gal et al. [40] for calibrating the model for active learning.

Since the softmax layer is assumed as a conversion between probability and target class prediction, how much of the softmax scores may be taken as probability is debatable. The neural network's training procedure aims to make the softmax scores of the training samples close to the target. Hence, if the model can achieve 100% training accuracy, it can simply increase the final weight layer to become extremely confident in the training set, however this makes the model excessively confident in any input. To deal with this issue, Gal et al. [40] demonstrated that by passing the input through the network several times with dropout enabled and then averaging the output softmax scores, we can approximate the posterior probability over the labels. Inference is achieved by training a model with dropout layers, as well as estimating posterior probability at test time with drop out layers.

Kuleshov et al. [39] proposed calibrating algorithm that is motivated by Platt scaling. To calibrate outcomes in model agnostic way, recalibration approaches train an auxiliary model on top of a trained predictor. This model will be trained somehow that when a predictor gives an event a chance of 0.8, it should happen roughly 80% of the time. Besides, sharp estimates are also required, which imply that probability should be near to zero or one. Suppose predictor $H: x \rightarrow (y, c)$, where x is input, y is output, and c is its probability. $R(H(x))$ is calibrated by fitting a regression R on c. Kuleshov et al. proposed an efficient and simple approach for finding R. In this regard, an isotonic regression for mapping empirical probabilities and predicted probabilities is used for R. Reliability plot [41] is the best way to assess calibrated outputs. In this regard, output probability (c) is grouped to 15 intervals, such as [0,0.06], [0.06,0.13], …, and average of estimated probabilities is plotted before and after calibration.

4.3 Results

To have consistent results on baseline model, the whole algorithm ran 5 times with shuffling. Each time the proposed model presented in Figure 4.2, is trained on the training set of MIT-

BIH Arrhythmia dataset and is evaluated on test set. Finally. Figure 4.4 shows the Accuracy, Area Under the Curve (AUC), F1-score and Matthew Correlation Coefficient (MCC) results of all runs on test set using boxplot. In average, 93.8 ± 1.6% Accuracy is achieved.

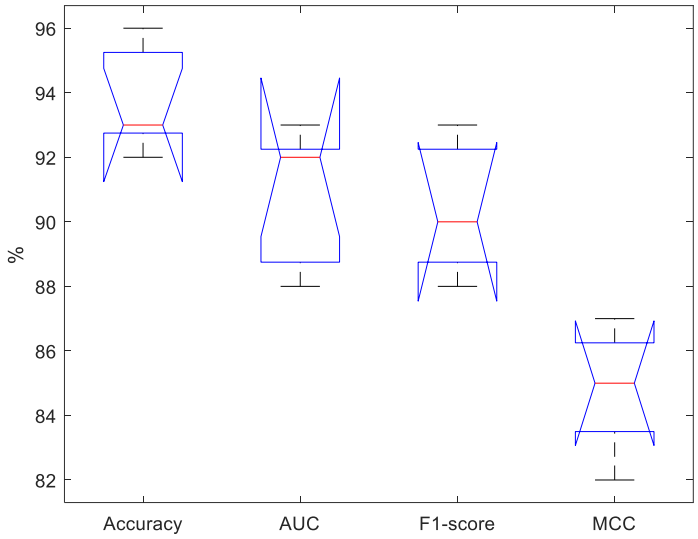

Figure 4-4. Performance of the arrhythmia detection model on MIT-BIH Arrhythmia Dataset using hold-out validation based on 5 times running with shuffling.

In the next step, the trained baseline model is evaluated on test set of extracted FECG NIFEA DB using proposed active learning method. Figure 4.5 shows an example of extracted FECG. All extracted signals quality is checked by doctor.

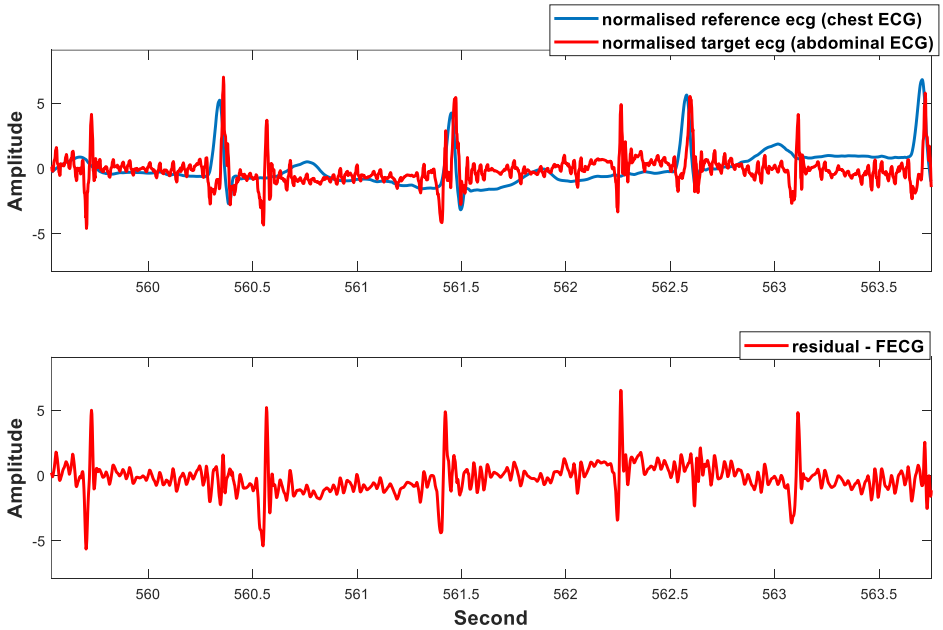

Figure 4-5. An example of extracted FECG from NIFEA DB.

Figure 4.6 shows the performance of active learning algorithm with different number of training samples before and after calibration. When number of training samples is zero, results

represent the transfer-learning approach performance. It is also worth mentioning that uncalibrated results presented in Figure 4.6 does not mean that calibration process is removed from active learning process, however, it shows the accuracy of model before applying calibration in each step. To shed light on it, the uncalibrated model in second iteration of active learning is trained on selected samples from calibrated model in the first iteration. The effect of detaching calibration from the proposed method is discussed in the discussion.

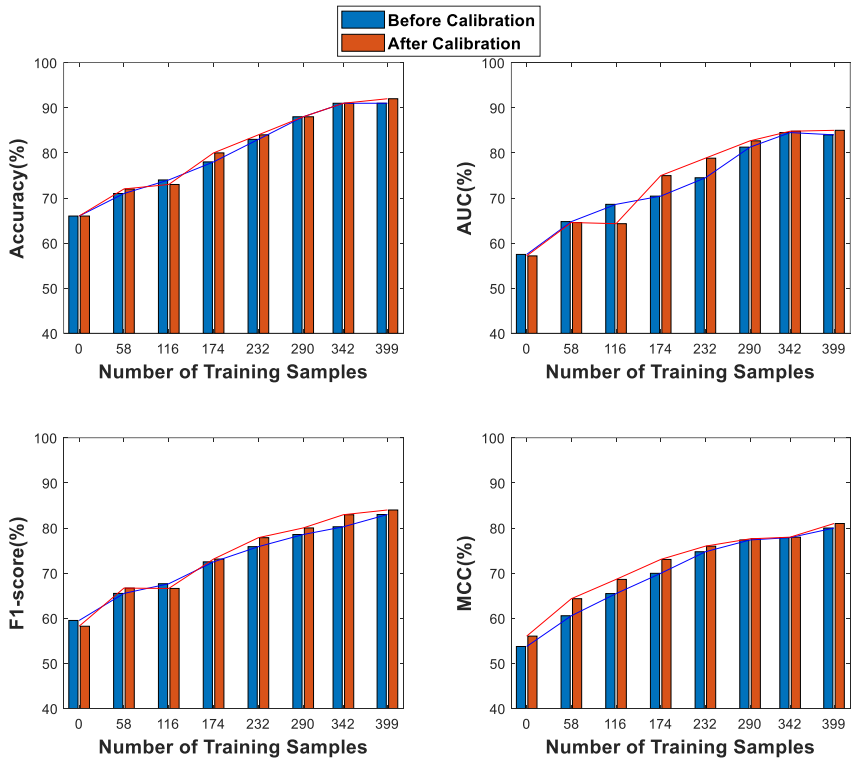

Figure 4-6. Performance of the arrhythmia detection model on test set of FECG NIFEA DB using active learning.

Training samples are selected in each step using lowest confidence samples in each cluster of encoded features. Figure 4.7 shows the t-SNE plot of all latent vectors acquired after training autoencoder (left image). Besides (right image), it shows the estimated clusters by OPTICS. Totally, 137 clusters are selected with minimum number of 5 samples in each cluster. From all clusters, only 58 clusters contain FECG samples. Hence, number of samples in the first epoch is 58 in the Figure 4.6.

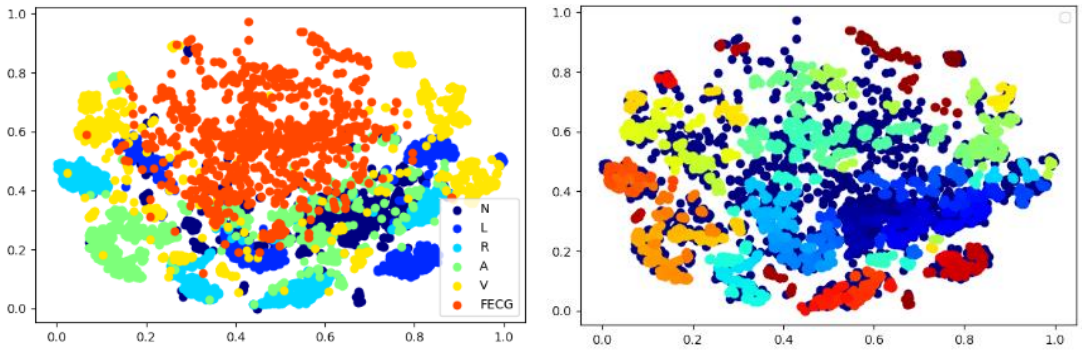

Figure 4-7. Left plot: t-SNE plot of latent features obtained from autoencoder training on adult (labeled data) and FECG dataset (unlabeled data). Right plot: Clustering latent features irrespective to their labels for acquiring data distribution. Each color in right subplot shows a cluster. There are 137 clusters, however we plot as much as possible. L: left bundle branch block beat; R: right bundle branch block beat; A: atrial premature beat; V: premature ventricular contraction.

The effect of calibration is demonstrated as reliability plots in Figure 4.8 for some iterations. The trained model predictions are underconfident and using 50% of the confident as threshold is not feasible for proposed active learning. However, the calibration helps to improve reliability of predictions; as a result, threshold 50% can be used after calibration. It is worth mentioning that reliability plots are shown for test set while calibration is performed on all training data from adult and fetal ECG.

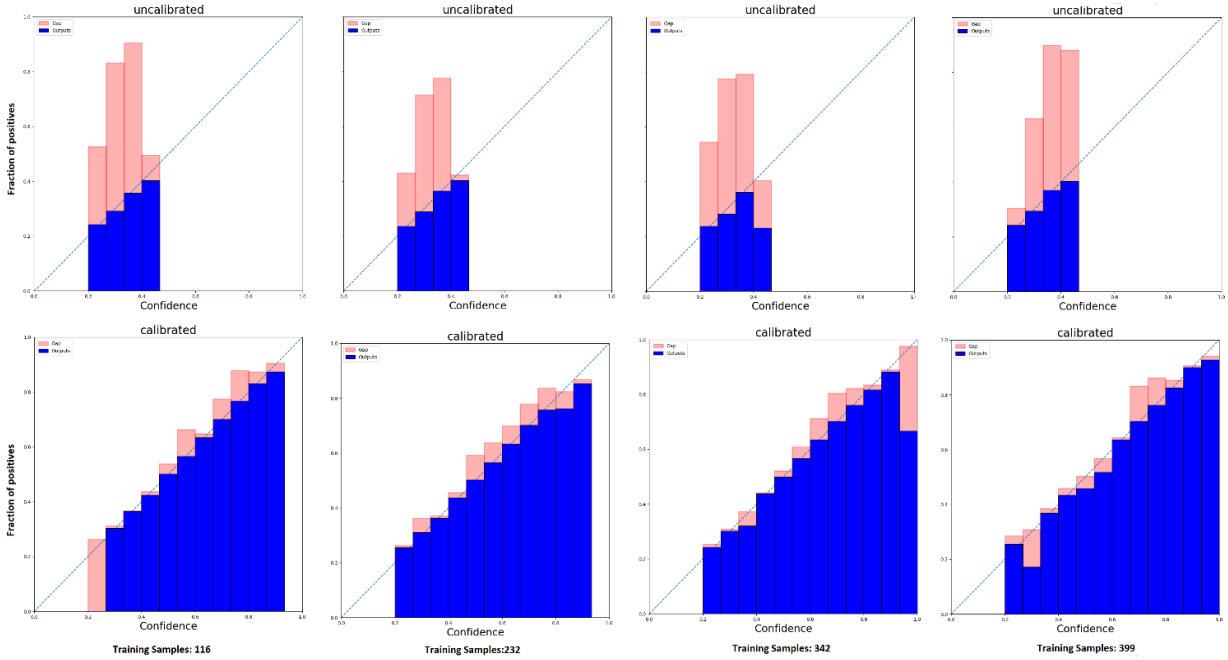

Figure 4-8. Top: Reliability plots before calibration. Bottom: Reliability plot after calibration. A complete reliability is indicated by a diagonal line. Red bars show the gap between accuracy and confidence. When the red bar crosses the diagonal, the accuracy exceeds the confidence, indicating that the model is not confident enough.

4.4 Discussion

The challenge of choosing the smallest possible sample of data to label and train a high-performance ML can be handled by Active Learning. The sampling process, wherein samples

are chosen for annotation by expert and trained using the model, is an essential element of active learning. We resolved the sampling problem by leveraging the autoencoder power to have a variety of samples and calibration to select the most uncertain samples. In the next, we conducted some ablation studies to evaluate influence each step of the proposed method.

While deep learning increases objective accuracy, they don't appear to be able to correctly communicate their confidence in the result [42]. A softmax as activation and cross-entropy loss are supposed to do the calibration job, however it seldom works that way in reality. Moreover, batch normalization is another factor that has negative effect on calibration regardless of hyperparameters. Therefore, we used the proposed calibration scheme on top of the model uncertainty predictions. On the other hand, the classification error does not change when the model depth and width is increased. However, the calibration appears to be deteriorating. This fact is reported by other researches too [37,42].

Nevertheless, we removed the calibration and applied the training. Since the threshold 50% on confidence is not applicable without calibration, we only selected the lowest confidence from each cluster. Figure 4.9 shows the comparison of the Accuracy with and without calibration. It is clear that calibration helped the process to reach the higher performance faster. Concisely, the proposed method could achieve 92% Accuracy on test set using 399 training samples, while without calibration 512 training samples is required which means more effort in annotation.

In the next ablation study, we removed the autoencoder and clustering for sampling from the dataset for annotation. Instead of that, we sorted predictions based on confidence after calibration and we selected 60 samples every iteration. 60 samples are selected to be comparable with proposed sampling approach. Figure 4.9 shows that the autoencoder and clustering approach helps the training to improve faster and with less effort. In other words, the proposed method without autoencoder requires 540 training samples to reach to the accuracy 92%. It is also worth mentioning that in most of the active learning iterations, the performance of the method without autoencoder is over than the method without calibration, which shows the importance of calibration.

The proposed deep learning approach is also trained without transfer-learning model. In other words, random weights are assigned to the network and the proposed active learning scheme is used for training. It is clear that transfer learning has a paramount effect on faster convergence. Furthermore, a model with random weight is trained in traditional way without active learning, while in every step 60 samples randomly are added to the training. The final comparison plot help to evaluate each step of the proposed method and show the effectiveness of the active learning.

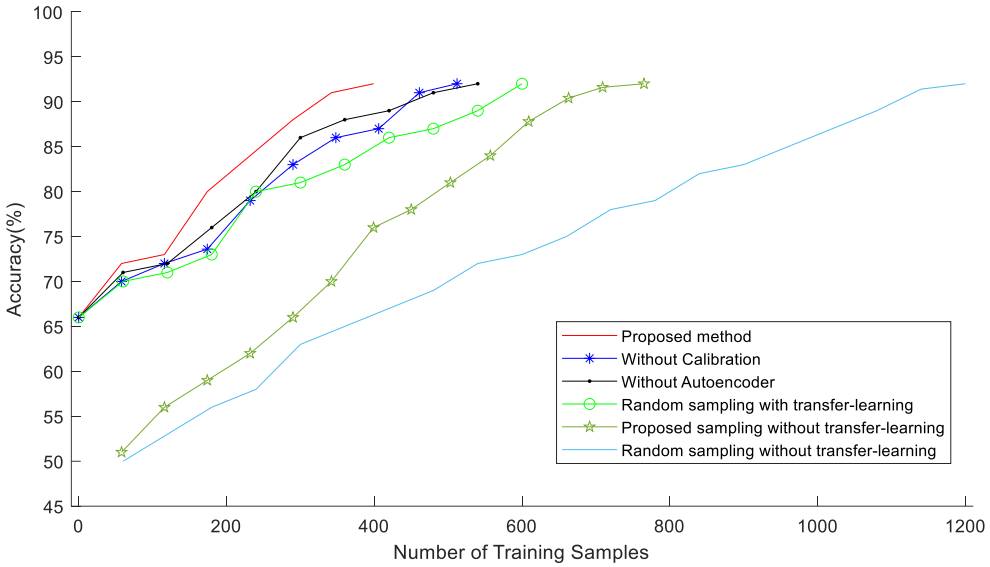

Figure 4-9. Ablation studies for evaluating the effectiveness of autoencoder, calibration, and transfer-learning in active learning. The proposed method can achieve 92% accuracy in much less iterations when it uses calibration, autoencoder and transfer-learning.

Currently, there is limited data on FECG arrhythmia, and more technological improvements are required to achieve cleaner signal that can accurately filter out maternal noise and baseline wandering. The early results of detecting FECG arrhythmia are encouraging; nevertheless, additional data is needed to fully comprehend its diagnostic accuracy in FFEG arrhythmia diagnosis.

4.5 Conclusion

We proposed a novel method for active learning of FECG anomaly detection based on recent advancements in autoencoders and probability calibration. First, we trained a model for detecting anomaly in adult ECG which could achieve 93.8% accuracy based on the MIT-BIH Arrhythmia Dataset. Then, the model is used for active transfer-learning approach. The sampling process of the proposed active learning is modified to select sample from all data distribution that is calculated based on latent feature of autoencoder. Moreover, the sampling process select the lowest confidence sample after model calibration, which improve the selection reliability. We evaluated the proposed approach performance by eliminating each important components and comparing the results with and without them. The proposed method could achieve 92% accuracy for FECG anomaly detection using 399 training samples. In contrast, training a model with random weight using active learning required twice annotation data. The annotation effort can even be increased about three times when there is no active learning and transfer-learning. The proposed active learning approach has potential to be used in clinical machine learning, where the annotation is costly and hard to achieve.

4.6 References

[1] J.A. Behar, L. Bonnemains, V. Shulgin, J. Oster, O. Ostras, I. Lakhno, Noninvasive fetal electrocardiography for the detection of fetal arrhythmias, Prenat. Diagn. 39 (2019) 178–187.

[2] E. Keenan, C. Karmakar, F.C. Brownfoot, M. Palaniswami, Personalized Anatomic Modeling for Noninvasive Fetal ECG: Methodology and Applications, IEEE Trans. Instrum. Meas. 70 (2021) 1–12.

[3] S. Strand, W. Lutter, J.F. Strasburger, V. Shah, O. Baffa, R.T. Wakai, Low-cost fetal magnetocardiography: a comparison of superconducting quantum interference device and optically pumped magnetometers, J. Am. Heart Assoc. 8 (2019) e013436.

[4] R.G. Sæderup, H. Zimmermann, D.H. Eiríksdóttir, J. Hansen, J.J. Struijk, S. Schmidt, Comparison of cardiotocography and fetal heart rate estimators based on non-invasive fetal ECG, in: 2019 Comput. Cardiol. CinC, IEEE, 2019: p. Page 1-Page 4.

[5] P. Chetandas, S. Zahiruddin, N. Jabeen, R. Baloch, F. Shaikh, Increasing rate of Caesarean Section Due to Non-Reassuring Cardiotocography, Open J. Obstet. Gynecol. 7 (2017) 351–357.

[6] T.Y. Euliano, S. Darmanjian, M.T. Nguyen, J.D. Busowski, N. Euliano, A.R. Gregg, Monitoring fetal heart rate during labor: a comparison of three methods, J. Pregnancy. 2017 (2017).

[7] A. Agostinelli, M. Grillo, A. Biagini, C. Giuliani, L. Burattini, S. Fioretti, F. Di Nardo, S.R. Giannubilo, A. Ciavattini, L. Burattini, Noninvasive fetal electrocardiography: an overview of the signal electrophysiological meaning, recording procedures, and processing techniques, Ann. Noninvasive Electrocardiol. 20 (2015) 303–313.

[8] E. Hernandez-Andrade, M. Patwardhan, M. Cruz-Lemini, S. Luewan, Early evaluation of the fetal heart, Fetal Diagn. Ther. 42 (2017) 161–173.

[9] A.V. Rajesh, R. Ganesan, Comprehensive study on fetal ECG extraction, in: 2014 Int. Conf. Control Instrum. Commun. Comput. Technol. ICCICCT, IEEE, 2014: pp. 1187–1192.

[10] N.J. Randall, P.J. Steer, I.A. Sutherland, Detection of the fetal ECG during labour by an intrauterine probe, J. Biomed. Eng. 10 (1988) 159–164.

[11] H. Li, P. Boulanger, A survey of heart anomaly detection using ambulatory Electrocardiogram (ECG), Sensors. 20 (2020) 1461.

[12] M. Anisha, S.S. Kumar, E.E. Nithila, M. Benisha, Detection of Fetal Cardiac Anomaly from Composite Abdominal Electrocardiogram, Biomed. Signal Process. Control. 65 (2021) 102308.

[13] M. Suganthy, S.I. Joy, P. Anandan, Detection of fetal arrhythmia by adaptive single channel electrocardiogram extraction, Phys. Eng. Sci. Med. (2021) 1–10.

[14] Z. Ebrahimi, M. Loni, M. Daneshtalab, A. Gharehbaghi, A review on deep learning methods for ECG arrhythmia classification, Expert Syst. Appl. X. 7 (2020) 100033.

[15] J.-H. Jang, T.Y. Kim, D. Yoon, Effectiveness of Transfer Learning for Deep Learning-Based Electrocardiogram Analysis, Healthc. Inform. Res. 27 (2021) 19–28.

[16] A.L. Goldberger, L.A. Amaral, L. Glass, J.M. Hausdorff, P.C. Ivanov, R.G. Mark, J.E. Mietus, G.B. Moody, C.-K. Peng, H.E. Stanley, PhysioBank, PhysioToolkit, and PhysioNet: components of a new research resource for complex physiologic signals, Circulation. 101 (2000) e215–e220.

[17] G.B. Moody, R.G. Mark, The impact of the MIT-BIH arrhythmia database, IEEE Eng. Med. Biol. Mag. 20 (2001) 45–50.

[18] V. Gupta, M. Mittal, Arrhythmia detection in ECG signal using fractional wavelet transform with principal component analysis, J. Inst. Eng. India Ser. B. 101 (2020) 451–461.

[19] S. Sekkate, M. Khalil, A. Adib, S.B. Jebara, A Multiresolution-Based Fusion Strategy for Improving Speech Emotion Recognition Efficiency, in: Int. Conf. Mob. Secure Program. Netw., Springer, 2019: pp. 96–109.

[20] J.R.F. Raj, K. Vijayalakshmi, S.K. Priya, Medical image denoising using multi-resolution transforms, Measurement. 145 (2019) 769–778.
[21] A. Boggess, F.J. Narcowich, A first course in wavelets with Fourier analysis, John Wiley & Sons, 2015.
[22] L. Wang, W. Sun, Y. Chen, P. Li, L. Zhao, Wavelet transform based ECG denoising using adaptive thresholding, in: Proc. 2018 7th Int. Conf. Bioinforma. Biomed. Sci., 2018: pp. 35–40.
[23] N. Sivannarayana, D.C. Reddy, Biorthogonal wavelet transforms for ECG parameters estimation, Med. Eng. Phys. 21 (1999) 167–174.
[24] B. Castro, D. Kogan, A.B. Geva, ECG feature extraction using optimal mother wavelet, in: 21st IEEE Conv. Electr. Electron. Eng. Isr. Proc. Cat No 00EX377, IEEE, 2000: pp. 346–350.
[25] S.S. Rathore, N. Tripathi, Suppression of Noise in ECG by Optimal Wavelet Transform, Solid State Technol. 63 (2020) 11757–11767.
[26] S.K. Dhull, K.K. Singh, ECG beat classifiers: a journey from ANN To DNN, Procedia Comput. Sci. 167 (2020) 747–759.
[27] M.R. Mohebbian, M.W. Alam, K.A. Wahid, A. Dinh, Single channel high noise level ECG deconvolution using optimized blind adaptive filtering and fixed-point convolution kernel compensation, Biomed. Signal Process. Control. 57 (2020) 101673.
[28] E. Eweda, Comparison of LMS and NLMS adaptive filters with a non-stationary input, in: 2010 Conf. Rec. Forty Fourth Asilomar Conf. Signals Syst. Comput., IEEE, 2010: pp. 1630–1634.
[29] X. Hua, J. Han, C. Zhao, H. Tang, Z. He, Q. Chen, S. Tang, J. Tang, W. Zhou, A novel method for ECG signal classification via one-dimensional convolutional neural network, Multimed. Syst. (2020) 1–13.
[30] A.F. Agarap, Deep learning using rectified linear units (relu), ArXiv Prepr. ArXiv180308375. (2018).
[31] B. Zhao, H. Lu, S. Chen, J. Liu, D. Wu, Convolutional neural networks for time series classification, J. Syst. Eng. Electron. 28 (2017) 162–169.
[32] G. Wang, C. Zhang, Y. Liu, H. Yang, D. Fu, H. Wang, P. Zhang, A global and updatable ECG beat classification system based on recurrent neural networks and active learning, Inf. Sci. 501 (2019) 523–542.
[33] S. Sinha, S. Ebrahimi, T. Darrell, Variational adversarial active learning, in: Proc. IEEECVF Int. Conf. Comput. Vis., 2019: pp. 5972–5981.
[34] V.V. Kuznetsov, V.A. Moskalenko, D.V. Gribanov, N.Y. Zolotykh, Interpretable Feature Generation in ECG Using a Variational Autoencoder, Front. Genet. 12 (2021).
[35] L. Van der Maaten, G. Hinton, Visualizing data using t-SNE., J. Mach. Learn. Res. 9 (2008).
[36] J.C. Dassun, A. Reyes, H. Yokoyama, M. Dolendo, Ordering Points to Identify the Clustering Structure Algorithm in Fingerprint-Based Age Classification, Virtutis Incunabula. 2 (2015) 17–27.
[37] Y. Gal, J. Hron, A. Kendall, Concrete dropout, ArXiv Prepr. ArXiv170507832. (2017).
[38] B. Lakshminarayanan, A. Pritzel, C. Blundell, Simple and scalable predictive uncertainty estimation using deep ensembles, ArXiv Prepr. ArXiv161201474. (2016).
[39] V. Kuleshov, N. Fenner, S. Ermon, Accurate uncertainties for deep learning using calibrated regression, in: Int. Conf. Mach. Learn., PMLR, 2018: pp. 2796–2804.
[40] Y. Gal, R. Islam, Z. Ghahramani, Deep bayesian active learning with image data, in: Int. Conf. Mach. Learn., PMLR, 2017: pp. 1183–1192.
[41] J.J. Thiagarajan, B. Venkatesh, D. Rajan, P. Sattigeri, Improving reliability of clinical models using prediction calibration, in: Uncertain. Safe Util. Mach. Learn. Med. Imaging Graphs Biomed. Image Anal., Springer, 2020: pp. 71–80.
[42] A. Singh, A. Bay, B. Sengupta, A. Mirabile, On the Dark Side of Calibration for Modern Neural Networks, ArXiv Prepr. ArXiv210609385. (2021).

5 BLIND, CUFF-LESS, CALIBRATION-FREE AND CONTINUOUS BLOOD PRESSURE ESTIMATION USING OPTIMIZED INDUCTIVE GROUP METHOD OF DATA HANDLING

The blood pressure (BP) is used to monitor an individual's health, particularly to treat and prevent hypertension. Starling *et al* [5.1]. findings demonstrated that elevated maternal blood pressure in the second and third trimesters may increase the risk of fetal growth and alter the body composition of newborns. There have been studies associated to pre-eclampsia, gestational hypertension, and premature delivery to blood pressures that would classify as stage 1 hypertension during pregnancy [5.2].

Mercury sphygmomanometer is one of the traditional arterial BP measuring techniques that has been the "gold standard" for over 100 years. Inflating a cuff around the arm to obstruct blood flow in the artery is the basis for this measurement. After the cuff is gently deflated, an expert must listen for Korotkoff sounds using a stethoscope positioned on the brachial artery. The need of a cuff in BP devices limits their size reduction and makes them more difficult to use. Moreover, they cannot be used for continuous BP measurement.

Recent method attempted to use ECG and PPG for indirect continuous BP measurement. Some methods also used two PPG measurements. These approaches need the recording of synchronized signals in separate locations, making the system both costly and complex. We propose a system that estimate BP (systolic and diastolic) by only one PPG signal from fingertip. This makes the system lightweight, portable and appropriate for day-to-day monitoring mother even in home setup.

The analysis and findings of this chapter is reported in the below mentioned published journal manuscript. The student contributed to writing the original draft, recording samples from subjects, implementing codes for regression, implementing different ML models for comparison, and revision of the manuscript:

Mohebbian, M.R., Dinh, A., Wahid, K. and Alam, M.S., 2020. Blind, cuff-less, calibration-free and continuous blood pressure estimation using optimized inductive group method of data handling. *Biomedical Signal Processing and Control*, *57*, p.101682.

[5.1] Starling, A.P., Shapiro, A.L., Sauder, K.A., Kaar, J.L., Ringham, B.M., Glueck, D.H., Galan, H.L. and Dabelea, D., 2017. Blood pressure during pregnancy, neonatal size and altered body composition: the Healthy Start study. *Journal of Perinatology*, *37*(5), pp.502-506.

[5.2] Sisti, G. and Williams, B., 2019. Body of evidence in favor of adopting 130/80 mm Hg as new blood pressure cut-off for all the hypertensive disorders of pregnancy. *Medicina*, *55*(10), p.703.

Blind, Cuff-less, Calibration-Free and Continuous Blood Pressure Estimation using Optimized Inductive Group Method of Data Handling

Mohammad Reza Mohebbian[1], Anh Dinh[1], Khan Wahid[1], Mohammad Sami Alam[1]

[1] Department of Electrical and Computer Engineering, University of Saskatchewan S7N 5A9, Saskatoon, Saskatchewan, Canada

Corresponding Author: Anh Dinh

Email: anh.dinh@usask.ca

Abstract

Traditionally, blood pressure (BP) is measured by cuff-based instruments, which is inconvenient and does not allow continuous measurement. In fact, continuous blood pressure monitoring is precious for gaining information about the health conditions of people. In this work, an algorithm is developed using a modified group method of data handling technique to estimate systolic BP (SBP) and diastolic BP (DBP) by only photo-plethysmogram (PPG) signal in a continuous manner. The estimation does not require to calibration and is done without any knowledge about significant features, and features are selected based on their competency. The Multi-parameter Intelligent Monitoring in Intensive Care dataset is used for training the system, and the hold-out validation is used in 7 runs by assuming 70% of the samples as a train set. Moreover, a designed hardware device is used for recording data on 15 subjects for testing the trained model on the real-world. As the state-of-the-art, four popular regression algorithms, including support vector machine, adaptive boosting, decision tree and random forest, are trained with conventional features, which use an electrocardiogram (ECG) and PPG signals simultaneously and compared with the proposed system. The root means square error (RMSE) and the mean absolute error (MAE) of the proposed algorithm is 3.47 ± 1.31 and 2.40 ± 1.01 mmHg for SBP and 4.67 ± 1.44 and 3.33 ± 1.61 mmHg for DBP respectively. Also, the RMSE of the proposed algorithm on recorded data by hardware device is 3.4 ± 0.6 and *4.5* ± 1.1 mmHg, and the MAE is 2.2 ± 0.7 and 3.0 ± 1.2 mmHg for SBP and DBP, respectively. The proposed algorithm is not dependent on synchronization of ECG and PPG, and it is promising compared to the state-of-the-art, especially in recorded data by new hardware.

Keywords: Continuous Blood Pressure, Machine learning, Cuff-less, Calibration-free, Blind Regression

5.1 Introduction

Blood pressure is a vital sign of use every day to monitor the health of an individual, especially to control and prevent hypertension and cardiovascular diseases (CVD) [1, 2]. In Europe, more than 4 million deaths each year is caused by CVD [3]. It is predicted that in, up to 23.3 million deaths can be caused by CVD until 2030 [4], since the number of people with high BP is doubled the past two decades [5]. Increasing or decreasing BP in unusual ways can also bring high risk damages to kidney, liver, brain, vessels heart and other organs [6]. Due to an enormous number of people are under the effect of blood pressure disorders, many researchers are working to improve BP measurement methods inconvenience and accuracy [7, 8]. One of the conventional arterial BP measurement methods that have been the "gold standard" for over 100 years is mercury sphygmomanometer [9]. This measurement is based on inflating a cuff around the arm to impede the blood flow in the artery. After the cuff is deflated slowly, it requires an expert to recognize the Korotkoff sounds by a stethoscope which is placed on the brachial artery. The cuff pressures at the first and the fifth Korotkoff sounds represent the SBP and DBP respectively. This method is called the auscultatory technique [10]. The requirement of a cuff in BP devices restricts the further reduction in size and limits the ease of their usage [11].

Another well-known method that is used occasionally for day to day home healthcare is automatic BP meters [12]. These devices are created based on oscillometry or tonometry and can be used without a trained person [13]. Oscillometry is similar to the auscultatory technique which uses a cuff around the arm or wrist. In this technique, while the cuff is being slowly deflated, a pressure transducer is used to record the pressure oscillation instead of detecting the Korotkoff sounds. The maximum oscillation in BP is called the mean arterial BP [14]. SBP and DBP are approximated from the mean blood pressure using the oscillation pattern. One of the main disadvantages of this method is the low precision through the approximation of SBP and DBP [15]. However, the tonometry-based method is different. Although the cuff exerts a pressure to the artery to press it against the bone, the pressure is not as intense as to occlude the artery completely [16]. Therefore, various tonometry technique, such as vascular unloading, pulse wave velocity (PWV) and pulse transit time (PTT) have been introduced in the literature [17, 18]. Nevertheless, these methods usually have some disadvantages. First, they usually have lower accuracy than cuff-based methods owing to the annoying interference that raises from smooth muscles inside the arterial wall [19, 20]. Moreover, the calibration process of these devices is still tricky due to their dependency to individual physiological parameter [21]. Various research in the literature concentrated on cuff-less blood pressure estimation [4, 12, 22, 23]. Poon and Zhang extracted pulse transit time (PTT) from PPG and ECG in 45 seconds and used Moens-Korteweg's formula for DBP and SBP estimation [12]. The results achieved a 2.8 ± 6.8 and a 0.9 ± 5.6 mmHg mean difference for DBP and SBP respectively [12]. However, they used the range of 122 ± 21 and 64 ± 9 mmHg for SBP and DBP estimation; hence, the algorithm works only in this limited range. Zheng et al. created a

wearable armband for measuring SBP by PTT analysis in 30 minutes intervals of ECG and PPG and achieved a 2.8 ± 8.2mmHg as the root mean square error (RMSE) [4]. Kachuee et al. designed two algorithms based on regression algorithms for estimating SBP and DBP in continuous method [22]. They achieved a mean absolute error (MAE) of 5.35 ± 6.14 and a 11.17 ± 10.09 mmHg for DBP and SBP respectively with the AdaBoost algorithm as the best method among different learners such as linear regression, decision tree, SVM and RF. Earlier of this research, they used support vector regression in another approach and achieved a 6.34 ± 8.45 and a 12.38 ± 16.17 mmHg for DBP and SBP respectively [23]. Attarpour et al.[24] used a synchronized PPG recording on fingertip and wrist and utilized a genetic algorithm to find an optimal feature subset among 38 features, for applying to a multi-layer neural network and achieved MAE 4.94 and 4.03 mmHg for SBP and DBP respectively. Liu et al. used only PPG signal and its second derivative for estimating BP MAE 8.5 ± 10.9 and 4.3 ± 5.8 mmHg for SBP and DBP respectively on Multi-parameter Intelligent Monitoring in Intensive Care (MIMIC) database [25]. They extracted 14 new features from PPG and its second derivative.

Concisely, using conventional features such as PTT and PWV, etc. need to record ECG with PPG or record two synchronized PPG in separate locations. This makes the system expensive and complicated. This paper presents a new method to estimate SBP and DBP based on simply recorded one PPG signal from the fingertip. The algorithm is based on signal processing and optimized group method of data handling (GMDH) algorithm, called Optimized Inductive GMDH (OIGMDH) [26], to estimate SBP and DBP in a cuff-less, calibration-free, precise and continuous approach without having information about significant features in PPG and without using the reference ECG signal. As such technique, this method is called a blind method. In this regard, the proposed framework does not need a synchronized recording of ECG and PPG and can be applied to various devices. The database for training framework is available at the UCI machine learning repository and also at the Phsysionet website called MIMIC [27]. Concisely, after pre-processing of plethysmograph signals, significant points are extracted. Then, optimized inductive learning based on modified group method of data handling for regression is trained with regularized least square and particle swarm optimization. The OIGMDH is applied on extracted points of the PPG to estimate the significant features and exerts weight to each feature by particle swarm optimization process to improve the accuracy of estimation of SBP and DBP at the same time. The rest of the paper is organized as follows: in the next section, information about the signals and formulation of methods used in this study is presented. Section 3 provides the results of the proposed method. The discussion is provided in section 4, along with conclusions.

5.2 Materials and methods

5.2.1 Datasets

In this study, the Multi-parameter Intelligent Monitoring in Intensive Care (MIMIC) dataset [27] is used for training the model. The dataset consists of a lot of parameters such as age,

heart rate, ECG, PPG, Bilirubin, Leukocytosis, Anemia and so on, which we used 30 seconds of Arterial Blood Pressure (ABP) signal, ECG and PPG from 12,000 subjects [27]. The SBP and DBP should be extracted from ABP by finding peaks and valleys.

Furthermore, an in-house device for recording ECG and PPG signal was built. Figure 5.1 shows the device which includes a Raspberry Pi 2 (RP2) and a PIC microcontroller to sample ECG and PPG signals at 362Hz and send to the RP2. The ECG sensing circuitries are also shown in Figure 5.1. The ECG sensing uses capacitive sensors, the Electric Potential Integrated Circuit (EPIC) [28], made by Plessey Semiconductors. These sensors are equivalent to the standard ECG patches. The electrodes are isolated from the human body being measured to have protection and safety. A circuit was designed and built to receive ECG signal on the fingertips. The EPIC sensors pick up the signals from the thumbs to generate an ECG waveform. The PPG sensor is a low-cost heart rate sensor made by Sparkfun Electronics [29]. This sensor sends a light beam toward the finger, and a receiver captures and amplifies the reflected light to provide the PPG waveform. These two waveforms ECG and PPG are digitized by a small microcontroller having 10-bit ADC before sending to the Raspberry Pi for processing and displaying the blood pressures.

(b)

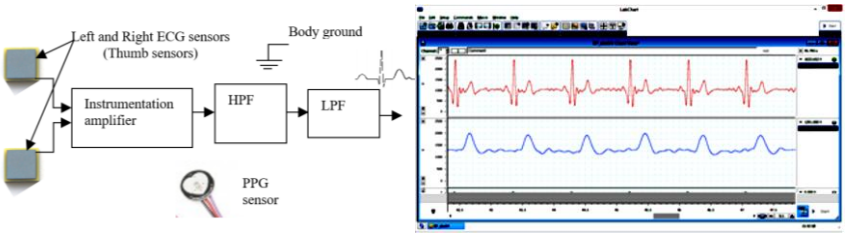

(c) (d)

Figure 5-1 A designed system based on Rasberry Pi (RP). (a) Top view with thumb ECG sensors, LCD, the PIC microcontroller is under the display to sample the signals and send to the Raspberry Pi, (b) Bottom view of the device showing the PPG sensor and the copper ground plate to ground the body to the circuit, (c) Simplified block diagram of the sensing system, and (d) ECG and PPG waveform displayed on an oscilloscope. The user places two thumbs at the ECG sensors while the two index fingers are in contact with the PPG sensor and ground underneath the RP. The device is powered with the USB of the RP power.

The trained system by the MIMIC database is applied for 15 subject signals in two minutes for each one. Each subject is selected from university students and the general public voluntarily and with different ethnicity. The experiments were conducted based on the Helsinki declaration principles and signed a written consent form. The outcome of the system is compared to the measured BP from the PortapresTM device as ground truth. The PortapresTM device is a portable ambulatory blood pressure monitoring system made by Finapres [30] which is depicted in Figure 5.2. This device is used in clinical diagnosis by other researchers [31], and it can be a reliable gold standard for continuous BP measurement.

Figure 5-2. The Portapres^{TM} device for measuring continuous BP

5.2.2 The proposed method

The structure of the OIGMDH is shown in Figure 5.3. Briefly, PPG signals are smoothed and filtered by Savitzky-Golay (SG) filter, then, are normalized. In the next step, significant points are extracted and fed into the inductive optimized learning procedure. The design of optimal inductive learning is based on the group method of data handling and regularized least square method that is combined with stochastic optimization, particle swarm optimization method. As the state-of-the-art, the OIGMDH is compared with four conventional machine learning algorithms, including AdaBoost, RF, SVM, and decision tree algorithm. The detailed information about each step mentioned above is provided in the sequel.

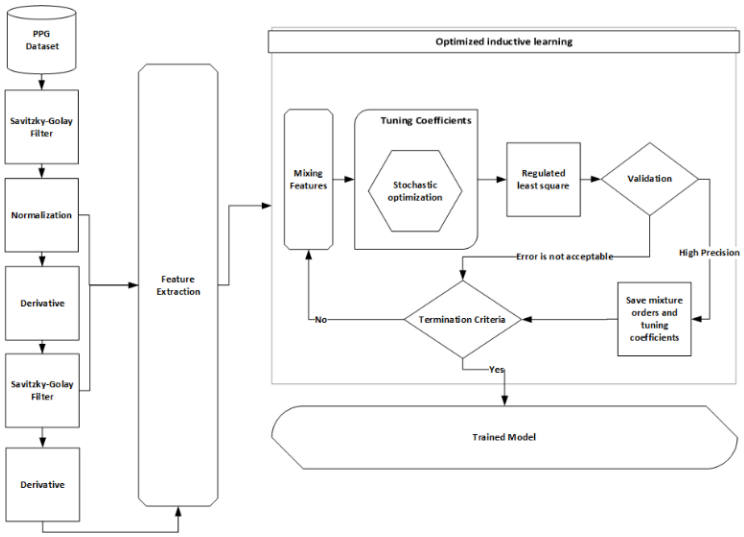

Figure 5-3. The block diagram of the proposed method. Left side is related to the pre-processing and extracting points of PPG and its derivatives. The optimized inductive learning block is the machine learning part which use different combination of features by creating mixing matrix. It uses PSO for tuning coefficients, then apply regulated least square for regression. This procedure continues until termination criteria is met.

5.2.3 Filtering

There are advance methods for de-noising PPG signals such as Empirical Mode Decomposition [32] and Discrete Wavelet Decomposition [33]. In this work, the Savitzky-Golay (SG) filter is used to remove baseline wandering (BW) and smooth the PPG as this is an FIR filter which is fast and easy to be implemented. The BW may be raised from the motion of the patients, changing electrode impedance or position, and also may be due to the instrument interferences. The SG filter fits consecutive subsets of contiguous data with a low-degree polynomial by the least square method. Then, the analytical solution of the least square method is used as a convolution coefficient for applying to other subsets.

SG is a simplified convolution of least-squares-fit for smoothing and computing derivatives of a signal. It applies weighted moving average filter on signal and this moving average filter is like a polynomial with certain order which is designed to preserve higher moments of the signal and to decrease the bias of the filter. SG filters can be designed efficiently using the polynomial approximation of an impulse sequence; hence their implementation on embedded systems is optimal [34]. In this work, for removing the BW, a first order SG filter is used as the first step. Then, a moving average filter is applied to the output of the previous step. According to Nahiyan and Amin, the output of the mentioned process is a close approximation of BW and subtracting this output from the original signal would give a BW corrected signal [35]. Since the BW frequency is usually less than 0.5 Hz, the window length can be considered 2 seconds. However, the SG filter is independent of the frequency domain, and for better precision, we can consider 0.5 seconds as window length which gives us full frequency range. The length of the SG filter should be odd, and we set it close to but shorter than the length of

the window. The edge of the windows is not smooth in the result of the windowing process. In this regard, a simple moving average filter with a length of 5% of the whole data is applied to the output of the SG filter. The standard deviation of the SG filter output, before and after applying moving average filter, is vital for creating a signal without BW artifact. In this case, if the standard deviation of the filtered signal is more prominent than 50% of the standard deviation of SG filtered signal, the original signal has no BW. Nahiyan and Amin have made this approach for removing ECG BW [35], and we modified this method for PPG signals. As an essential step, the SG filter should be used for the smoothing signal after taking derivative in every step. Also, a mean average filter is used after each SG implementation to reduce the effect of windowing.

5.2.4 PPG normalization and feature extraction

In normal circumstances, because of the pre-processing section, some features in the signal have a reduced amplitude. Therefore, an algorithm is required to boost some waves without bolding noise peaks. In this regard, normalization is used to equalize the amplitude. Sharma and Kumar Sharma used logarithmic transformation [36] as below:

$$y_l = \log_e\left(1 + \frac{C y_n^2(n)}{m_{y_n^2(n)}}\right) \qquad (5.1)$$

Where, y_n^2 is normalized signals that are obtained by dividing the signal to its maximum, C is a constant and $m_{y_n^2(n)}$ is the average of normalized signal. The normalized squaring signal reduces noise amplitudes regarding the higher amplitude of the systolic peak of PPG. If C has a significant value, the noise peaks may be intensified. Therefore, choosing an appropriate constant is paramount and according to the literature and trial and test, a $C = 5$ has been chosen [36]. The normalization process is also applied after taking every derivative of the signals in order to maintain signals between 0 and 1 for further processing.

In this work, we used time domain features, and we assigned suggested names to essential points on the PPG and its derivatives. Also, for simplicity, we call first and second derivative of PPG as the velocity of PPG (VPG) and acceleration of PPG (APG). The main points of PPG have introduced in Table 5.1. These points are also illustrated in Figure 5.4.

Table 5-1. Important points on PPG and its derivatives.

Signal	Wave Name	Suggested Name
PPG	Systolic Peak	S
	Dicrotic Notch	N
	Diastolic Peak	D
VPG	Min slope in the systolic period	x
	Max slope in the systolic period	w
	Max slope in the diastolic period	u
APG	a wave	a
	b wave	b
	c wave	c
	d wave	d
	e wave	e

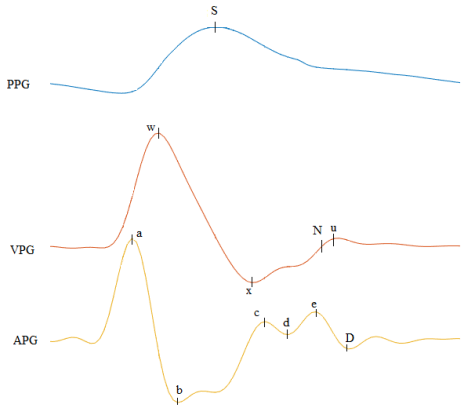

Figure 5-4. Important points on PPG, VPG, and AVG. The first (top) signal is an epoch of PPG. The second and third signals are the first and second derivatives of PPG respectively. Points a and w are maximum in APG and VPG respectively; b and x are the minimum points of APG and VPG respectively; e and c are the local maximum of APG; d is the local minimum in APG between e and c; D is local minimum in APG after e. Notch or N point can be recognized between D and S when VPG is zero; S is maximum point of PPG and u is the local maximum in VPG.

Five points, including a, b, c, d, and e, are formed for every heartbeat in the APG signal and are the local minima and maxima which can be identified by thresholding which is explained in the following. As shown in Figure 5.4, a, b, c and d waveforms show a complete cycle of systole whereas the onset of diastolic is represented by e waveform. We set a to zero when a wave is formed and based on this reference other point times are calculated. For the assessment of vasoactive agents and vascular aging, Takazawa et al. are the pioneer who used the derivation of the PPG signal [37]. Later on, VPG and APG waveforms are cited by many researchers [38, 39], and they started to examine the b/a ratio as an indicator for arterial

stiffness [40], blood lead concentration [41], essential hypertension [38], and age progression [42]. For evaluating vascular aging and for the screening of arteriosclerotic disease, other researchers found that b/a, c/a, d/a, and e/a are also useful [37, 43].

Moreover, D refers to Diastolic wave, N refers to Notch and S refers to Systolic wave. Before the signal is reached to steady state, Diastolic peak is detected by finding local minima of the second derivative of PPG. The Dicrotic Notch or N point can be recognized between D and S when the first derivative of the signal is zero. The Dicrotic point is "a secondary upstroke in the descending part of a PPG, and it is corresponding to the transient increase in aortic pressure upon closure of the aortic valve" [44] and it is an alternative time reference point to measure local pulse wave velocity in the carotid artery

In this proposed method, the thresholding process is used to find the extremums. The detection threshold is calculated as follows: the absolute amplitude of the signal was sorted (s), the cumulative squared value of s was calculated, and points that are greater than 60% maximum cumulative squared is used as the detection threshold. Two hundred milliseconds is used as a minimum distance between detected systolic points since according to the Barbieri et al., heartbeat interval has a specific range physiologically [45].

5.2.5 Optimal inductive learning

Ivakhnenko was the first who proposed Group Method of Data Handling (GMDH) [26]. It has been applied in many areas for data science and machine learning [46, 47]. For the improvement of performance in current algorithms, the optimized inductive GMDH algorithm finds interactions in data and select an optimal network using stochastic optimization and regularized the least square. The same approach is used by Marateb et al. for un-balanced classification problem [47]. The general relation between input and output of a GMDH model is indicated by the discreet form of Volterra function which is called as Kolmogorov-Gabor polynomial and defined as Equation 5.2.

$$\boldsymbol{y = w_0 + \sum_{i=1}^{n} w_i x_i + \sum_{i=1}^{n}\sum_{j=1}^{n} w_{ij} x_i x_j + \sum_{i=1}^{n}\sum_{j=1}^{n}\sum_{k=1}^{n} w_{ijk} x_i x_j x_k + \cdots} \qquad \textbf{(5.2)}$$

The weights of w are calculated by the least square error that is a regression technique. In other words, the output of this function tries to minimize its difference with real-value. In the traditional GMDH, all possibilities of two independent variables are taken into consideration to create regression polynomial, and each combination of two independent variables is called a neuron. These neurons build layers of the network. The output of the neuron k is called Y_k that is calculated by $Y_k = AW_k$ and can be achieved by the least square method as Equation 5.3.

$$\boldsymbol{W_k = (A^T A)^{-1} A^T Y_k} \qquad \textbf{(5.3)}$$

Where, A is the mixing matrix that can be defined as Equation 5.4, which has m sample of observations. These observations are called p and q. For each observation of p and q, we have a neuron for the first layer. Neurons which are better than the specific threshold is chosen for the next layer. This threshold is called selection pressure, and we choose it by trial and test. In the next layer, the new matrix A is created by the output of previous neurons but with the same mixing process. This process continues until termination criteria are met. The number of layers expected accuracy or time of learning process can be set as termination criteria.

$$\boldsymbol{A}=\begin{bmatrix} \mathbf{1} & \boldsymbol{x_{1p}} & \boldsymbol{x_{1q}} & \boldsymbol{x_{1p}x_{1q}} & \boldsymbol{x_{1p}^2} & \boldsymbol{x_{1q}^2} \\ \mathbf{1} & \boldsymbol{x_{2p}} & \boldsymbol{x_{2q}} & \boldsymbol{x_{2p}x_{2q}} & \boldsymbol{x_{2p}^2} & \boldsymbol{x_{2q}^2} \\ \vdots & \vdots & \vdots & \vdots & \vdots & \vdots \\ \mathbf{1} & \boldsymbol{x_{mp}} & \boldsymbol{x_{mq}} & \boldsymbol{x_{mp}x_{mq}} & \boldsymbol{x_{mp}^2} & \boldsymbol{x_{mq}^2} \end{bmatrix} \qquad (5.4)$$

5.2.6 Mixing feature

The mixing matrix A can be designed differently to befitting for proposed problem. The detected points in PPG and its derivative contain information of some physiological actions. These features are used in other researches as significant features [12, 39, 41]. Mixing matrix enables the algorithm to find significant features without having information about them. Changing the mixing matrix is also done in other research for gaining better result [47]. In this work, the mixing matrix A is defined as:

$$\boldsymbol{A}=\begin{bmatrix} \mathbf{1} & \boldsymbol{|x_{1p}-x_{1q}|^{\alpha}} & \boldsymbol{\beta^{\frac{|x_{1p}-x_{1q}|}{x_{1p}}}} & \boldsymbol{\gamma^{\frac{|x_{1p}-x_{1q}|}{x_{1q}}}} & \boldsymbol{\frac{x_{1p}^{\omega}}{x_{1q}^{\mu}}} & \mathbf{log}\,(\mathbf{1}+\boldsymbol{x_{1q}^{\psi}x_{1p}^{\phi}}) \\ \mathbf{1} & \boldsymbol{|x_{2p}-x_{2q}|^{\alpha}} & \boldsymbol{\beta^{\frac{|x_{2p}-x_{2q}|}{x_{2p}}}} & \boldsymbol{\gamma^{\frac{|x_{2p}-x_{2q}|}{x_{2q}}}} & \boldsymbol{\frac{x_{2p}^{\omega}}{x_{2q}^{\mu}}} & \mathbf{log}\,(\mathbf{1}+\boldsymbol{x_{2q}^{\psi}x_{2p}^{\phi}}) \\ \vdots & \vdots & \vdots & \vdots & \vdots & \vdots \\ \mathbf{1} & \boldsymbol{|x_{mp}-x_{mq}|^{\alpha}} & \boldsymbol{\beta^{\frac{|x_{mp}-x_{mq}|}{x_{mp}}}} & \boldsymbol{\gamma^{\frac{|x_{mp}-x_{mq}|}{x_{mq}}}} & \boldsymbol{\frac{x_{mp}^{\omega}}{x_{mq}^{\mu}}} & \mathbf{log}\,(\mathbf{1}+\boldsymbol{x_{mq}^{\psi}x_{mp}^{\phi}}) \end{bmatrix} \qquad (5.5)$$

where, $\alpha, \beta, \gamma, \omega, \mu, \psi$ and ϕ are tuning coefficients that will be discussed in the next section, and p and q are observation. This mixing matrix includes every possible combination of detected points and can calculate each interval time that may have significant relation with BP. Instead of logarithm function, one can use sin, cos, $cosh$, $sinh$ or other nonlinear functions [47] to discover the nonlinear relationship between PPG points and BP; nevertheless, we chose logarithm function since it provides better performance in training process with the the trial and test.

Forasmuch as mixing matrix uses detected points on PPG for one cycle, one can take the average of mixing matrix for several cycles to have more stable features. For simplicity, we used this averaging technique before applying tuning coefficients. The expanding sliding window which is used for feature extraction has some consequences on the precision of the algorithm which will be discussed in the discussion.

5.2.7 Tuning coefficients

According to Equation 5.5, the mixing matrix contains regression coefficients $\alpha, \beta, \gamma, \omega, \mu, \psi$ and ϕ that can affect the estimation of BP. As an instance, assume that the time between systolic point and Dicrotic Notch is a significant feature; however, this relation between the time difference of these points and BP may be nonlinear and square form of this difference time has better correlation with BP. The stochastic optimization algorithm is required in this step to find the best coefficients which can create significant relation with BP value. Particle Swarm Optimization (PSO), is a population-based, meta-heuristics method that is inspired by flocking birds [48]. This method is used as stochastic optimization with the same internal parameters and topology that Mohebbian et al. used in another approach [49]; except the number of iteration is set to 10 and the cost function is based on the regularized least square method, and root mean square error which will be described in the next sections. In each PSO iteration, m number of the sample divided to train and validation set. Then, in the train set, W_k is calculated based on a regularized least square method and applied to the validation set. The result of the validation set, directing the PSO algorithm to choose a better coefficient. This procedure is exerted for each neuron of the network in every layer during the learning process of GMDH.

5.2.8 Regularized Least Square

As described in Equation 5.3, the least square method is used in traditional GMDH method. In this work, the regularized least square method is used instead of the least square method for some reasons. First, the least square method depends on $(A^T A)^{-1}$, which can make a problem in computing in singular value or near singular value. Also, the least square may provide a good result in the train, but it cannot guarantee high precision in the test set. Therefore, to apply the further constraint, Hoerl and Kennard used a small constant λ which is added to the diagonal entries of matrthe ix $(A^T A)^{-1}$ and called it ridge regression [50]. In this regard, Equation 5.3 can be rewritten as Equation 5.6.

$$\boldsymbol{W_k = (A^T A + \lambda I)^{-1} A^T Y} \qquad \textbf{(5.6)}$$

Where I is the identity matrix. This constraint means that the norm of the regression coefficients matrix W_k for neuron kth is equal to one; hence, the regression coefficients are in a unit n-sphere. The ridge regression has bias comparing to the least square. However, at the cost of bias, it reduces the variance and reduces the mean square error [50]. The OIGMDH can work with other regression algorithms instead of least square and its derivatives. However, the least square method is optimum and has straightforward computation.

5.2.9 State-of-the-art

In machine learning approaches, ensemble machine learning has been shown to have a better consistent performance than single instance methods such as radial basis functions, kernel machines, or k-nearest neighbor [51]. Ensemble machine learning algorithms are divided into two categories, including sequential and parallel ensemble methods. In sequential ensemble methods such as AdaBoost [52], base learners are generated sequentially. While, in parallel

ensemble methods such as RF, base learners are generated in parallel; therefore, the error can be decreased dramatically by averaging [53]. The optimal inductive learning algorithm that is described in previous sections uses both sequential and parallel ensemble method. Moreover, it has an inner feature selection based on the mixing matrix.

For comparing the result of the proposed algorithm, we used four popular machine learning methods, including SVM, decision tree, AdaBoost and RF algorithm in two scenarios. First, we use synchronized ECG and PPG signal from MIMIC and extract CF that will be discussed in the next section. Then, four machine learning algorithms are trained and the results of the test set of MIMIC database and also recorded data from the designed device are evaluated. Second, we train the proposed method with MIMIC database and the results of the trained network on the test set of MIMIC database and recorded data are assessed. Features that are extracted from PPG and ECG are listed below:

1. The time interval between ECG R-peak and systolic peak in PPG.
2. The time interval between ECG R-peak and minimum peak in PPG.
3. The time interval between ECG R-peak and maximum slope in PPG.
4. Heart rate
5. Mean, median and standard deviation of R-R interval in ECG.
6. The time interval between systolic peak and Dicrotic Notch point after it.
7. The ratio between the systolic peak and the first Dicrotic Notch point after it.
8. The ratio between the systolic peak and the first diastolic point after it.
9. The area under the PPG curve in the time interval from minimum peak to maximum slope in PPG.
10. The area under the PPG curve in the time interval from maximum slope to systolic peak in PPG.
11. The area under the PPG curve in the time interval from systolic peak to Dicrotic Notch point in PPG.
12. The area under the PPG curve in the time interval from Dicrotic Notch point to a minimum peak in PPG.

Figures 5.5 and 5.6 illustrate the mentioned features more appropriately.

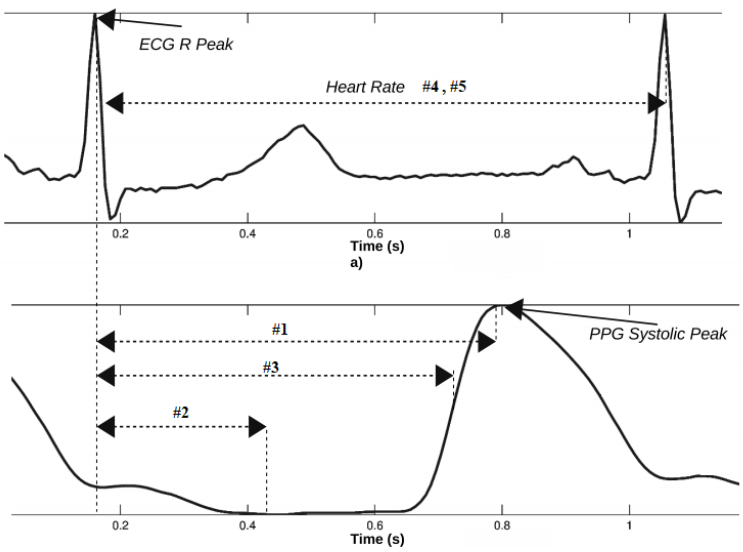

Figure 5-5. Illustration of conventional features 1 to 5 via ECG and PPG. Pulse Transit Time features are obtained by calculating the time distance between the ECG R-peak and three points on the PPG signal, which are the PPG maximum peak (feature number 1), the PPG minimum (feature number 2) and the point at which the maximum slope of the PPG waveform occurs (feature number 3). The feature number 4 and 5 are related to the heart rate and statistical analysis of R-R interval.

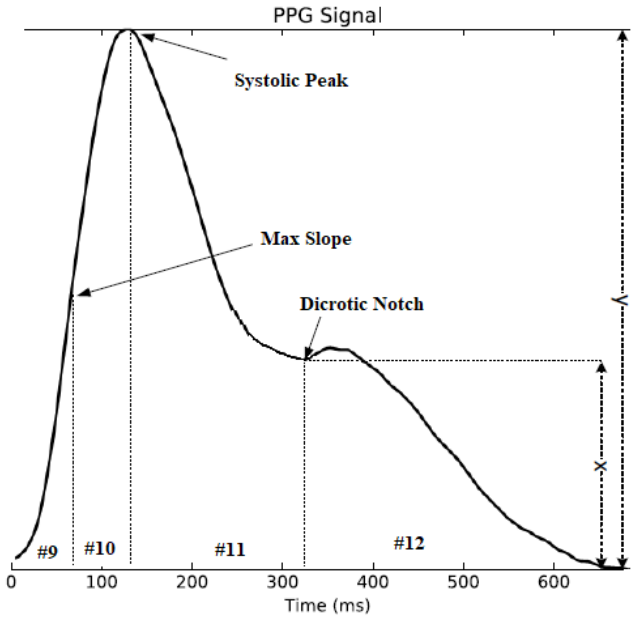

Figure 5-6. A PPG epoch and a representation of some conventional features. Features number 9, 10, 11 and 12 are the partial area under the PPG curve. The feature number 7 is equal to $\frac{x}{y}$ and the feature number 8 can be calculated in a same way.

Features 5.1, 5.2 and 5.3 are selected because they represent the pulse arrival time or pulse wave velocity [21]. Moreover, they are depended to the elasticity of vessels [21]. According to Mancia [54], there is mutual information between heart rate and BP. Therefore the heart rate is selected as a significant feature. The Dicrotic Notch point is "a secondary upstroke in the descending part of a PPG, and it is corresponding to the transient increase in aortic pressure upon closure of the aortic valve" [44], and it is an alternative time reference point to measure local pulse wave velocity in the carotid artery [55]. The area under the PPG curve is related to the peripheral resistance [56] and is used for PPG analysis and blood pressure estimation in the literature [57].

Support vector machine regression or SVMR constructs a set of hyperplanes in a high dimensional space, which can be used for regression [58]. In this work, we called it SVM since this algorithm is an application of the conventional SVM. In this study, the radial basis function kernels were used, and the radius of the RBF kernel should be appropriately set to avoid poor regression. The method proposed by Cherkassky et al. was used for selecting parameters [59].

Decision Tree divides dataset to a small part and uses entropy to calculate the information of the subsets [60]. In this work C4.5 decision tree is used since it can handle continuous attributes, and its implementation is straightforward.

The RF algorithm resamples the training dataset several times and creates a decision tree model for samples. In the RF algorithm, each tree in the ensemble is created with bootstrap samples. Also, instead of using all features, some features are selected randomly. Eventually, trees have less correlation and their averaging lead to reducing variance are selected as the selected model [53]. In this work, the number of trees for the RF algorithm is set to 30. In the same manner, adaptive boosting or AdaBoost is used in this research for training weak learners and combining them to make a strong classifier.

5.3 Results

As discussed in the state-of-the-art section, four scenarios are targeted. First, results on the online dataset using conventional features (CF) selection and four machine learning approaches are validated. Then, the trained system is used for estimating BP in the recorded data with the same method. Next, OIGMDH is applied to the online dataset, and the trained system is used for the recorded data from the designed device.

5.3.1 Results on the online dataset

The results of predicting DBP and SBP by four machine learning approaches, including RF, decision tree, SVM and AdaBoost algorithm, are evaluated by hold-out validation and considering the 70% samples as the train set. Conventional features are described in the state-of-the-art section. Concisely, the mean absolute error and root mean square error of each

method is calculated by running the algorithm seven times. Moreover, the mean difference plot and the scatter plot of the test set are depicted for the worst case in 7 runs. The mean-difference plot is also called Bland-Altman plot [61]. The Bland-Altman plots are broadly used to assess the comparative among two unique instruments or two estimations strategies. This plot helps to distinguish proof of any efficient measurement or outlier existence. The mean difference can be recognized by the one-sample t-test method, and the estimated bias can be adjusted by subtracting the mean difference from the new method. The average difference ±1.96 standard deviations of the difference, which is called limits of agreement, shows the significance of the new model. The R-squared measure of goodness of fit is also calculated for better comparison [62].

The result of four different method is shown in Table 5.2.

Table 5-2. Results of conventional features (CF) with four different machine learning algorithms on MIMIC data.

		RF algorithm with CF	**SVM algorithm with CF**	**Decision Tree algorithm with CF**	**AdaBoost algorithm with CF**
SBP	*RMSE (*mmHg*)*	5.9 ± 2.4	*6.8* ± 2.6	*7.2* ± 2.1	*9.2* ± 3.3
	*MAE (*mmHg*)*	3.9 ± 3.4	*4.1* ± 3.4	*4.2*± 2.9	*5.1*± 2.9
DBP	*RMSE (*mmHg*)*	7.3 ± 3.0	*7.8* ± 3.1	*8.4* ± 3.0	*11.1* ± 3.6
	*MAE (*mmHg*)*	2.2 ±2.2	*5.3* ± 2.9	*5.7*± 2.6	*6.9*± 3.1

The RF algorithm performance is more significant than other conventional methods. The RMSE of the RF method for the SBP estimation is 5.90±2.43 with MAE of 3.98±3.40. The RMSE of the RF method for DBP estimation is 7.35±3.01 with MAE of 2.25±2.21. Figure 5.7 and 8 show the scatter plot and the Bland-Altman plot for the RF method. The same plots for other methods are presented in the supplementary material.

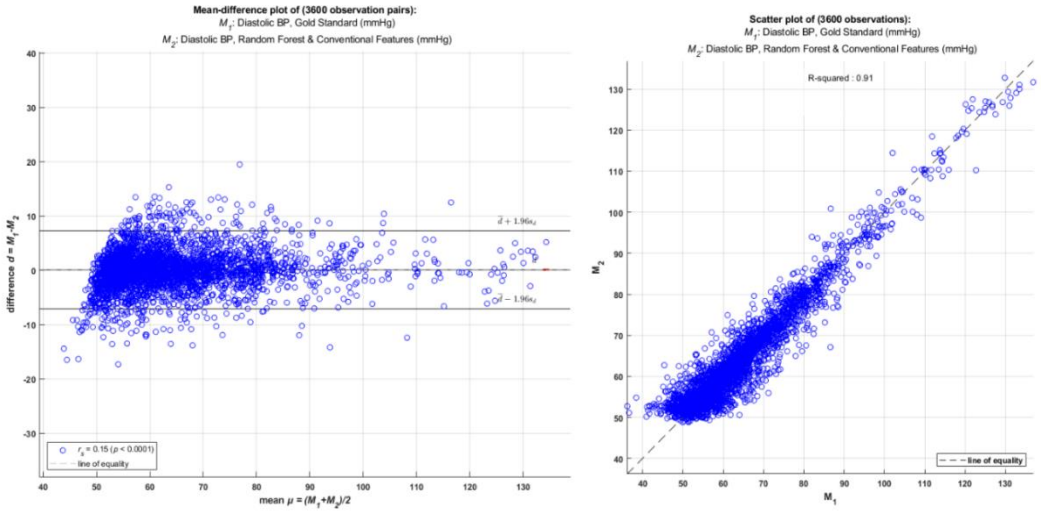

Figure 5-7. The mean difference plot or the Bland-Altman plot (left) and the scatter plot (right) of the test-set for the worst case among 7 runs of random forest algorithm with conventional features by hold-out validation for estimating DBP; The R-squared coefficient is 0.91 for DBP estimation.

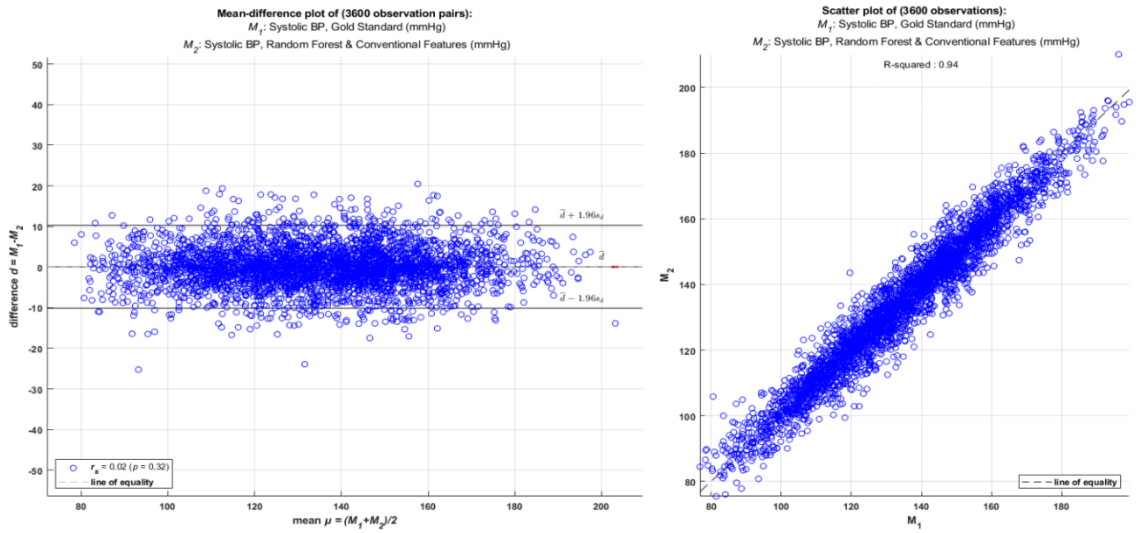

Figure 5-8. The mean difference plot or the Bland-Altman plot (left) and the scatter plot (right) of the test-set for the worst case among 7 runs of random forest algorithm with conventional features by hold-out validation for estimating SBP; The R-squared coefficient is 0.94 for SBP estimation

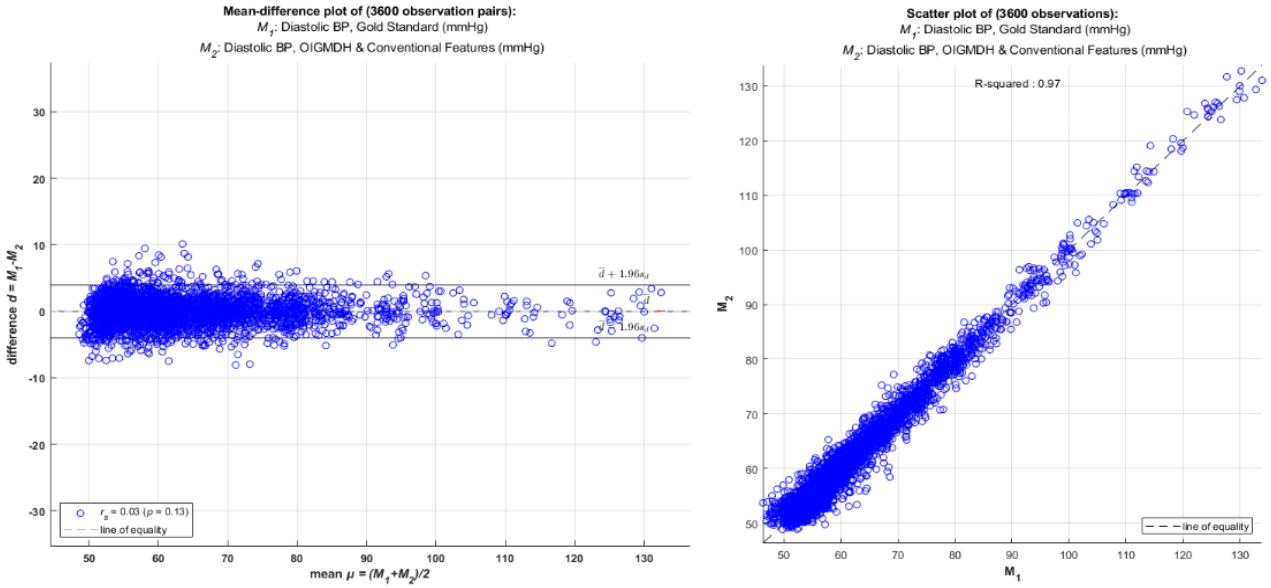

Figure 5-9. The mean difference plot or the Bland-Altman plot (left) and the scatter plot (right) of the test-set for the worst case among 7 runs of IOGMDH with conventional features by hold-out validation for estimating DBP; The R-squared coefficient is 0.97 for DBP estimation.

The online dataset is also used for training by the OIGMDH. Similar to previous results, the mean absolute error and root mean square error is calculated by running algorithm seven times and each time with hold-out validation by considering the 70% samples as the train set. Figure 5.9 and 5.10 show the mean difference plot and the scatter plot. For SBP, the RMSE is 3.47±1.31, MAE is 2.40±1.01 mmHg. Also, for DBP, the RMSE is 4.67±1.44, and MAE is 3.33±1.61 mmHg. Figure 5.9 and Figure 5.10 show the scatter plot and the Bland-Altman plot for the OIGMDH method.

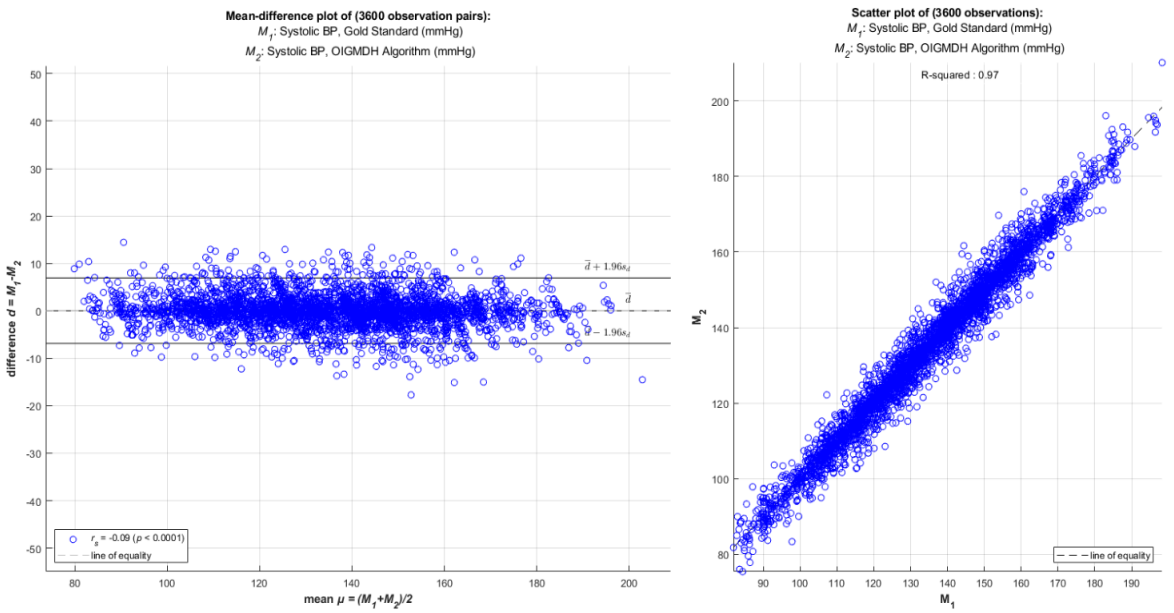

Figure 5-10. The mean difference plot or the Bland-Altman plot (left) and the scatter plot (right) of the test-set for the worst case among 7 runs of IOGMDH with conventional features by hold-out validation for estimating SBP; The R-squared coefficient is 0.97 for SBP estimation.

5.3.2 Results on recorded signals

Since the RF algorithm has better performance than other algorithms, we used this trained machine learning algorithm on 15 subjects to compare the outcome of the system to the measured BP from the PortapresTM device in two minutes for each person and with 10-second sliding window length. The result is shown in Table 5.3. Trained OIGMDH by online dataset is also used for estimating on recorded signals. Significant points are extracted from 2 minutes of the PPG signal for each person with a sliding window length of 10 seconds. Averaging on mixing matrix is taken into consideration for every window before tuning coefficients. Table 5.3 represents the results on the recorded database.

Table 5-3. Results of the trained RF algorithm with CF and the trained OIGMDH on recorded data regarding the Portapres™ results as the gold standard on 15 people

Method	BP	RMSE (mmHg)	MAE (mmHg)
RF algorithm with CF	*SBP*	*8.0 ± 5.8*	***7.0 ± 5.0***
	DBP	*7.8 ± 4.5*	***6.8 ± 3.9***
OIGMDH	*SBP*	*3.4 ± 0.6*	***2.2 ± 0.7***
	DBP	*4.5 ± 1.1*	***3.0 ± 1.2***

5.4 Discussion

5.4.1 Sliding window effect

In this study, pure signal processing principles and the optimized inductive learning, based on the GMDH, is used for predicting SBP and DBP. Moreover, the conventional method of features extraction from PPG and ECG and traditional machine learning algorithms, based on the literature review, is used for comparing the result of OIGMDH. In the conventional method, regarding the frame size for extracting features in the learning process, the designed regression system would work differently. In other words, the precision of the estimated BP is severely based on the sliding window. As an instance, the BP value can be estimated in 5 seconds with less precision, or it can be predicted in 20 seconds with better precision. Figure 5.11 illustrates the error of these algorithms (root mean square error) in different frame size. The tradeoff between precision and nearly real-time processing should be taken into consideration to be able to create a device for measuring BP continuously

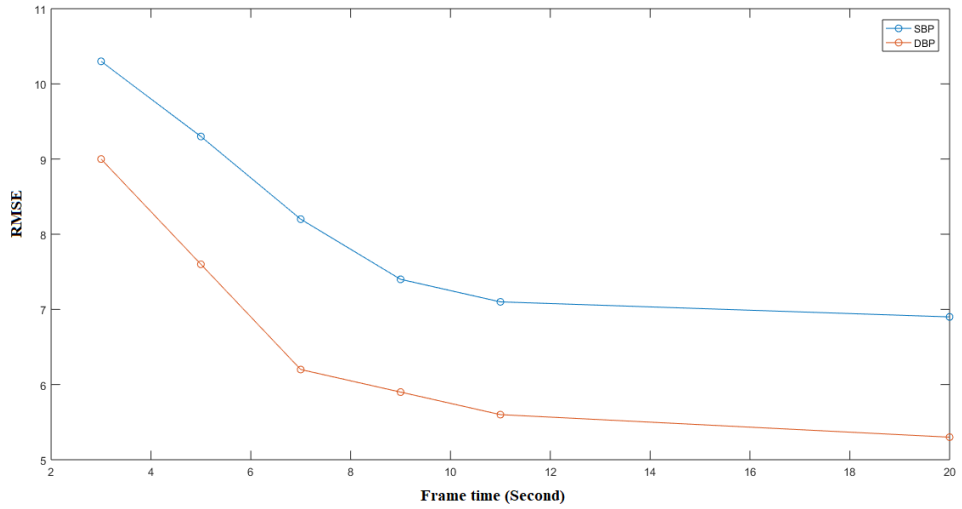

Figure 5-11. The relation between sliding window length for feature extraction and RMSE of estimated BP by RF algorithm

On the other hand, the effect of sliding window length on OIGMDH is depicted in Figure 5.12. Sliding window length has not paramount effect on the precision of the algorithm. Hence, continuous BP measurement with better precision is possible.

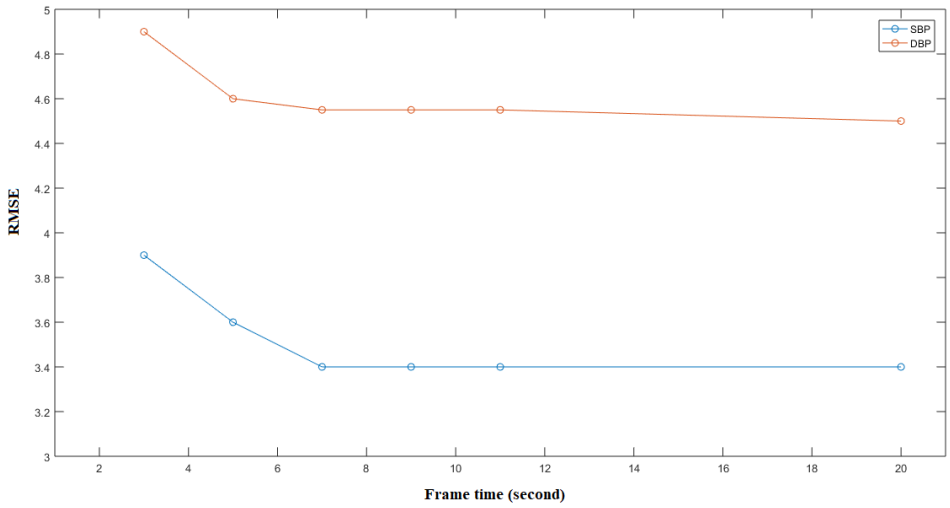

Figure 5-12. The relation between sliding window length for feature extraction and RMSE of estimated BP by IOGMDH

5.4.2 Performance and properties of the proposed method

Table 5.4 is provided for comparing trained OIGMDH, RF algorithm and modern methods which are reported in the literature. In this Table, the range of BP, the time for estimation of BP and the MAE are also compared.

The CF in the combination of machine learning algorithm works promising on the online dataset but not that confident on the recorded dataset. This error can be raised from a slight delay between ECG and PPG recording. Placing the PPG sensor in different places for recording can also change the results, since PPG synchronization with ECG would be under effect. Therefore, pulse transit time has variation and is not a trustable parameter for training with one dataset and using in another. Also, the physiological factors are more important than electronic delays. According to the literature, estimating BP by PTT and PWV features need calibration [63]. Because these features depends on the physiological factors such as age, race, gender and so on [20] and also they are time-dependent and different between day and night [4]. Also, there is a delay between electrical phenomenon of R wave and ejection of the blood which differ from person to person [64]. The OIGMDH algorithm is only using the PPG signal, and mentioned lags do not have any effect on its prediction. Therefore, it is possible to train a system with a dataset and use this trained system on other signals. The more similar method to this study is done by Liu et al. [25] in which PPG and APG is used for BP estimation. However, they used age, weight, height and gender as other significant feature. Poon and Zhang extracted pulse transit time (PTT) from PPG and ECG in 45 seconds and used MoensKorteweg's formula for DBP and SBP estimation [12]. The results achieved a 2.8±6.8 and a 0.9±5.6 mmHg mean difference for DBP and SBP respectively. However, there are three major different with proposed method. First, they used the range of 122 ± 21 and 64 ± 9 mmHg for SBP and DBP estimation; hence, the algorithm works only in this limited range. Second, they used ECG and

PPG simultaneously; while proposed method uses only PPG. The Poon and Zhang method need 45 second and it cannot be considered real-time and their acquired error has high standard deviation.

Table 5-4. Comparing with other methods

Method	Type of signals	BP	Range [min-max] (mmHg)	MAE (mmHg)	Meantime analysis
RF and CF on the online dataset	*ECG and PPG*	*SBP*	*[81-197]*	2.2 ± 2.2	**10 second**
		DBP	*[51-128]*	3.9 ± 3.4	
RF and CF on recorded signals	*ECG and PPG*	*SBP*	*[81-197]*	7.0 ± 5.0	**10 second**
		DBP	*[51-128]*	6.8 ± 3.9	
OIGMDH on the online database	*Fingertip PPG*	*SBP*	*[81-197]*	2.4 ± 1.0	**5 second**
		DBP	*[51-128]*	3.3 ± 1.6	
OIGMDH on the recorded signal	*Fingertip PPG*	*SBP*	*[81-197]*	2.2 ± 0.7	**5 second**
		DBP	*[51-128]*	3.0 ± 1.2	
Kachuee *et al.* [22]	ECG and PPG	*SBP*	*[81-178]*	11.1 ± 10.0	**Depends on subject heart rates**
		DBP	*[60-128]*	5.3 ± 6.1	
Kachuee *et al.* [23]	ECG and PPG	*SBP*	*[81-178]*	12.3 ± 16.1	**NA**
		DBP	*[60-128]*	6.3 ± 8.4	
Attarpour et al. [24]	*Wrist and Fingertip PPG*	*SBP*	*NA*	4.9 ± 5.9	**NA**
		DBP	*NA*	4.0 ± 5.5	
Poon and Zhang [12]	*ECG and PPG*	*SBP*	*[101-143]*	0.9±5.6	**45 second**
		DBP	*(55-73]*	2.8±6.8	
Zheng *et al.* [4]	ECG and PPG	*SBP*	*[80-210]*	2.8 ± 8.2	**30 minute**
		DBP	*NA*	NA	
Liu et al. [25]	*Fingertip PPG*	*SBP*	*NA*	8.5 ±1.0	**Depends shape of APG**
		DBP	*NA*	4.3 ± 5.8	

NA: Not available

The Bland-Altman plot of traditional machine learning algorithm with CF method is presented in supplementary materials.

5.4.3 Significant Features

The proposed method uses blind feature selection and searches every possible interaction between a pair of features using mixing matrix in Equation 5.5. The explanation of significant features is complicated. However, the four most crucial features which are selected by the

IOGMDH in the first layer is shown in Table 5.5 with their weights. The PSO algorithm approximates these weights.

Table 5-5. The most significant features in the first layer of IOGMDH

Selected points		Weights $\{\alpha, \beta, \gamma, \omega, \mu, \psi, \phi\}$
a	*b*	***{0.8, 0.4, 0.1, 0.3, 0.2, 0.3,0.1}***
c	*b*	***{0.5, 0.9, 0.2, 0.7, 0.6, 0.1,0.2}***
a	*w*	***{0.6, 0.1, 0.1, 0.2, 0.9, 0.4,0.3}***
S	*a*	***{1.0, 0.4, 0.2, 0.2, 0.3, 0.1,0.5}***

The interpretation of the selected features is difficult since it is a complex feature set. As an example, Table 5.4 shows that a and b are selected as significant points. Therefore, the mixing matrix of these points can be represented using Equation 5.5:

$$\boldsymbol{A}=\begin{bmatrix} \mathbf{1} & \left|\boldsymbol{a_{1p}}-\boldsymbol{b_{1q}}\right|^{\mathbf{0.8}} & \mathbf{0.4}\frac{|a_{1p}-b_{1q}|}{a_{1p}} & \mathbf{0.1}\frac{|a_{1p}-b_{1q}|}{b_{2q}} & \frac{b_{1q}^{0.3}}{a_{1p}^{0.2}} & \mathbf{log}\left(\mathbf{1}+\boldsymbol{a_{1p}^{0.3}b_{1q}^{0.2}}\right) \\ \mathbf{1} & \left|\boldsymbol{a_{2p}}-\boldsymbol{b_{2q}}\right|^{\mathbf{0.8}} & \mathbf{0.4}\frac{|a_{2p}-b_{2q}|}{a_{2p}} & \mathbf{0.1}\frac{|a_{2p}-b_{2q}|}{b_{2q}} & \frac{b_{2q}^{0.3}}{a_{2p}^{0.2}} & \mathbf{log}\left(\mathbf{1}+\boldsymbol{a_{2p}^{0.3}b_{2q}^{0.2}}\right) \\ \vdots & \vdots & \vdots & \vdots & \vdots & \vdots \\ \mathbf{1} & \left|\boldsymbol{a_{mp}}-\boldsymbol{b_{mq}}\right|^{\mathbf{0.8}} & \mathbf{0.4}\frac{|a_{mp}-b_{mq}|}{a_{mp}} & \mathbf{0.1}\frac{|a_{mp}-b_{mq}|}{b_{mq}} & \frac{b_{mq}^{0.3}}{a_{mp}^{0.2}} & \mathbf{log}\left(\mathbf{1}+\boldsymbol{a_{mp}^{0.3}b_{mq}^{0.2}}\right) \end{bmatrix} \quad \textbf{(5.7)}$$

In this regards, the distance between a and b is selected for creating a mixing matrix. However, there is no previous analysis of correlation between these complex set of features and BP, and that is why this method is called blind. Moreover, this mixing matrix is multiplied by another mixing matrix during layers of the network and can find the optimized interactions between features. Other non-linear functions can also be used for evaluating the interaction of the features.

Finally, the main limitation of this study is the number of patient population in the recorded database, and further studies should be evaluated on a larger population. Finally, assessing the performance of the model on datasets from different institutions is required in addition to an internal validation.

5.5 Conclusion

In conclusion, the work proposes a new algorithm for measuring BP without calibration and cuff. The technique uses only the PPG signal to continuously estimate both systolic and diastolic blood pressures in real time. The proposed algorithm is promising compared with state-of-the-art models and offers a new tool in clinical approaches. The developed program and recorded database are available to interested readers upon request.

5.6 References

[1] Sarrafzadegan N, Hassannejad R, Marateb HR, Talaei M, Sadeghi M, Roohafza HR, et al. PARS risk charts: A 10-year study of risk assessment for cardiovascular diseases in Eastern Mediterranean Region. PloS one. 2017;12:e0189389.

[2] Wolf-Maier K, Cooper RS, Banegas JR, et al. Hypertension prevalence and blood pressure levels in 6 european countries, canada, and the united states. JAMA. 2003;289:2363-9.

[3] Nichols M, Townsend N, Scarborough P, Rayner M. Cardiovascular disease in Europe: epidemiological update. European heart journal. 2013;34:3028-34.

[4] Zheng Y-L, Yan BP, Zhang Y-T, Poon CC. An armband wearable device for overnight and cuff-less blood pressure measurement. IEEE transactions on biomedical engineering. 2014;61:2179-86.

[5] Forouzanfar MH, Liu P, Roth GA, Ng M, Biryukov S, Marczak L, et al. Global burden of hypertension and systolic blood pressure of at least 110 to 115 mm Hg, 1990-2015. Jama. 2017;317:165-82.

[6] Peter L, Noury N, Cerny M. A review of methods for non-invasive and continuous blood pressure monitoring: Pulse transit time method is promising? Irbm. 2014;35:271-82.

[7] Thomas G, Drawz PE. BP Measurement Techniques What They Mean for Patients with Kidney Disease. Clinical Journal of the American Society of Nephrology. 2018:CJN. 12551117.

[8] Boonyasai RT, Carson KA, Marsteller JA, Dietz KB, Noronha GJ, Hsu YJ, et al. A bundled quality improvement program to standardize clinical blood pressure measurement in primary care. The Journal of Clinical Hypertension. 2018;20:324-33.

[9] Wadhwani R, Siddiqui NI, Sharma B. Assessment of accuracy of mercury sphygmomanometer and automated oscillometric device of blood pressure measurement in population of normal individuals. Asian Journal of Medical Sciences. 2018;9:17-24.

[10] Beevers G, Lip GY, O'brien E. ABC of hypertension: Blood pressure measurement: Part II—Conventional sphygmomanometry: technique of auscultatory blood pressure measurement. BMJ: British Medical Journal. 2001;322:1043.

[11] Pickering TG. What will replace the mercury sphygmomanometer? Blood pressure monitoring. 2003;8:23-5.

[12] Poon C, Zhang Y. Cuff-less and noninvasive measurements of arterial blood pressure by pulse transit time. Engineering in Medicine and Biology Society, 2005 IEEE-EMBS 2005 27th Annual International Conference of the: IEEE; 2006. p. 5877-80.

[13] Walma E, Prins A, Mulder P, Hoes A. Accuracy of an oscillometric automatic blood pressure device: the Omron HEM403C. Journal of human hypertension. 1995;9:169-74.

[14] Bada HS, Korones SB, Perry EH, Arheart KL, Ray JD, Pourcyrous M, et al. Mean arterial blood pressure changes in premature infants and those at risk for intraventricular hemorrhage. The Journal of pediatrics. 1990;117:607-14.

[15] Rabi DM, Daskalopoulou SS, Padwal RS, Khan NA, Grover SA, Hackam DG, et al. The 2011 Canadian Hypertension Education Program recommendations for the management of hypertension: blood pressure measurement, diagnosis, assessment of risk, and therapy. Canadian Journal of Cardiology. 2011;27:415-33. e2.

[16] Cheng H-M, Lang D, Tufanaru C, Pearson A. Measurement accuracy of non-invasively obtained central blood pressure by applanation tonometry: a systematic review and meta-analysis. International Journal of Cardiology. 2013;167:1867-76.

[17] Benetos A, Okuda K, Lajemi M, Kimura M, Thomas F, Skurnick J, et al. Telomere length as an indicator of biological aging: the gender effect and relation with pulse pressure and pulse wave velocity. Hypertension. 2001;37:381-5.

[18] Smith RP, Argod J, Pépin J-L, Lévy PA. Pulse transit time: an appraisal of potential clinical applications. Thorax. 1999;54:452-7.

[19] Payne R, Symeonides C, Webb D, Maxwell S. Pulse transit time measured from the ECG: an unreliable marker of beat-to-beat blood pressure. Journal of Applied Physiology. 2006;100:136-41.

[20] Gesche H, Grosskurth D, Küchler G, Patzak A. Continuous blood pressure measurement by using the pulse transit time: comparison to a cuff-based method. European journal of applied physiology. 2012;112:309-15.

[21] Chen W, Kobayashi T, Ichikawa S, Takeuchi Y, Togawa T. Continuous estimation of systolic blood pressure using the pulse arrival time and intermittent calibration. Medical and Biological Engineering and Computing. 2000;38:569-74.

[22] Kachuee M, Kiani MM, Mohammadzade H, Shabany M. Cuffless blood pressure estimation algorithms for continuous health-care monitoring. IEEE Transactions on Biomedical Engineering. 2017;64:859-69.

[23] Kachuee M, Kiani MM, Mohammadzade H, Shabany M. Cuff-less high-accuracy calibration-free blood pressure estimation using pulse transit time. Circuits and Systems (ISCAS), 2015 IEEE International Symposium on: IEEE; 2015. p. 1006-9.

[24] Attarpour A, Mahnam A, Aminitabar A, Samani H. Cuff-less continuous measurement of blood pressure using wrist and fingertip photo-plethysmograms: Evaluation and feature analysis. Biomedical Signal Processing and Control. 2019;49:212-20.

[25] Liu M, Po L-M, Fu H. Cuffless Blood Pressure Estimation Based on Photoplethysmography Signal and Its Second Derivative. International Journal of Computer Theory and Engineering. 2017;9:202.

[26] Ivakhnenko A, Ivakhnenko G. The review of problems solvable by algorithms of the group method of data handling (GMDH). Pattern Recognition And Image Analysis C/C Of Raspoznavaniye Obrazov I Analiz Izobrazhenii. 1995;5:527-35.

[27] Saeed M, Villarroel M, Reisner AT, Clifford G, Lehman L-W, Moody G, et al. Multiparameter Intelligent Monitoring in Intensive Care II (MIMIC-II): a public-access intensive care unit database. Critical care medicine. 2011;39:952.

[28] PS25255 EPIC Ultra High Impedance ECG Sensor Advance Information. Data Sheet 291955

[29] Pulse Sensor - SEN-11574 - SparkFun Electronics. Pulse Sensor.

[30] Finapres Medical Systems | Products - Portapre.

[31] Imholz BP, Wieling W, van Montfrans GA, Wesseling KH. Fifteen years experience with finger arterial pressure monitoring: assessment of the technology. Cardiovascular research. 1998;38:605-16.

[32] Orphanidou C. Derivation of respiration rate from ambulatory ECG and PPG using ensemble empirical mode decomposition: Comparison and fusion. Computers in biology and medicine. 2017;81:45-54.

[33] Tang SD, Goh YS, Wong MD, Lew YE. PPG signal reconstruction using a combination of discrete wavelet transform and empirical mode decomposition. Intelligent and Advanced Systems (ICIAS), 2016 6th International Conference on: IEEE; 2016. p. 1-4.

[34] Agarwal S, Rani A, Singh V, Mittal AP. Performance Evaluation and Implementation of FPGA Based SGSF in Smart Diagnostic Applications. Journal of medical systems. 2016;40:63.

[35] Nahiyan KT, Al Amin A. Removal of ECG Baseline Wander using Savitzky-Golay Filter Based Method. Bangladesh Journal of Medical Physics. 2017;8.

[36] Sharma T, Sharma KK. QRS complex detection in ECG signals using locally adaptive weighted total variation denoising. Computers in biology and medicine. 2017;87:187-99.

[37] Takazawa K, Tanaka N, Fujita M, Matsuoka O, Saiki T, Aikawa M, et al. Assessment of vasoactive agents and vascular aging by the second derivative of photoplethysmogram waveform. Hypertension. 1998;32:365-70.

[38] Liang Y, Chen Z, Ward R, Elgendi M. Hypertension assessment via ECG and PPG signals: An evaluation using MIMIC database. Diagnostics. 2018;8:65.

[39] Shahrbabaki SS, Ahmed B, Penzel T, Cvetkovic D. Photoplethysmography derivatives and pulse transit time in overnight blood pressure monitoring. Engineering in Medicine and Biology Society (EMBC), 2016 IEEE 38th Annual International Conference of the: IEEE; 2016. p. 2855-8.

[40] Rubins U, Grabovskis A, Grube J, Kukulis I. Photoplethysmography analysis of artery properties in patients with cardiovascular diseases. 14th Nordic-Baltic Conference on Biomedical Engineering and Medical Physics: Springer; 2008. p. 319-22.

[41] Utami N, Setiawan AW, Zakaria H, Mengko TR, Mengko R. Extracting blood flow parameters from Photoplethysmograph signals: A review. Instrumentation, Communications, Information Technology, and Biomedical Engineering (ICICI-BME), 2013 3rd International Conference on: IEEE; 2013. p. 403-7.

[42] Russoniello CV, Zhirnov YN, Pougatchev VI, Gribkov EN. Heart rate variability and biological age: Implications for health and gaming. Cyberpsychology, Behavior, and Social Networking. 2013;16:302-8.

[43] Watanabe N, Bando YK, Kawachi T, Yamakita H, Futatsuyama K, Honda Y, et al. Development and Validation of a Novel Cuff-Less Blood Pressure Monitoring Device. JACC: Basic to Translational Science. 2017;2:631-42.

[44] Dawber TR, THomas Jr HE, McNamara PM. Characteristics of the dicrotic notch of the arterial pulse wave in coronary heart disease. Angiology. 1973;24:244-55.

[45] Barbieri R, Matten EC, Alabi AA, Brown EN. A point-process model of human heartbeat intervals: new definitions of heart rate and heart rate variability. American Journal of Physiology-Heart and Circulatory Physiology. 2005;288:H424-H35.

[46] Rayegani F, Onwubolu GC. Fused deposition modelling (FDM) process parameter prediction and optimization using group method for data handling (GMDH) and differential evolution (DE). The International Journal of Advanced Manufacturing Technology. 2014;73:509-19.

[47] Marateb HR, Mohebian MR, Javanmard SH, Tavallaei AA, Tajadini MH, Heidari-Beni M, et al. Prediction of dyslipidemia using gene mutations, family history of diseases and anthropometric indicators in children and adolescents: The CASPIAN-III study. Computational and Structural Biotechnology Journal. 2018;16:121-30.

[48] Eberhart R, Kennedy J. A new optimizer using particle swarm theory. Micro Machine and Human Science, 1995 MHS'95, Proceedings of the Sixth International Symposium on: IEEE; 1995. p. 39-43.

[49] Mohebian MR, Marateb HR, Mansourian M, Mañanas MA, Mokarian F. A hybrid computer-aided-diagnosis system for prediction of breast cancer recurrence (HPBCR) using optimized ensemble learning. Computational and structural biotechnology journal. 2017;15:75-85.

[50] Hoerl AE, Kennard RW. Ridge regression: Biased estimation for nonorthogonal problems. Technometrics. 1970;12:55-67.

[51] Dietterich TG. Ensemble methods in machine learning. International workshop on multiple classifier systems: Springer; 2000. p. 1-15.

[52] Hastie T, Rosset S, Zhu J, Zou H. Multi-class adaboost. Statistics and its Interface. 2009;2:349-60.

[53] Liaw A, Wiener M. Classification and regression by randomForest. R news. 2002;2:18-22.

[54] Mancia G, Ferrari A, Gregorini L, Parati G, Pomidossi G, Bertinieri G, et al. Blood pressure and heart rate variabilities in normotensive and hypertensive human beings. Circulation research. 1983;53:96-104.

[55] Hermeling E, Reesink KD, Kornmann LM, Reneman RS, Hoeks AP. The dicrotic notch as alternative time-reference point to measure local pulse wave velocity in the carotid artery by means of ultrasonography. Journal of hypertension. 2009;27:2028-35.

[56] Wang L, Pickwell-MacPherson E, Liang Y, Zhang YT. Noninvasive cardiac output estimation using a novel photoplethysmogram index. Proc of 31st IEEE EMBS. 2009:1746-9.

[57] Elgendi M. On the analysis of fingertip photoplethysmogram signals. Current cardiology reviews. 2012;8:14-25.

[58] Basak D, Pal S, Patranabis DC. Support vector regression. Neural Information Processing-Letters and Reviews. 2007;11:203-24.

[59] Cherkassky V, Ma Y. Practical selection of SVM parameters and noise estimation for SVM regression. Neural networks. 2004;17:113-26.

[60] Smith L, Tansley J. Decision tree analysis. Google Patents; 2004.

[61] Bland JM, Altman DG. Measuring agreement in method comparison studies. Statistical methods in medical research. 1999;8:135-60.

[62] Cameron AC, Windmeijer FA. An R-squared measure of goodness of fit for some common nonlinear regression models. Journal of econometrics. 1997;77:329-42.

[63] Mccombie DB, Reisner AT, Asada HH, Shaltis P. Wearable pulse wave velocity blood pressure sensor and methods of calibration thereof. Google Patents; 2010.

[64] Klabunde R. Cardiovascular physiology concepts: Lippincott Williams & Wilkins; 2011.

6 ECG COMPRESSION USING OPTIMIZED B-SPLINE

In previous chapters, we have implemented methods for removing noises and artifacts from signals, extracting FECG from abdominal ECG, extracting blood pressure from PPG and detecting anomaly in FECG and ECG with least training data and high performance.

Real-time health monitoring is a challenge that becoming increasingly important, since it can help in early diagnosis and improve the quality of care, especially for cardiac diseases which is very risky. Real-time recording, transmission, viewing, processing, monitoring, and storage, on the other hand, still need additional research, especially as data grows larger. Using the compression technique is a solution to reduce the size of data which is investigated by many researchers. However, encoding and decoding of compressed data is a barrier for real-time processing, especially anomaly detection that sometimes need fast response.

Due to physician shortages and rural location, getting prenatal care might be difficult. Multiple prenatal visits are required to collect basic fetal measures, which adds to the patient's stress. Pregnant women's access to prenatal treatment may be aided through remote monitoring. Remote monitoring has been found to be beneficial in high-risk pregnancies, particularly in women with gestational hypertension and diabetes [6.1]. Compressing signal enables monitoring numerous patients through wireless network in limited bandwidth. Moreover, it can pave the way of distance monitoring of maternal and fetal cardiac status. When data is compressed, it can solve many problems: bandwidth use will be reduced, transmission speed will rise, and the risk of data loss will be reduced.

In this chapter, a lossy compression technique based on a combination of B-spline fitting and ant colony optimization is utilized for compression. The proposed method is applied to ECG signals from the MIT-BIH Arrhythmia Database and 15 recorded ECG using designed hardware. The compression ratio and the percentage root mean square difference show the superior performance of the proposed method regarding the state-of-the-art methods in the literature. Finally, the diagnosis distortion and the size of transmission or restoring is compared with when data is uncompressed. The whole design offers an effective way of using ECG on distributed systems like in a tele-health monitoring.

The analysis and findings of this chapter is under-review in Multimedia Tools and Applications journal. The student contributed to writing the original draft, recording samples, evaluating the compressed signal, implementing optimization and compression and revising the paper.

[6.1] Van Den Heuvel, J.F., Groenhof, T.K., Veerbeek, J.H., Van Solinge, W.W., Lely, A.T., Franx, A. and Bekker, M.N., 2018. eHealth as the next-generation perinatal care: an overview of the literature. *Journal of medical Internet research*, *20*(6), p.e9262.

ECG Compression using optimized B-spline

Mohammad Reza Mohebbian, Khan A.Wahid

Department of Electrical and Computer Engineering, University of Saskatchewan S7N 5A9, Saskatoon, Saskatchewan, Canada

Corresponding Author: Mohammad Reza Mohebbian

Email: mom158@usask.ca

Abstract

Electrocardiogram (ECG) is widely used in the medical field due to non-invasive detecting cardiac anomalies. Transmission, storage and monitoring are necessary for all ECG platforms, from conventional ECG recording methods to portable and wearable approaches. In this regard, compression algorithms are used for reducing data size which make transmitting and storing easier. In this work, an efficient near lossless compression technique is designed that can be used for monitoring and visualization. The compression technique used a combination of B-spline interpolation and ant colony optimization. since the B-Spline coeffcients of the signal are calculated as compressed data, the signal can be visualized without decompression which can save time respecting to state-of-the-art techniques. The MIT-BIH Arrhythmia Database and 15 recorded ECG are used for validation. Averagely, 7.8 ± 1.1 compression ratio and 2.3 ± 1.4 % percentage root-mean-square difference are achieved. Moreover, the experimental analysis proves the superiority of the proposed technique over state-of-the-art techniques and ensures efficient compression, as well as preserving the quality of the original ECG.

Keywords: *ECG, Signal Compression, B-Spline, near lossless*

6.1 Introduction

An Electrocardiogram (ECG) is a physiological signal which can be used for the diagnosis of heart diseases [1]. Traditional ECG uses twelve electrodes for measuring heart activity for a short time. Holter is another standard method for recording ECG that record the heart activity with a duration of 24 hours or more [2]. Besides, emerging wireless sensor networks (WSNs) and the internet of things helped to bring new technologies like wearable ECG and WSN-based ECG, which need transmitting signals [3]. Depending on application types, the ECG signal can

be recorded with 100 to 500 Hz sampling frequency [4] and as an example, three channels of 24 hours ECG can typically take over two hundred megabytes. Therefore, transmitting signal is a challenge that would be more difficult with increasing resolution, sampling frequency, number of channels, and number of signals. Signal compression is one of the solutions for sending and storing signals [5]. However, the compressing and decompressing parts need to be fast and with least loss, especially for monitoring vital signs which are very important to be visualized precisely and real-time.

Effective ECG compression focuses on efficient transmission and data storage without missing essential diagnostic information. In the literature, there are several ways for compressing the ECG signal: time domain compression, transform domain compression, compression by parameter extraction, and hybrid approach [6]. In the time domain compression approach, the original time-domain ECG signal characteristics are examined, and redundant data points are eliminated. This approach is reasonably quick to process since no substantial data translation or transformation is required [7]. The transform domain compression approach, on the other hand, works by transforming the original signal to a frequency or spatiotemporal signal. As a result, it takes longer to process than the first approach, despite the fact that it compresses data more efficiently [8]. The third ECG compression approach is parameter extraction compression. This technique needs the extraction of complicated features from the signal. The features are determined using a variety of learning approaches, which are subsequently employed to compress the original signal and then conserved for decompress [9]. Dictionary learning [10], and deep learning [11] are two examples of modern feature extraction approaches. To develop an effective compression strategy, the hybrid compression approach integrates the details from time-domain, transform-domain, and parameter extraction methods [12]. The final two approaches are more computationally intensive than the first two. As a result, they demand additional processing time and resources.

Nonetheless, compression and reconstruction performance may be enhanced even further. This paper uses a time domain approach based on combination of the B-spline interpolation and the ant colony optimization for ECG compression. The proposed method improves the Quality Score (QS), which are well-known metrics for signal compression [13]. Due to using time domain and B-Spline technique, the data compression is fast and compressed data can be used for visualization and monitoring purposes without decompression owing to B-spline characteristics. The MIT-BIH Arrhythmia Database and 15 recorded ECG are utilized for evaluating the performance of compression.

The rest of the paper is organized as follows: in the next section, information about the datasets and formulation of methods used in this study is presented. Section 3 provides the results of the proposed method. The discussion is provided in Section 4, along with conclusions.

6.2 Methods

6.2.1 Datasets

For real system testing, a device for recording the ECG signal is built. The device is made by a Raspberry Pi 2 (RP2) and a PIC microcontroller to sample ECG signals at 360 and send it to the RP2. The ECG sensing uses capacitive sensors, the Electric Potential Integrated Circuit (EPIC), made by Plessey Semiconductors [14]. These sensors are equivalent to the standard ECG patches. The electrodes are isolated from the human body being measured to have protection and safety. A circuit was designed and built to receive an ECG signal on the fingertips. The EPIC sensors pick up the signals from the thumbs to generate an ECG waveform. The ECG waveform is digitized by a small microcontroller having 10-bit ADC before sending it to the Raspberry Pi. A total of 15 signals from different subjects are recorded in one minute. Each subject is selected among university students with the general public voluntarily and ethic approval.

Moreover, 48 signals, from the MIT-BIH Arrhythmia Database are used for justification [15]. The reason for using MIT-BIH is that many other studies used this database and comparison with other methods would be easier [16]. The ECG recordings were acquired from BIH Arrhythmia Laboratory which studied 47 subjects and recorded 48 two-channel ambulatory ECG recordings of half-hour lengths. The recordings were digitized at 360 samples/second/channel which had an 11-bit resolution over 10mV range.

6.2.2 Proposed method

The block diagram of the proposed method is depicted in Figure 6.1. In summary, signals are filtered and normalized. Then the rectangular windowing is applied on signals to segment signals to small sections. In the next step, the compression algorithm which is made by combination of ant colony optimization and B-spline interpolation is used for compressing each segment. After compression, signals are reconstructed, and performance metrics are calculated for evaluating the proposed method. More details are provided in next subsections.

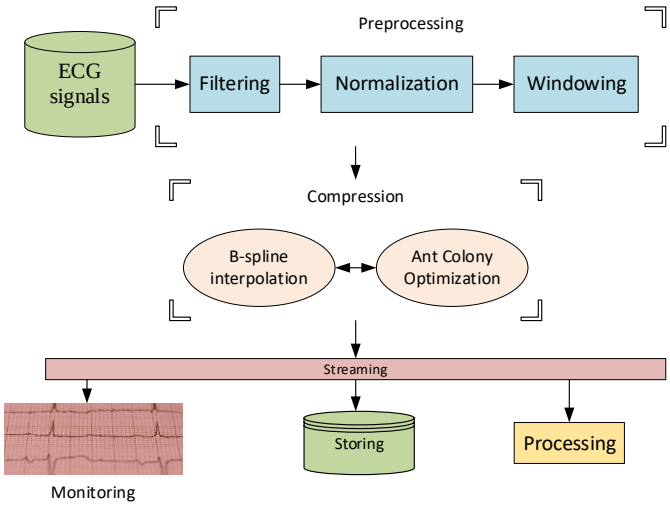

Figure 6-1. The block diagram of the proposed method

6.2.2.1 Preprocessing

ECG signals are commonly contaminated by various noises throughout collecting and transmission in the real world. Multiresolution, a branch of the wavelet transform, has produced excellent results in noise reduction processing in a variety of disciplines, including ECG signal [17], speech signal [18], and images [19]. Multiresolution, on the other hand, is highly dependent on selected wavelet threshold and wavelet function. The best choice for finding maximum decomposition level is stopping decomposition when the signal becomes shorter than the FIR filter length for a specific wavelet [20]. Moreover, many scholars perceived the Symlet wavelet transform to be the best wavelet family for ECG denoising [21, 22].

In this regard, we used Sym4 [21–24] for denoising and the threshold for filtering coefficient is selected based on Wang et al. [21] method that use adaptive thresholding for each level. If a consistent global threshold is used, the same frequency band may be removed at different decomposition levels, causing the original signal to deviate from its original shape.

Then, signals are linearly normalized in range of 0-255 to be quantized using 8 bits. The rectangular sliding window with length of the second is performed for segmenting. Next, the B-spline fitting algorithm is combined with ant colony optimization and applied to the signal window. The detail of compression is provided in the next step.

6.2.2.2 B-spline fitting

Basis spline (B-Spline) is a spline function that has minimal support regarding the given smoothness, degree and domain partition. Using B-spline for curve fitting problem has several merits respect to polynomial fits. High order polynomials tend to oscillate; while the B-spline is smooth and well behaved. The adjacency of local polynomials for creating a piecewise regression may produce discontinuities in connecting pieces. While the B-spline is continuous, and its polynomial segments have continuous derivatives. Furthermore, exact or approximate fitting a signal using B-spline is computationally efficient [25].

Suppose $\{c\}_{i=0}^{n}$ are control points. The B-spline curve of degree p can be defined as Equation 6.1

$$\boldsymbol{g(t) = \sum_{i=0}^{n} c_i N_i^p(t)} \qquad \textbf{(6.1)}$$

Where, $N_i^p(t)$ is the B-spline basis function which is defined on knot vector $U = \{t_0, t_1, \dots, t_{n+p+1}\}$ while $t_i \leq t_{i+1}$; $i = [0, n+p]$. The basic function $N_i^p(t)$ can be defined recursively as Equation 6.2 and 6.3.

$$N_i^0(t) = \begin{cases} 1 & t \in [t_i, t_{i+1}) \\ 0, otherwise \end{cases} \quad (6.2)$$

$$N_i^p(t) = \frac{t-t_i}{t_{i+p}-t_i} N_i^{p-1}(t) + \frac{t_{i+p+1}-t}{t_{i+p+1}-t_{i+1}} N_{i+1}^{p-1}(t) \qquad p \geq 1 \qquad (6.3)$$

The interior knots of U are knots with an index of $i = [p+1, n]$ and they denoted by m_i. Interior knots can be categorized into active and inactive knots. If $(p+1-m_i)$th order derivative of $c(t)$ is discontinuous in t_i, knot t_i is called active. The kth order derivative of $c(t)$ can be defined as Equation 6.4 and 6.5.

$$g^{(k)}(t) = \prod_{i=1}^{k}(p+i-1) \sum_{i=k}^{n} c_i^{(k)} N_i^{p-k}(t) \qquad (6.4)$$

$$c_i^{(k)} = \begin{cases} c_i & k = 0 \\ \frac{c_i^{k-1} - c_{i-1}^{k-1}}{t_{i+p+1-k} - t_i}, & k > 0 \end{cases} \quad 6.5)$$

Suppose the ECG samples are represented by y_j, where $j \in [1, N]$ corresponds to the sample indices. The least-square problem can be defined as the following Equation.

$$e = \frac{1}{N} \sum_{j=1}^{N} \big(g(j) - y_j\big)^2 \qquad (6.6)$$

Where g is defined in Equation 6.1 and is the B-spline. For having a continuous regression this equation subjects to $g(1) = y_1$ and $g(N) = y_N$.

The least-square norm is an unbiased estimation when the signal is corrupted by white zero-mean noise. Moreover, when measurement data is stochastic process and the error follows Gaussian distribution, the least square method gives the minimum estimated variance [26].

According to Karczewicz et al. [27] the cubic ($p = 4$) B-spline is an appropriate choice for ECG compression, regarding the computational cost and accuracy. Therefore, the number and location of knots and control parameters (c_i in Equation 6.1) should be optimized for the curve-fitting problem. The Ant Colony Optimization is used for optimization which is elaborated in the next subsection.

6.2.2.3 Ant Colony Optimization

The B-spline fitting problem depends on the number of knots, knots position, and control parameters and according to Equation 6.2 and 6.3, knots have non-linearity characteristics. In this regard, the objective function (Equation 6.6) is a non-convex function and may have several local minima. Therefore, using stochastic optimization can increase the chance of finding a global optimum. Furthermore, increasing the number of knots increases redundancy

and makes the compression harder. Therefore, the compression ratio (CR) should also be used in optimization objective. The cost function is provided in Equation 6.7, where e is defined in Equation 6.6 and μ is tuning parameters for balancing CR and means square difference.

$$\boldsymbol{Cost} = \frac{\boldsymbol{e}}{\boldsymbol{CR}} \qquad (\mathbf{6.7})$$

The Ant Colony Optimization (ACO) is a stochastic optimization technique that is inspired by the behavior of ants for finding their path from colony to food source [28]. In ACO, ants try to find the minimum cost path in problem space and help each other by pheromone trails in finding the optimum solution. The problem should be presented as a graph in which the probability for selecting node j from the node i for ant k is P_{ij}^{k} and is defined as Equation 8.

$$\boldsymbol{P_{ij}^{k}} = \frac{\boldsymbol{\tau_{ij}^{\alpha}\,\eta_{ij}^{\beta}}}{\boldsymbol{\sum_{l\in v_i^k}\tau_{il}^{\alpha}\,\eta_{il}^{\beta}}} \qquad \mathbf{(6.8)}$$

Where τ is the level of pheromone trail between two nodes, η is the visibility from one node to another, α denotes to how much the pheromone trail has an influence on final probability and is set to 0.5, β represents the influence of visibility from one node to another which is set to 1.2, v_i^k is the neighborhood of node i that ant k has not visited yet. When an ant cross from node i to j, it deposits pheromone based on Equation 6.9.

$$\boldsymbol{\tau_{ij} = \tau_{ij} + \sum_{k=1}^{n}\Delta\tau_{ij}^{k}} \qquad \textbf{Equation 6.9)}$$

Wherein, $\Delta\tau_{ij}^{k}$ is the amount pheromone that ant k deposited between node i and j. If the arc between node i and j belongs to the full tour constructed by ant k, $\Delta\tau_{ij}^{k}$ will be $\frac{1}{l}$ where l is the length of the tour. Moreover, a pheromone trail between nodes i and j is evaporated with evaporation rate ρ. Hence, the τ will be updated by the weight of (1-ρ). For improving the convergence rate of the algorithm, optimized parameters for each signal window are used as initial points for the next signal window. The termination criteria are set to 50 iterations of algorithm, and it can also be set for reaching an acceptable error with an appropriate compression ratio. Furthermore, all optimized coefficients are based on 8-bit resolution.

6.2.3 Validation

The CR and PRD of selected signals from MIT-BIH and recorded signals are evaluated. The percentage root-mean-square difference (PRD) and compression ratio (CR) are provided in the following equations as performance indices.

$$\boldsymbol{PRD} = \mathbf{100} \times \sqrt{\frac{\boldsymbol{\sum_i(\bar{y}_i - y_i)^2}}{\boldsymbol{\sum_i y_i^2}}} \qquad \mathbf{(6.10)}$$

$$\boldsymbol{CR} = \frac{\boldsymbol{Number\ of\ Bits\ in\ uncompressed\ signal}}{\boldsymbol{Number\ of\ Bits\ in\ compressed\ signal}} \qquad \mathbf{(6.11)}$$

Where, $\hat{y}_i$ is the ith approximated of the signal. The decline in the quality of reconstruction is often followed by a rise in CR. Therefore, the quality score (QS) is defined to represent the tradeoff between compression efficiency and reconstruction quality as seen in the Equation 6.12.

$$\boldsymbol{QS} = \frac{\boldsymbol{CR}}{\boldsymbol{PRD}} \qquad \textbf{(6.12)}$$

Comparing the cost function in Equation 6.7 and the QS function reveals that both are showing same tradeoff. In other words, the QS is inverse of the cost function that we intent to minimize. For calculating that how much percent of the signal is compressed the Equation 6.13 can be used.

$$\boldsymbol{CR}\ (\%) = (\mathbf{1} - \frac{\textit{Number of Bits in compressed signal}}{\textit{Number of Bits in uncompressed signal}}) \times \mathbf{100} \qquad \textbf{(6.13)}$$

For diagnostic distortion analysis purposes, the mean value of the original ECG signal and the restored signal are calculated and then subtracted from them. Using Daubechies 9/7 biorthogonal Wavelet filters up to 5 levels, all signals are decomposed. The QRS complex typically has the highest amplitude and the widest spectrum, therefore the QRS complex is visible on all levels. It is more noticeable in the second and third levels, though. On the first two levels, the P and T waves are not apparent and are primarily belong to four and five levels. The deviation between the original signal's Wavelet coefficients and the reconstructed signal's Wavelet coefficients is determined by the percentage root mean square difference, referred to as Wavelet PRD (WPRD). Finally the Wavelet Energy based Diagnostic Distortion (WEDD) is calculated by the weighted average of WPRD in all levels [29].

$$\boldsymbol{WEDD} = \sum_{l=1}^{L+1} \boldsymbol{w_l}\ \boldsymbol{WPRD_l} = \sum_{l=1}^{L+1} \boldsymbol{w_l}\ \sqrt{\frac{\sum_{k=1}^{K_l}[d_l(k) - \widetilde{d_l(k)}]^2}{\sum_{k=1}^{K_l}[d_l(k)]^2}},\ \mathbf{l} = \mathbf{1}, \mathbf{2}, \mathbf{3}, \ldots \mathbf{L} \qquad \textbf{(6.14)}$$

Where, $WPRD_l$ is the error in l-th sub band, and $d_l(k)$ and $\widetilde{d_l(k)}$ are the k-th wavelet coefficient in l-th sub band of original and reconstructed signal, respectively.

6.3 Experimental results and discussion

6.3.1 Results

For every second, ACO is utilized for fitting a series of B-spline. As an instance, for the first 180 samples of one of the recorded signals which are depicted in Figure 6.2, 12 knots are selected, and 15 control points are optimized by ACO with a 10-bit resolution. Therefore, instead of sending 150 10-bit samples, 27 8-bit samples are sent. Hence, the PRD 3.6 and CR 6.9 is achieved.

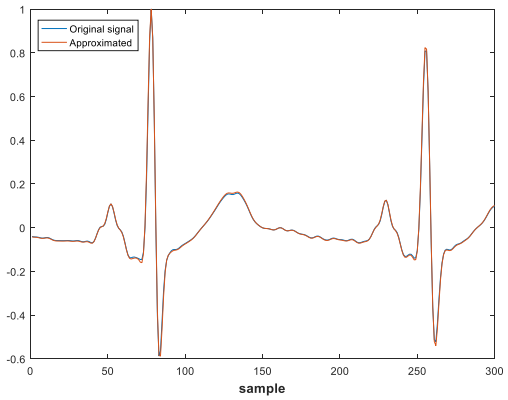

Figure 6-2. The approximated ECG with the proposed method for one of the recorded signals.

The performance of the compression is provided in Table 6.1. According to Table 6.1, improving CR leads to increasing PRD and decreasing CR makes PRD better. For having a comprehensive comparison, the overall range of PRD and CR is provided. Moreover, WEDD is shown for evaluating diagnostic distortion. WEDD can be in different range, such as excellent (0-4.6), very good (4.6-7), good (7-11.2), not bad (11.2-13.6), and bad (>13.6) [29]. According to Table 6.1, the diagnostic distortion is marked in very good range, which means the proposed method does not remove important part of signals.

Table 6-1. The result of the proposed method.

Dataset	CR		PRD (%)		WEDD	
	Average ± std	[min, max]	Average ± std	[min, max]	Average ± std	[min, max]
MIT-BIH	7.8 ± 1.0	[6.8, 8.3]	2.3 ± 1.4	[1.3, 3.4]	4.2 ± 2.3	[3.6, 6.2]
Recorded signals	8.1 ± 1.3	[7.0, 8.9]	2.1 ± 1.0	[1.4, 3.5]	3.8 ± 1.9	[3.4, 5.9]

std: standard deviation; CR: Compression Ratio; PRD: Percentage Root mean square; WEDD: Wavelet energy based diagnostic distortion; Difference. min: minimum; max: maximum.

The proposed method for compression and anomaly awareness is performed by MATLAB (The MathWorks Inc., Natick, MA, USA) with a Core-i7 3.6 GHz CPU with 8 GB of RAM. The computational time for 150 samples of the signal in the compression, decompression is 1.6 ± 0.9 seconds with Matlab. Since compiling a program, rather than interpreting, can improve the speed, C++ implementation of the proposed algorithm is evaluated and as the result, the computational time is decreased to 0.09 ± 0.01 second. Defining a process as a real-time is a debate and depends on the application, however, latency about 6 to 20 millisecond can be supposed near real-time [22].

6.3.2 Comparison of compression performance

The proposed method is compared with similar research, reported in the literature, in Table 6.2 and it has a better-quality score (QS) respecting other methods. Having a low Percentage Root

means square Difference beside a high compression is the merit of the proposed method. As instances, Polania *et al.* [30] performed simultaneous orthogonal matching pursuit and could achieve a better PRD than this research, but with a less CR. Mamaghanian *et al*. [31] compared discrete wavelet transform (DWT) and sparse binary sensing and report a real-time performance for the sparse binary method but with low precision that has 9% PRD. Chae et al. [32] also used a modified TH-DWT and only test one signal. Moreover, there is no systematic real-time validation. Elgandi and Ward [33] used adaptive linear predictors and obtained a compression ratio 6.4 along with QRS detection. Their method is real-time, but the proposed method is superior. The proposed method is also compared with recent method that is proposed by Jha CK [34], wherein the wavelet transform and empirical mode decomposition are combined. Although, their method has higher compression ratio, but the proposed method can achieve better PRD which leads to a better QS. Overall, the QS of the proposed method is superior to other methods.

Table 6-2. Comparing the proposed method with other methods in the literature.

Reference	Year	Method	Test Dataset	CR(%)	CR	PRD (%)	QS
[30]	2011	Simultaneous Orthogonal Matching Pursuit	One record from MIT-BIH	86.1	7.2	2.5	2.8
[31]	2011	Compressive Sensing	All records in MIT-BIH	70.5	3.4	9.0	0.3
[35]	2012	Wavelet Transform	10 records from MIT-BIH	75.0	4.0	1.6	2.5
[36]	2013	Encoding with Modified Thresholding	4 records from MIT-BIH	81.4	5.4	2.7	2.0
[32]	2013	Compressive Sampling	One record from MIT-BIH	60.0	2.5	9.0	0.2
[37]	2016	DCT-IV based compression algorithm	48 records from MIT-BIH	84.8	6.6	2.6	2.5
[12]	2016	Combining of EMD and wavelet transform	11 records from MIT-BIH	93.9	16.6	7.3	2.2
[38]	2017	Embedded zerotree wavelet	5 records from MIT-BIH	95.0	20	10.6	1.8
[33]	2017	Prior knowledge in compressed sensing	11 records from MIT-BIH	84.3	6.4	3.7	1.7
[9]	2018	Downsampling using decimator	105 records from QT Database	82.7	5.8	1.9	3.0
[39]	2020	Block-Sparsity-based Joint Compressive Sensing	48 records from MIT-BIH	47.3	1.9	4.7	0.4
[34]	2021	Combining of EMD and wavelet transform	48 records from MIT-BIH	95.3	21.5	6.8	3.1
Current Study	2021	Proposed Method	48 records from MIT-BIH	87.1	7.8	2.3	3.4
			15 Recorded signals	87.6	8.1	2.1	3.8

6.3.3 Ablation studies

Two ablation studies are performed to evaluate effect of window length and optimization algorithm. In the first ablation study, window length including 0.25, 0.5, 1, 2 and 3 seconds are compared on performance. In this regard, signal are segmented using defined window length and proposed method is applied on it. Figure 6.3 shows the CR, PRD (%) and QS for different window length. The best QS is achieved by setting window length to 1 second. By reducing window length, the PRD can improve, however the CR is increased since number of knots and other parameters are increased. On the other hand, increasing the window length improve compression ratio but the error can increase.

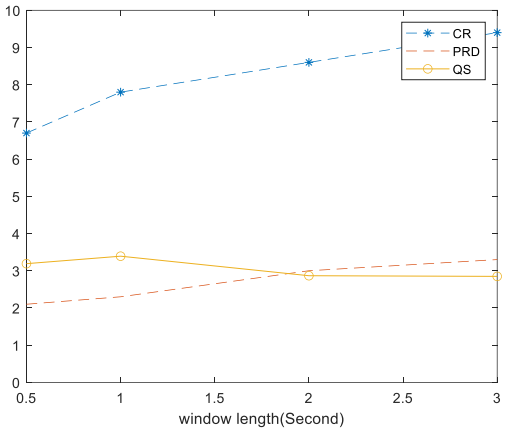

Figure 6-3. The effect of changing window length on the performance. The optimum window length is 1 second, since the QS is in the best condition.

In the second ablation study, the genetic algorithm (GA) and particle swarm optimization (PSO) algorithm are also tested on parts of the data for measuring performance. In multiple runs, PSO and GA converge to the identical optimum solution which is found by ACO. However, their convergence rate is a little slower than ACO. Figure 6.4 shows a comparison between the convergence rate of three algorithms. The cost function is mentioned in Equation 6.7.

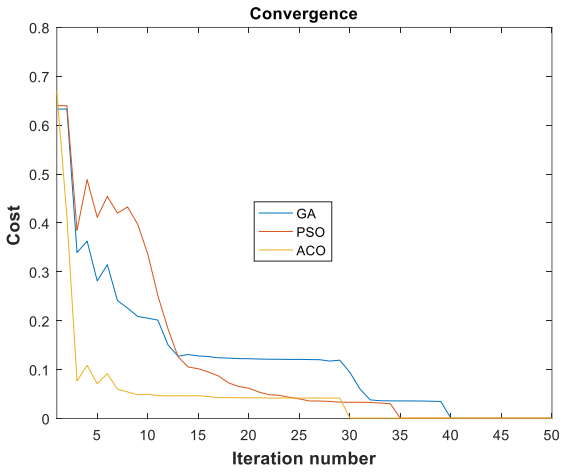

Figure 6-4. Convergence rate of the ACO for B-spline fitting problem comparing to the Genetic Algorithm (GA) and Particle Swarm Optimization (PSO) algorithm.

The proposed method works property on ECG. Nevertheless, it can be applied on other signals such as PPG or arterial blood pressure. The limitation of the current study is that the proposed method cannot be applied to high-frequency signals such as EEG or EMG due to the noisy-like waveform. In other words, when the signal has high frequency components and has a lot of variation, the estimated number of knots and control points is high, and the compression cannot achieve a good CR.

6.4 Conclusion

The paper proposed a time domain compression algorithm for ECG signal. It utilized a combination B-spline interpolation and ant colony optimization on MIT-BIH Arrhythmia Database and some recorded ECG. The technique achieved higher efficiency in terms of quality score. Ablation studies showed that optimum window length for the compression is 1 second. Moreover, changing the stochastic optimization algorithm does not influence on final result. The speed of the proposed method is evaluated which show real-time performance. Furthermore, the Wavelet Energy based Diagnostic Distortion is also used to assess preserving the quality of the reconstructed ECG signal for diagnosis purposes. Overall, the proposed method can compete with state-of-the-art methods and has potential to be used in real-time clinical applications.

6.5 References

1. Goldberger A (2018) Goldberger's Clinical Electrocardiography. Elsevier
2. Jha CK, Kolekar MH (2018) Classification and compression of ECG signal for holter device. In: Biomedical signal and image processing in patient care. IGI Global, pp 46–63
3. Rosu M, Pasca S (2018) WBAN based long term ECG monitoring. In: Wearable technologies: concepts, methodologies, tools, and applications. IGI Global, pp 952–971
4. Qurraie SS, Afkhami RG (2017) ECG arrhythmia classification using time frequency distribution techniques. Biomed Eng Lett 7:325–332

5. Hussein AF, Hashim SJ, Aziz AFA, et al (2017) A real time ECG data compression scheme for enhanced bluetooth low energy ECG system power consumption. J Ambient Intell Humaniz Comput 1–14
6. Chowdhury MH, Cheung RC (2019) Reconfigurable architecture for multi-lead ecg signal compression with high-frequency noise reduction. Sci Rep 9:1–12
7. Abenstein JP, Tompkins WJ (1982) A new data-reduction algorithm for real-time ECG analysis. IEEE Trans Biomed Eng 43–48
8. Alam MS, Rahim NMS (2008) Compression of ECG signal based on its deviation from a reference signal using discrete cosine transform. In: 2008 International Conference on Electrical and Computer Engineering. IEEE, pp 53–58
9. Elgendi M, Al-Ali A, Mohamed A, Ward R (2018) Improving remote health monitoring: A low-complexity ECG compression approach. Diagnostics 8:10
10. Tian X, Zhu Q, Li Y, Wu M (2020) Cross-Domain Joint Dictionary Learning for ECG Reconstruction from PPG. In: ICASSP 2020-2020 IEEE International Conference on Acoustics, Speech and Signal Processing (ICASSP). IEEE, pp 936–940
11. Yildirim O, San Tan R, Acharya UR (2018) An efficient compression of ECG signals using deep convolutional autoencoders. Cogn Syst Res 52:198–211
12. Wang X, Chen Z, Luo J, et al (2016) ECG compression based on combining of EMD and wavelet transform. Electron Lett 52:1588–1590
13. Blanco-Velasco M, Cruz-Roldán F, Godino-Llorente JI, et al (2005) On the use of PRD and CR parameters for ECG compression. Med Eng Phys 27:798–802
14. Kuronen E (2013) Epic Sensors in electrocardiogram measurement
15. Moody GB, Mark RG (2001) The impact of the MIT-BIH arrhythmia database. IEEE Eng Med Biol Mag 20:45–50
16. Wang F, Ma Q, Liu W, et al (2019) A novel ECG signal compression method using spindle convolutional auto-encoder. Comput Methods Programs Biomed 175:139–150
17. Gupta V, Mittal M (2020) Arrhythmia detection in ECG signal using fractional wavelet transform with principal component analysis. J Inst Eng India Ser B 101:451–461
18. Sekkate S, Khalil M, Adib A, Jebara SB (2019) A Multiresolution-Based Fusion Strategy for Improving Speech Emotion Recognition Efficiency. In: International Conference on Mobile, Secure, and Programmable Networking. Springer, pp 96–109
19. Raj JRF, Vijayalakshmi K, Priya SK (2019) Medical image denoising using multi-resolution transforms. Measurement 145:769–778
20. Boggess A, Narcowich FJ (2015) A first course in wavelets with Fourier analysis. John Wiley & Sons
21. Wang L, Sun W, Chen Y, et al (2018) Wavelet transform based ECG denoising using adaptive thresholding. In: Proceedings of the 2018 7th International Conference on Bioinformatics and Biomedical Science. pp 35–40
22. Sivannarayana N, Reddy DC (1999) Biorthogonal wavelet transforms for ECG parameters estimation. Med Eng Phys 21:167–174
23. Castro B, Kogan D, Geva AB (2000) ECG feature extraction using optimal mother wavelet. In: 21st IEEE Convention of the Electrical and Electronic Engineers in Israel. Proceedings (Cat. No. 00EX377). IEEE, pp 346–350
24. Rathore SS, Tripathi N (2020) Suppression of Noise in ECG by Optimal Wavelet Transform. Solid State Technol 63:11757–11767
25. Unser M, Aldroubi A, Eden M (1991) Fast B-spline transforms for continuous image representation and interpolation. IEEE Trans Pattern Anal Mach Intell 13:277–285
26. Avkiran NK (2018) An in-depth discussion and illustration of partial least squares structural equation modeling in health care. Health Care Manag Sci 21:401–408
27. Karczewicz M, Gabbouj M (1997) ECG data compression by spline approximation. Signal Process 59:43–59

28. Dorigo M, Di Caro G (1999) Ant colony optimization: a new meta-heuristic. In: Proceedings of the 1999 congress on evolutionary computation-CEC99 (Cat. No. 99TH8406). IEEE, pp 1470–1477
29. Manikandan MS, Dandapat S (2007) Wavelet energy based diagnostic distortion measure for ECG. Biomed Signal Process Control 2:80–96
30. Polania LF, Carrillo RE, Blanco-Velasco M, Barner KE (2011) Compressed sensing based method for ECG compression. In: 2011 IEEE international conference on acoustics, speech and signal processing (ICASSP). IEEE, pp 761–764
31. Mamaghanian H, Khaled N, Atienza D, Vandergheynst P (2011) Compressed sensing for real-time energy-efficient ECG compression on wireless body sensor nodes. IEEE Trans Biomed Eng 58:2456–2466
32. Chae DH, Alem YF, Durrani S, Kennedy RA (2013) Performance study of compressive sampling for ECG signal compression in noisy and varying sparsity acquisition. In: 2013 IEEE International Conference on Acoustics, Speech and Signal Processing. IEEE, pp 1306–1309
33. Elgendi M, Mohamed A, Ward R (2017) Efficient ECG compression and QRS detection for e-health applications. Sci Rep 7:1–16
34. Jha CK, Kolekar MH (2021) Empirical mode decomposition and wavelet transform based ECG data compression scheme. IRBM 42:65–72
35. Mishra A, Thakkar F, Modi C, Kher R (2012) ECG signal compression using compressive sensing and wavelet transform. In: 2012 Annual International Conference of the IEEE Engineering in Medicine and Biology Society. IEEE, pp 3404–3407
36. Kumar R, Kumar A, Pandey RK (2013) Beta wavelet based ECG signal compression using lossless encoding with modified thresholding. Comput Electr Eng 39:130–140
37. Luo C-H, Ma W-J, Juang W-H, et al (2016) An ECG acquisition system prototype design with flexible PDMS dry electrodes and variable transform length DCT-IV based compression algorithm. IEEE Sens J 16:8244–8254
38. Ziran P, Guojun W, Jiang H, Shuangwu M (2017) Research and improvement of ECG compression algorithm based on EZW. Comput Methods Programs Biomed 145:157–166
39. Kumar S, Deka B, Datta S (2020) Multichannel ECG compression using Block-Sparsity-based joint compressive sensing. Circuits Syst Signal Process 39:6299–6315

7 CONCLUSION AND FUTURE DIRECTION

7.1 Summary and conclusion

This thesis presents potential improvement in cardiac status monitoring of fetal and maternal using artificial intelligence. Developing an end-to-end monitoring system using the defined methodology in each section leads to a novel, easy-to-use, non-invasive, continuous, robust to noise, and efficient evaluation of maternal and fetal cardiac status during pregnancy.

In chapter 2, a robust method for deconvolution of biomedical signals is presented. The suggested method is tested in two different ways. First, the suggested method is used for single-channel ECG denoising in conditions with a very low signal-to-noise ratio. Second, the suggested technique extracts the QRS complex from a single thoracic channel from a maternal ECG. This study shows that the proposed algorithm works in harsh situations, wherein SNR is very low, such as -20 dB, or when the naked eye's ECG signal is not detectable. In these situations, the algorithm can improve the SNR by about 31 dB steps.

In chapter 3, we introduced a method for converting maternal abdominal ECG to fetal ECG. We trained a generative network that can either synthesize Maternal ECG or extracting FECG. The proposed method does not need pairing maternal and fetal ECG for training, and this feature eliminates the lack of enough dataset for training a deep learning model. Moreover, the proposed method does not need tuning, and probability calibration strategies applied to the trained model showed that the model has enough generalization.

The technology to accurately measure FECG is mainly unavailable, which is the fundamental reason for its exclusion from clinical settings. As a result, there has not been much study linking ECG features to FECG outcomes on a broad scale, despite the high similarity of ECG and FECG. Moreover, the lack of gold standard datasets for FECG anomaly detection is another reason FECG arrhythmia detection using deep learning has not achieved much success like other fields where deep learning gained high performance. This is partly due to the absence of comprehensive clinical information about fetal cardiac function and partly due to the low signal-to-noise ratio of FECG compared to the maternal ECG. As explained in previous chapters, we tried to cancel noises, robust design systems for FECG extraction.

Chapter 4 designed an anomaly detection system for FECG using a pretrained system based on adult ECG anomaly detection using the least FECG training sample. The proposed active learning strategy for training could achieve 92% accuracy for FECG anomaly detection using

399 training samples; in contrast, training a model with random weight using active learning required twice annotation data. The annotation effort can even be increased three times when there is no active learning and transfer learning. The proposed active learning approach can be used in clinical machine learning, where the annotation is costly and hard to achieve.

In chapter 5, extracting blood pressure using only PPG signal is investigated. Previous cuff-less methods used a combination of ECG and PPG. The proposed method does not need to synchronize ECG and PPG signals, and only one electrode (PPG) can predict blood pressure with high precision. Continuous measuring blood pressure using only one signal that is more robust against motion than ECG recording techniques is one of the merits of the proposed method. We assumed that designing the proposed hardware, which is cheap to create, eases the monitoring of maternal blood pressure during pregnancy and enables controlling pre-eclampsia, gestational hypertension, and premature delivery.

Finally, in chapter 6, a compression approach is suggested for compressing ECG signals. The proposed method can apply to biomedical signals that are smooth like ECG, such as PPG and FECG. The proposed compression scheme has low diagnosis distortion, which means it can maintain signal quality for diagnosing anomalies after decompression. Moreover, the decompression phase is faster than state-of-the-art methods with similar compression ratios but slower than the proposed method.

All these goals can be combined in an end-to-end system for maternal and fetal cardiac monitoring. The mother's PPG and AECG are recorded to provide data into the system. A denoising method is then applied to each signal to remove artifacts. The AECG is then converted to FECG, and anomaly detection is performed. Simultaneously, blood pressure is calculated from the PPG signal. Acquired data may be compressed and used to fill a status report, or it can be used individually to investigate a specific issue.

7.2 Future research direction

The United States has the greatest maternal mortality rate of any developed country, continuing to climb. Cardiovascular disease is the leading cause of morbidity and death during pregnancy and the postpartum period. Cardiac arrhythmias are another prevalent pregnancy problem in women who have underlying structural heart disease. There are many variables in practice since there is not much data on effectively caring for pregnant women with heart disease. However, the current study can help to monitor and store data to correlate these treatment techniques with mother and fetal outcomes.

Developing and testing an end-to-end system using combination of all proposed objectives is the ideal goal of this project. Considering the size of the AI-powered monitoring device along with computational performance, especially for running deep learning algorithms, is one of the challenges. Custom components might lower the system's size and power, allowing it to be portable and run longer, resulting in higher diagnostic completion rates. Optimizing models

using advanced neural architectural search, knowledge distillation and pruning neural netowkrs are some of the potential future works for implementing the proposed objectives.

Finally, this study was evaluated with limited sample size and datasets. Further testing and analysis are required to evaluate the generalization and real efficiency of each step.

APPENDIX

Publications

1. Mohebian, M.R., shahim Vedaei, S., Wahid, K.A., Dinh, A., Marateb, H.R. and Tavakolian, K., 2021. Fetal ECG Extraction from Maternal ECG using Attention-based CycleGAN. *IEEE Journal of Biomedical and Health Informatics*.
2. Mohebbian, M.R., Alam, M.W., Wahid, K.A. and Dinh, A., 2020. Single channel high noise level ECG deconvolution using optimized blind adaptive filtering and fixed-point convolution kernel compensation. Biomedical Signal Processing and Control, 57, p.101673.
3. Mohebbian, M.R., Dinh, A., Wahid, K. and Alam, M.S., 2020. Blind, cuff-less, calibration-free and continuous blood pressure estimation using optimized inductive group method of data handling. Biomedical Signal Processing and Control, 57, p.101682.

Other publications

1. Mohebbian, M.R., Sohag, M.H.A., Vedaei, S.S. and Wahid, K.A., 2020. Automated Detection of Bleeding in Capsule Endoscopy using on-chip Multispectral Imaging Sensors. IEEE Sensors Journal.
2. Mohebbian, M., Walia, E., Habibullah, M., Stapleton, S. and Wahid, K.A., 2021. Classifying MRI motion severity using a stacked ensemble approach. Magnetic Resonance Imaging, 75, pp.107-115.
3. Marateb, H.R., Nezhad, F.Z., Nosouhi, M., Esfahani, Z., Fazilati, F., Yusefi, F., Amiri, G., Far, N.M., Rastegari, M., Mohebbian, M.R. and Wahid, K.A., 2021. Prosthesis Control Using Undersampled Surface Electromyographic Signals. In Analysis of Medical Modalities for Improved Diagnosis in Modern Healthcare (pp. 89-112). CRC Press.
4. Habibullah, M., Mohebian, M.R., Soolanayakanahally, R., Wahid, K.A. and Dinh, A., 2020. A cost-effective and portable optical sensor system to estimate leaf nitrogen and water contents in crops. *Sensors*, *20*(5), p.1449.
5. Mohebbian, M.R., Hassan, A.M., Wahid, K.A. and Babyn, P., 2020, June. Multi-Frame Low-Dose CT Image noise reduction using Adaptive Type-2 Fuzzy filter and Fast-ICA. In 2020 IEEE Region 10 Symposium (TENSYMP) (pp. 690-693). IEEE.
6. Hasan, A.M., Mohebbian, M.R., Wahid, K.A. and Babyn, P., 2020. Hybrid-Collaborative Noise2Noise Denoiser for Low-Dose CT Images. IEEE Transactions on Radiation and Plasma Medical Sciences, 5(2), pp.235-244.
7. Khan, A.H., Sohag, M.H.A., Vedaei, S.S., Mohebbian, M.R. and Wahid, K.A., 2020, July. Automatic detection of intestinal bleeding using an optical sensor for wireless capsule endoscopy. In 2020 42nd Annual International Conference of the IEEE Engineering in Medicine & Biology Society (EMBC) (pp. 4345-4348). IEEE.
8. Habibullah, M., Mohebian, M.R., Soolanayakanahally, R., Bahar, A.N., Vail, S., Wahid, K.A. and Dinh, A., 2020. Low-cost multispectral sensor array for determining leaf nitrogen status. Nitrogen, 1(1), pp.67-80.
9. Vedaei, S.S., Fotovvat, A., Mohebbian, M.R., Rahman, G.M., Wahid, K.A., Babyn, P., Marateb, H.R., Mansourian, M. and Sami, R., 2020. COVID-SAFE: an IoT-based system for automated health monitoring and surveillance in post-pandemic life. IEEE Access, 8, pp.188538-188551.

10. Rahman, K.M., Mohammed, S.K., Vedaei, S.S., Mohebbian, M.R., Chafjiri, F.S. and Wahid, K.A., 2021. A low complexity lossless Bayer CFA image compression. Signal, Image and Video Processing, pp.1-9.

Archives

11. Mohebbian, M.R., Walia, E. and Wahid, K.A., 2021. Which K-Space Sampling Schemes is good for Motion Artifact Detection in Magnetic Resonance Imaging?. arXiv preprint arXiv:2103.08516.

12. Mohebbian, M.R., Vedaei, S.S., Wahid, K.A. and Babyn, P., 2021. Multiclass Anomaly Detection in GI Endoscopic Images using Optimized Deep One-class Classification in an Imbalanced Dataset. arXiv preprint arXiv:2103.08508.